Knot theory and entanglement in biopolymers

Agnese Barbensi
St Catherine's College
University of Oxford

A thesis submitted for the degree of
Doctor of Philosophy
Trinity 2020

A Spring, e a tutto il tempo passato insieme.

Acknowledgements

I want to devote a few words to all the people who enabled me to complete this work. First, I wish to thank my advisors Dorothy, Heather and Marc, for all their help and constant support during these three years. I honestly couldn't have hoped for better mentors and I will always be grateful for the opportunity they gave me.

Thanks to Professor Ulrike Tillmann and to Professor Cristian Micheletti for acting as my assessors, and for all their useful corrections and remarks that definitely improved this thesis.

A special thank goes to Professor Andrzej Stasiak; I learned so much from him, and having the chance to work with him has been a privilege. I would like to thank my collaborator Dimos Goundaroulis as well. Working with him has been great and so much fun! I can't miss to mention Paolo, Matthias, Mehdi, Marco, Paolo, Francesco and all the topologists who listened to my maths questions during these years. Thanks to the applied topology group, and to all the people I interacted with at the Mathematical Institute. I feel so lucky I have had the opportunity to work in such a friendly yet productive environment.

To my partner Daniele, none of this could have been possible without you. I can't wait for our next adventure! Finally, thanks to my dad Nicola and to my sister Irene for all their support and love. Babbo, questa tesi e' in parte anche tua. Grazie di tutto!

Abstract

This thesis is divided into two parts, each summarising one of the main projects I have undertaken since the beginning of my DPhil. In the first project, we study the graph associated to a knot K, whose vertices are diagrams representing K, and edges represent single Reidemeister moves. We prove that the isomorphism type of this graph is a complete knot invariant, up to mirroring. This framework suggests a discretised model to study the action of some enzymes on knotted DNA molecules. More specifically, we use a grid diagrams based model to investigate the topological consequences of intersegmental passages occurring in circular DNA molecules. We suggest a grid diagrams-based calculation as a new and computationally convenient framework for investigating knotting probabilities in biopolymers.

Recent studies classify the topology of proteins by analysing the distribution of their projections using knotoids. In the second project, using a double branched cover construction, we prove a correspondence between knotoids and strongly invertible knots. This correspondence allows us to study knotoids through tools and invariants coming from knot theory. By using the theory we developed, we investigate the topological relation between knotoids differing by small perturbations on the direction of projection. We then apply our results to infer information on the global topology of knotted proteins.

Introduction

The foundations of this thesis are rooted in low-dimensional topology, and my research includes applications of knot theory to the study of entanglement phenomena in biopolymers, and the development of mathematical theory tailored to this goal. The results of this thesis can be broadly split into two areas: DNA topology and protein entanglement.

The spatial arrangement of many biopolymers has profound effects on several cellular processes. Most famously, the helical conformation of DNA creates topological problems during replication and other processes. These problems are addressed by specific enzymes, whose main function is to change the molecules' topology. In the past decades the expertise of many biologists, mathematicians and other scientists contributed to create a consistent picture explaining many aspects of the functioning of such enzymes (see *e.g.* [17] for a survey). Still, many central questions remain unanswered, and the study of these mechanisms moved from being restricted to the case of "short" DNA molecules (such as bacterial plasmids) to encompass the extreme complexity of entire chromosomes [102]. As a consequence, the cutting edge research in DNA topology increasingly relies on the use of sophisticated topological and computational tools.

In a somewhat similar way, the three dimensional structure of other biopolymers is known to play a key role in their well-functioning. Remarkably, proteins can present phenomena of entanglement as well. The first example of a knot in a protein dates back to 1994, and many more have been identified since [30, 122, 80, 58]. It is known that the knotted domains of some families of proteins have been conserved through evolution [113], and recent studies [108, 113] suggest that the presence of knots in proteins has a prominent biological purpose. Figuring

out whether this is the case is still an open and interesting question in biology, and as for the case of DNA topology, it requires the combined effort of scientists with very different backgrounds, such as biology, chemistry, physics and mathematics.

Organization of the thesis

This dissertation is divided into two thematic parts. Part I contains our work on the actions of certain specific families of enzymes on circular DNA molecules. After introducing the problem and the setting in Chapter 1, we give a discretised model for the set of all the configurations taken by a knot as an infinite graph, whose edges represent local continuous deformations of the embedded curve. In Chapter 2 we investigate the properties of this graph, and we prove, among other things, that the isomorphism type of this graph is a complete knot invariant, up to mirroring.

We then include crossing changes to our set of local deformations, and in Chapter 3 we exploit our framework to model the configuration space of a knotted DNA molecule undergoing the action of such enzymes as a graph, in which each vertex is a diagram representing a specific configuration, and edges represent the action of type II topoisomerases. By replacing classical diagrams with a combinatorial version, this provides a purely topological and computationally convenient framework that can be used to investigate the functioning of such enzymes.

Part II deals with the problem of entanglement in linear biopolymers. Since proteins can be modelled as open curves in space, it is not straightforward to meaningfully characterise their entanglement. Knotoids are a recent generalisation of knots that deals with this issue. After an introduction carried out in Chapter 4, Chapter 5 is devoted to our work on knotoids, in which we construct a series of knotoid invariants through a double branched cover construction.

Recent studies classify the topology of proteins by analysing the distribution of their projections using knotoids. The approximation of this distribution depends on the number of projection directions that are sampled. In Chapter 6 we exploit

the framework developed in 5 to investigate the relation between knotoids differing only by small perturbations of the direction of projection. We then apply our results to infer information about the global topology and geometry of knotted proteins.

All the results in Part I are joint with Daniele Celoria, Heather Harrington, Andrzej Stasiak and Dorothy Buck [7, 8], while the results in Part II are joint with Dorothy Buck, Heather Harrington, Marc Lackenby and Dimos Goundaroulis [5, 9]

Contents

Part I

DNA topology

Chapter 1

Introduction to Part I

DNA (Deoxyribonucleic acid) is a molecule that carries all the genetic instructions used in the growth, development, functioning and reproduction of all known living organisms and of many viruses. DNA's secondary and tertiary structures are strongly related to the molecule's geometry and topology, and mathematical tools are becoming increasingly essential to understand the functioning of these molecules (see *e.g.* [10] and [17] for introductions to DNA topology). DNA is made up of repeated nucleotides: a sugar, a phosphate and one of four heterocyclic bases. These are called adenine, cytosine, guanine and thymine, and they are denoted by the letters A,C, D, and T. All the genetic information of the organism are contained in the bases sequence. These nucleotides are stacked upon each other to form a chain, defining the primary structure of DNA.

The first description of the secondary structure of DNA (based on the X-ray images of Rosalind Franklin) is due to Francis Crick and James Watson [130]. They proposed that these nucleotides are stacked upon each other forming the famous double helix. In this double helix, phosphates and sugars form the backbones of the ladder, while the bases (paired with the rule A-T, C-G) form the steps. This helical geometric structure is quite common in macromolecules.

One of the most interesting features of DNA's tertiary structure is that the axis of these molecules can be coiled in space, creating *supercoiled* DNA (for more details, see [10] and [17]). Even if the axis of DNA is often linear (as in human genomic DNA), in many cases (as in many viruses, bacteria and in human mitochondrial DNA) the ends of the backbones of the double helix close to form circular

molecules. Remarkably, circular DNA molecules may become knotted and linked as the product of replication or other cellular processes, and these can be noxious for the well functioning of the cell. As we will further see in what follows, biological processes such as replication, transcription and recombination are influenced by and can change the topology and geometry of DNA molecules. For this reason, there are enzymes whose main function is exactly to regulate the topology of DNA molecules [10, 17]. One of the most important family of such enzymes is called Topoisomerases. Topoisomerases act by binding at the molecule, breaking one or two strands of the DNA's double helix, passing another segment of DNA through the break, and finally rejoining the break. Depending on whether they break one or two strands of the double helix, Topoisomerases are divided into two different families, called type I and type II respectively. These enzymes, in addition to being of vital importance for replication [23] as well as of several other cellular processes [129], are often used as targets for antibacterial and anticancer drugs [66, 19].

1.1 Modelling DNA molecules as twisted ribbons

Double stranded, covalently closed DNA molecules can be modelled as twisted ribbons $S^1 \times I$ embedded in the 3-space $\mathbb{R}^3$ (more details can be found in [10] and [17]). In this setting, the two edges of the ribbon (representing the backbones of the double helix) are two curves linked around each other. The image of the core $S^1 \times \{1/2\}$ of the ribbon (*i.e.* the central axis of the double helix) can be viewed as a closed curve in space, that is, a *mathematical knot*. The main function of type I topoisomerases is to regulate the amount of supercoiling, thus, they control how much DNA's axis is coiled in space. They perform this task by binding to the DNA molecule, making a transient break in one of the two DNA backbones. They then reseal the break after passing the other backbone around, as in Figure 1.1.

As shown on the right-hand side of Figure 1.1, the effect of an action of type I topoisomerase is to change the "amount of linking"[1] between the two edges of the ribbon.

[1]Thus, to change by ± 1 the *linking number* between the two edges of the ribbon. For a definition of the linking number, see *e.g.* [105].

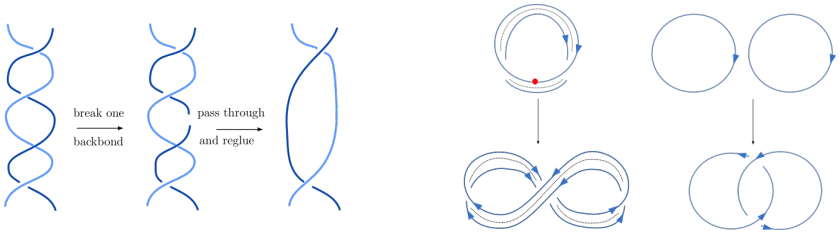

Figure 1.1: Type I topoisomerases control the amount of supercoiling in double stranded DNA molecules.

The class of topoisomerases known as type II act on double stranded DNA molecules by breaking both strands of a segment, that are then bridged by the bound enzyme [124]. Subsequently, a distinct double stranded segment (either from the same molecule or from another one) is passed through, and the cut is resealed [10], see Figure 1.2.

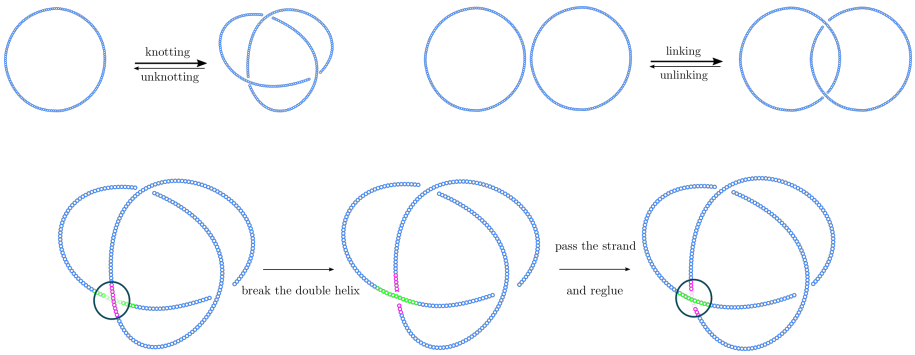

Figure 1.2: Action of type II topoisomerase. The main function of these enzymes is to regulate the amount of knotted and linked DNA molecules.

One of the main function of type II topoisomerases is to regulate the amount of knotted DNA molecules. Indeed, an action of type II topoisomerases has the effect of *changing a crossing* in a projection of the curve representing the core of the ribbon. This operation often results in transforming the *knot type* of a DNA molecule.

1.2 The unknotting function of type II topoisomerases

Type II topoisomerases' ability to cleave and reseal plays a fundamental role in the well functioning of the cell. Indeed, Type II topoisomerases are of vital importance for the proper functioning of DNA replication [23] and of several other cellular processes [129]. As mentioned earlier, DNA knots are known to be damaging for the cell [32]. Therefore, they should be quickly unknotted by DNA topoisomerases. It has been observed in reactions performed in vitro that when type II topoisomerases act on randomly cyclized DNA molecules (*i.e.* molecules having the equilibrium level of knotting), the level of knotting decreases markedly [106]. Thus, type II topoisomerases manifest a preference to disentangle rather then the opposite. This is somehow remarkable, since being knotted is a global phenomenon, and type II topoisomerases act locally. In the last decades several possible explanations for this behaviour have been proposed [106, 126, 132, 118, 18, 82, 81]. For nice surveys on this topic see [124, 11, 125, 104].

The first attempt to model the action of these enzymes is due to Rybenkov *et al.* [106], where the functioning of type II topoisomerases is explained by assuming that the enzymes form clamps that actively slide along the DNA, which results in concentrating DNA entanglements and thus it facilitates their disentanglement by the enzyme. Since active sliding mechanism was not confirmed experimentally, the same leading authors hypothesised that type II topoisomerases create a sharp bend in the gate segment, providing a *preferred orientation* that directs the passage of the transient segment from inside to outside the bend formed by the gate [126].

According to this model, the enzyme first bind two segments, while a third one functions as transient segment. Years later, simulations in [111] seemed to disprove the knot-trapping hypothesis. A similar three-segments mechanism (without the knot-trapping) was later suggested by Roca and collaborators [118]. Yan et al. [132] conjectured that the enzymes must activate the strand-passage reaction by binding two segments of the molecules, before the cut and reseal is performed in another position.

More recently, Buck and Zechiedrich [18] suggested that type II topoisomerases preference to unknot may be due to their ability to recognise specific *inter-hooked*

juxtaposed segments as sites of strand passages. The idea is that topoisomerases may use local information to recognise *hooked* juxtapositions of strands (that is, a portion of the molecule, seen as a knot in space, where two strands are curved toward each other, see Figure 1.3)[2] and selectively perform there the strand passage.

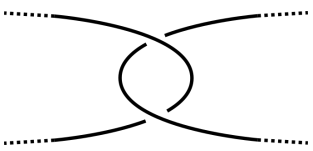

Figure 1.3: A local example of a hooked juxtaposition.

Several previous works (*e.g.* [82, 81, 20]) have confirmed this hypothesis. Earlier approaches have been varied, and used several different ways to model the dynamics of knotted DNA molecules. More physically and biologically realistic models (*e.g.* [133, 26, 27]) allow to include important features of DNA molecules, such as the effect of the presence of supercoiling [10].

Less realistic and more simple approaches to this and related problems, (*e.g.* simulations in the lattice [82, 81] and in the equilateral chain [20, 40, 57] models), employed randomization algorithms to ensure uniformity of sampling and to produce systems exhibiting global and detailed balance while undergoing a given type of intersegmental passages. More precisely, in the lattice model [82, 81], in order to uniformly sample knotted configurations of a given knot type it is necessary to start from a (possibly partial) initial seed configuration. New conformations are then generated from the starting one using a Monte Carlo algorithm. A similar approach is adopted in the equilateral chain model [20, 40, 57], where the initial seed configuration often resembles the ideal one [110]. One of the main aspects of our work is the creation of a simplified new model that tackles these problems.

Our aim here is to propose a new, computationally convenient, purely topological, and intrinsically randomized framework to examine how the interconversion rates between different knot types depend on the local geometry of regions where

[2] A more precise definition of hooked juxtapositions can be given in terms of curvature and tangent vectors, and can be found in [18].

the intersegmental passages occur. The main idea behind our model is that the dynamic of the action of DNA topoisomerases on circular DNA molecules can be encoded by local transformation on planar projections containing the information of over/underpassing segments (*i.e.* knot diagrams).

Previous simulations in the lattice model [82, 81] enabled exact enumeration of configurations up to a given length, and random sampling (achieved using a Monte Carlo algorithm) for higher lengths. However, their analysis was restricted to very few different knot and link types. Simulations in the equilateral chain model [20, 40, 57] included several, more complex, knot types (and also, in related models [133] and to some extent, the presence of supercoiling) but exact enumeration is out of reach in this setting.

Here instead we look at the knot reduction rates in a minimal model amenable to exact enumeration, where uniformity of sampling is intrinsic and built-in, and we demonstrate how most of the behaviours observed in more complex, 3-dimensional models can be recovered in our setting as well. Our model, being purely combinatorial and topological in nature, and essentially 2-dimensional, can not provide precise quantitative answers on problems such as computing the absolute knotting probabilities (see the discussion in Sections 3.1 and 3.3), that can be more realistically addressed in the equilateral chain and cubic lattice models. As we discuss in more details in Section 3.3, our model provides a new and complementary approach to investigate certain statistical and probabilistic properties of knotted polymers.

1.3 Knots and their diagrams

Through this dissertation, a *knot* is defined as a smooth embedding of the circle S^1 into the 3-dimensional sphere S^3 or into the euclidean space $\mathbb{R}^3$. Sometimes we call knots also the images of such embeddings. Two knots K_0 and K_1 are considered *equivalent*, written $K_0 \sim K_1$, if their corresponding embeddings are related by an *ambient isotopy*. Recall that an ambient isotopy is a smooth map

$$F : S^3 \times I \longrightarrow S^3$$

such that $F(\cdot, t)$ is a diffeomorphism for every t. Thus, two knots K_0 and K_1 are equivalent if and only if there exist such F taking the image of the first to the image of the second. A knot is called *trivial* (or we refer to it as the *unknot*) if it is equivalent to the standard planar embedding of S^1 in S^3.

We will often call *knot types* the equivalence classes of knots under the ambient isotopy equivalence relation. Analogously, we call *link* an embedding of a disjoint union $S^1 \sqcup S^1 \cdots \sqcup S^1$ of n circles into the sphere S^3. The image of each circle is called a *component* of the link, and a *link type* is the equivalence class of such an embedding, up to ambient isotopy. Thus, a knot is a link with only one component. The set of knot types in S^3 will be denoted by $\mathcal{K}(S^3)$.

The goal of knot theory is to distinguish and classify knots up to ambient isotopy. This is achieved through the use of *knot invariants*, *i.e.* maps from the set of knots to some structured object like a group or a ring, such that they take the same value on two knots K_0 and K_1 whenever $K_0 \sim K_1$. A knot invariant is called *complete* when it is injective; in other words, two knots share the same image under it if and only if they are equivalent. Some of the most versatile knot invariants take the form of polynomials or integers. During this dissertation, we will make use of several knot invariants, but since most of them are well known and widely used, we will often avoid going into the details of their definitions, and omit to prove that they are in fact unchanged under ambient isotopy.

Knots are often studied through their *diagrams*. A diagram for a knot K in S^3 is just a projection of the knot into a 2-dimensional plane or sphere, such that the only singularities are transverse double points. Each intersection point is called a *crossing*, and it is endowed with the information of which strand is passing over (for more details and precise definitions see *e.g.* [105]). Some examples of knot diagrams are shown in Figure 1.5. Every knot type admits infinitely many diagrams representing it.

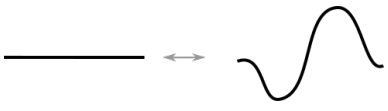

Figure 1.4: Example of a local planar isotopy acting on an arc.

Many simple knot invariants can be defined using diagrams. For example, the *crossing number* of a knot K is defined as the smallest number of crossings of any diagram of the knot. A *planar isotopy* can modify locally a knot diagram by moving slightly an arc as in Figure 1.4, or by displacing a whole diagram, without creating or removing any crossing. We consider two diagrams to be *equivalent* if they differ only by a planar isotopy. The set of diagrams representing K, taken up to equivalence, is denoted by $\mathcal{D}(K)$.

Remark 1.3.1. By considering S^2 rather than D^2 as the ambient space we get a "smaller" set of diagrams; for example, the two diagrams of the left trefoil shown in Figure 1.5 are planar isotopic on the 2-sphere but not on the plane. In our work, we mostly deal with diagrams in S^2.

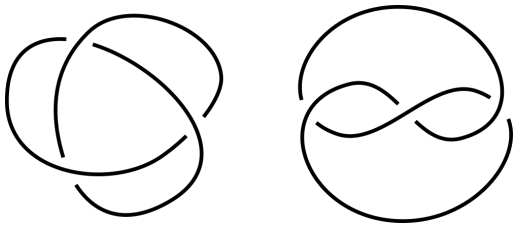

Figure 1.5: These two diagrams of the left trefoil are planar isotopic on S^2, but not on D^2.

After giving an orientation to a diagram $D \in \mathcal{D}(K)$, we can define its *writhe* as the sum of the signs of the crossings [3]. The last definition we will need is the *mirror* $D_{\mathbf{mir}}$ of a diagram D, which is just the diagram obtained by switching all crossings in D. The knot type of $D_{\mathbf{mir}}$ is called the *mirror* of K, and it is denoted by $K_{\mathbf{mir}}$. A knot is said to be *amphichiral* if it is unchanged under mirroring of its diagrams, and *chiral* otherwise.

One of the most fundamental results in knot theory is Reidemeister's Theorem [103] stating that two diagrams represent the same knot type if and only if they are related by a finite sequence of local moves, known as Reidemeister moves, described in Figure 1.6.

[3]Note that the writhe of a knot diagram is invariant under change of orientation, since the sign of each crossing does not change after reversing the orientation of the diagram.

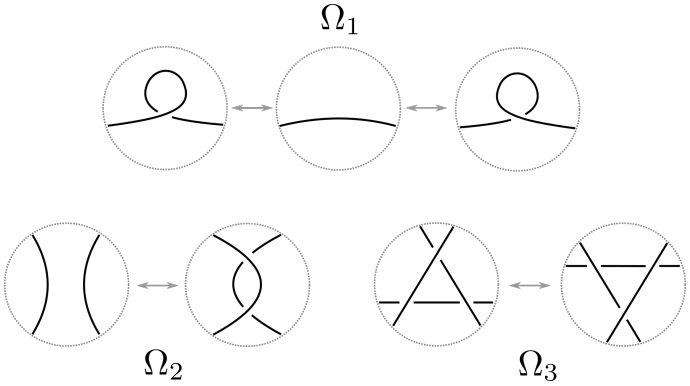

Figure 1.6: The standard Reidemeister moves on knot diagrams. Ω_1 adds/removes a curl. Ω_2 separates overlapping strands and Ω_3 allows the passage of a strand over (or under) a crossing.

In other words, Reidemeister's Theorem tells us that any ambient isotopy between two different embeddings representing equivalent knot types can be decomposed (at a diagrammatic level) as a finite sequence of Reidemeister moves and planar isotopies. Thus, the *configuration space* of a knot, *i.e.* the set of all the embeddings contained in the equivalence class of a knot type K, can be modelled as an infinite graph, in which the vertices are the diagrams representing K, and edges represent single Reidemeister moves.

Definition 1.3.2. *Given a knot $K \subset S^3$ define the* Reidemeister graph *of K, $\mathcal{G}(K)$ as the graph whose vertices are the diagrams of K on the 2-sphere (up to isotopies of S^2), and has an edge between two diagrams* iff *they are connected by a single Reidemeister move. If we replace diagrams in S^2 with planar diagrams, we obtain the planar Reidemeister graph $\mathcal{G}_P(K)$.*

In what follows we will use the term *Reidemeister graphs* or $\mathcal{R}$-graphs to denote both $\mathcal{G}(K)$ and $\mathcal{G}_P(K)$. The properties of this graphs are the subject of Chapter 2. Our main result is that the isomorphism type of $\mathcal{G}(K)$ is a complete knot invariant, up to mirroring. All the results in Chapter 2 are joint with Daniele Celoria [7].

1.4 Crossing changes

As we mentioned in Section 1.1, the strand passage induced by a single action of type II topoisomerase corresponds to performing a *crossing change* on the corresponding knot diagram, as shown in Figure 1.7.

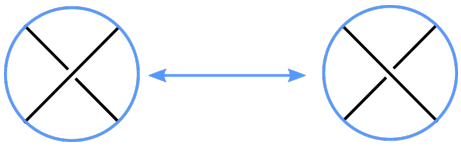

Figure 1.7: Changing a crossing in a knot diagram.

This can be also seen in the bottom line of Figure 1.2. The crossing where the change is performed is highlighted with a circle in both the starting and resulting diagram. Thus, understanding which knots can be obtained from one another through a single crossing change is of particular interest for biologists.

Besides the biological relevance, crossing changes between knots are deeply connected with various topics in low-dimensional topology, such as surgery theory, double branched covers (through the well known Monetesinos trick [92]) and the theory of smooth 4-manifolds [97]. Unfortunately, understanding how different knot types are related through crossing changes is perhaps one of the most complicated topics in knot theory, and even some apparently simple questions remain still unanswered.

For example, define the *unknotting number* $u(K)$ of a knot K as the minimum number of crossing changes required to transform K into the trivial knot[4]. Its value is known for all the knots with crossing number less or equal than 9, and for many infinite families of knots (*e.g.* for torus knots[5]). Even if several different tools have been developed and extensively used to find bounds for it (*e.g.* Heegaard Floer homology [98, 96], the Blanchfield pairing [16], *etc*), and despite its natural definition, detecting the unknotting number of a knot is a really hard problem

[4]It is a classical result [105] that any knot type can be transformed into the trivial knot by a finite sequence of crossing changes.

[5]The notion of torus knots is revised in Appendix A.1

(according to KnotInfo [22] there are still knots with crossing number 10 whose unknotting number is unknown).

As a further and more general example, the minimum number of crossing changes needed to pass from one knot type to another is called the *Gordian distance* between these two knots, and the *Gordian table* is a matrix M, whose entry $m_{i,j}$ is the Gordian distance between the i_{th} and j_{th} knot type. Even for knots with crossing number less than 9 there are still undetermined distances in this table. For instance, the minimal number of crossing changes needed to pass from the figure eight knot 4_1 to the torus knot 5_1 remains unknown[6] [93].

As anticipated in Section 1.2, the biases manifested by type II topoisomerases suggest another question regarding crossing changes between different knot types. Indeed, to understand the functioning of these enzymes it is crucial not only to know which knot types are connected through single strand passages, but also to quantify the intensity of such exchanges. As an example, out of the 2309 knots having minimal crossing number less or equal than 12, 505 are known to have unknotting number 1. The probability that a random strand passage leads to unknotting highly depends on the starting knot type, as shown by simulations in the equilateral chain model[7] [40] and using knots in the cubic lattice[8] [81].

1.5 The graph of knot diagrams

Any knotted configuration can be represented by knot diagrams, and every deformation between two different configurations can be represented by a finite sequence of local moves (*i.e.* Reidemeister moves and crossing changes) between the corresponding diagrams. Thus, we can represent the configuration space of knots as an

[6]Here and in the rest of the thesis, we use Alexander-Briggs notation of knots. The first number of the notation indicates the minimal crossing number of a given knot type. The second number, written in subscript, is an enumeration among those knots sharing the same minimal crossing number.

[7]In this model, a polymer is modelled as a collection of N segments of the same length.

[8]The cubic lattice is the graph in $\mathbb{R}^3$ whose vertices are all the points having integer coordinates and whose edges consist of straight arcs of length 1 connecting these vertices. A lattice polygon, or a knot, on the simple cubic lattice is a piecewise linear, simple closed curve such that each linear piece of it is a unit length segment with its endpoints on the cubic lattice.

infinite graph, whose vertices consist of knot diagrams up to planar isotopy, and edges represent either crossing changes or single Reidemeister moves. We will call this graph the *blown-up Gordian graph*, and a precise definition is given in Section 2.5.

The blown-up Gordian graph is connected and locally finite, and it presents several interesting combinatorial features, as discussed in Chapter 2. The blown-up Gordian graph provides a purely topological and discretised framework to look at the intensity of crossing changes-mediated passages between different knot types. In Chapter 3 we exploit this framework to investigate the biases manifested by type II topoisomerases. By using a slightly modified version of the blown-up Gordian graph as a model, we will test the simplification power of the geometric selection of sites, validating the hooked juxtaposition hypothesis [18].

Chapter 2

The Reidemeister Graph is a complete knot invariant

Graphs are not a new tool in knot theory. For example, the *Gordian graph* is a well known graph in knot theory; its vertices are given by knot types, and two knots have an edge between them whenever they are related by a single crossing change. This graph can be thought of as describing knot theory at "large scales". The Gordian graph is however very ill behaved: each vertex of this graph has infinite valence, vertices at distance 2 are connected by infinitely many distinct minimal paths [4], and for every $n \geq 1$ there are embeddings of the graphs $\mathbb{Z}^n$ into it [88]. This pathological nature of the Gordian graph makes it usually difficult to pinpoint its properties.

The aim of this chapter is to study the opposite point of view: instead of zooming out on the set of all knots, we will describe a way to observe "under the microscope" each knot type. To this end, we associate to each knot type $K \subset S^3$ a graph, the Reidemeister graphs $\mathcal{G}(K)$ and $\mathcal{G}_P(K)$, having a vertex for each diagram of K, and an edge between two diagrams whenever one can be converted into the other by a single Reidemeister move, as explained in Definition 1.3.2. The Reidemeister graphs are always locally finite, and many of its properties can be studied through combinatorial techniques.

This chapter is structured as follows: after giving some definition in Section 2.1, in Section 2.2 we analyse some local properties of these graphs; in particular we will classify all short paths in them (Theorem 2.2.2), and examine the change in

valence between adjacent vertices. These technical results are going to be crucial to establish the main result of the chapter. As a preliminary step we will prove in Theorem 2.2.23 that the graph can detect which Reidemeister move corresponds to each of its edges, and define a related notion of *diagram complexity*.

Section 2.3 instead deals with global properties of the $\mathcal{R}$-graphs; we show that unsurprisingly they are non-planar (Proposition 2.40) and not hyperbolic (Proposition 2.3.1). In addition we show that each Reidemeister graph has only one thick end (Proposition 2.3.3), and compute the homology groups of an associated simplicial complex, following Miyazawa's definition [91].

In Section 2.4 we are going to prove the main result of this chapter, concerning the completeness of the S^2-Reidemeister graph invariant:

Theorem 2.0.1. *The S^2-Reidemeister graph is a complete knot invariant up to mirroring; that is $\mathcal{G}(K) \equiv \mathcal{G}(K')$ iff $K' = K$ or K_{mir}.*

Indeed the proof of this theorem will guarantee a stronger result (Proposition 2.4.3): the isomorphism type of the graph does not only distinguish all knots, but contains enough information to recover some diagrams of the knot (up to mirroring). Moreover, all this data can be extracted from finite portions of the graph (Corollary 2.4.4).
We remark that, unlike the previously known complete invariants -such as knot complement [44], quandles [60] and conormal tori [38]- the proof of completeness for the S^2-graph is substantially more elementary, and self contained.

Finally, in Section 2.5 we define yet another kind of graph, relating the Gordian and Reidemeister graphs by a "blowup" construction.

All the results in this chapter are joint with Daniele Celoria.

2.1 The graph

We start by giving some precise definitions of the well known objects we are going to use extensively in the following. A knot diagram $D \in \mathcal{D}(K)$ can be thought of as a 4-valent graph in D^2 or S^2, by disregarding the crossing information. In

order to avoid confusion, we are going to refer the 4-valent graph associated to a diagram as the *knot projection*. We will call an *arc* each portion of a diagram or projection which connects two crossing points, and denote by $\alpha(D)$ the number of arcs in D. By the handshaking lemma we have $\alpha(D) = 2cr(D)$, where $cr(D)$ is the number of crossings in D. From now on, we are going to assume that, unless otherwise stated, each diagram D contains at least one crossing.

The complement of a planar knot projection is composed of polygons, with the exception of the *external* region which is a punctured polygon; we will call this external part a polygon as well. As is customary we denote by $p_k(D)$ the number of polygons with k-edges.

We have

$$\alpha(D) = \frac{1}{2}\sum_{k\geq 1} k \cdot p_k(D), \tag{2.1}$$

and the number of regions in $S^2 \setminus D$ is $\sum_{k\geq 1} p_k(D)$.

We say that a planar diagram D is *periodic* if there exists a non-trivial rotation of the projection plane taking D to itself, and a knot K is periodic if it admits a periodic diagram. The *order of periodicity* is then just the order of the rotation acting on the diagram.

A diagram on the 2-sphere is said to be *periodic* if there is a non-trivial finite order, orientation preserving self-diffeomorphism of the sphere, that takes it to itself. The $(2n+1, 2)$-torus knots are an example of knots that exhibit a D_{2n+1} periodicity[1] on the 2-sphere and cyclic periodicity of order 2 or d (with $d|2(2n+1)$) on the plane.

Conversely, a knot which does not admit any periodic diagram is said to be *non-periodic*.

Recall the set of Reidemeister moves shown in Figure 1.6. Note that this set of moves is not *minimal* (cf. [100] for the statement in the oriented case); in fact one of the two Ω_1 moves could be discarded (Figure 2.7). However the choice of this slightly larger set will be crucial in the proof of all the upcoming results. In what follows we will find it convenient to divide the Ω_2 moves in two kinds; the first ones consist of those Ω_2 moves performed on the configuration in Figure 2.1, which is

[1]Here D_m denotes the dihedral group of order $2m$.

called a *tentacle*. We will denote them by Ω_T, and call them *tentacle moves*. In

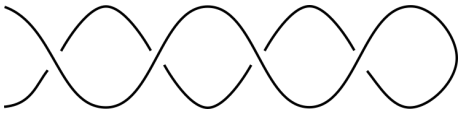

Figure 2.1: A tentacle configuration of height 3. Note that the crossings have alternating signs.

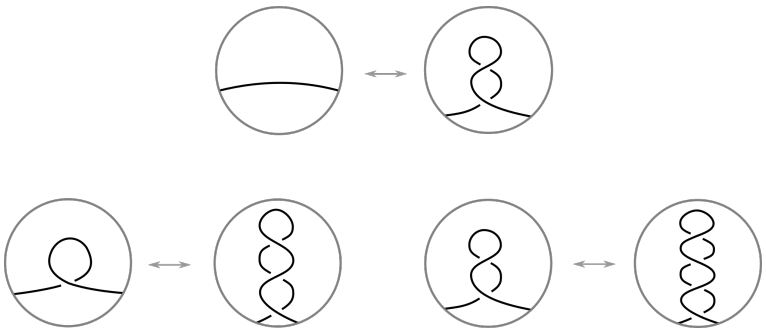

Figure 2.2: The tentacle moves. In the top part of the figure a tentacle move creating a tentacle configuration of height 1 is shown; such a move always arises as the superposition of an arc on itself.

other words, Ω_T moves are the Ω_2 moves that create a tentacle (and their inverses), as in Figure 2.2. We will say that a tentacle configuration has *height* m if it can be expressed as the composition of $m+1$ Ω_1 moves (with alternating signs). In particular a tentacle of height 1 is the result of performing two Ω_1s with opposite curls, or a Ω_T move in which the two affected strands belong to the same arc (top of Figure 2.2). A tentacle of height m contains $m-1$ sub-tentacles of heights $m-1,\dots,1$ as sub-configurations.

The other kind (which we will simply call Ω_2) instead is any other Reidemeister move of type 2. The reason for this distinction will become apparent in the next sections (see Theorem 2.2.2); in fact we are going to prove that tentacle moves are intrinsically distinguished from the other moves (Theorem 2.2.23).

Additionally, if Ω denotes a Reidemeister move which is not a Ω_3, there are two cases, according to whether we are doing or undoing the move. Hence, when necessary, we are going to denote a move by Ω^+ or Ω^- if it increases (respectively decreases) the crossing number.

Recall the definition of the two basic versions of the object we are going to study throughout the rest of the chapter.

Definition. *Given a knot $K \subset S^3$ define the* Reidemeister graph *of K, $\mathcal{G}(K)$ as the graph whose vertices are the diagrams of K on the 2-sphere (up to isotopies of S^2), and has an edge between two diagrams* iff *they are connected by a single Reidemeister move. If we replace diagrams in S^2 with planar diagrams, we obtain the planar Reidemeister graph $\mathcal{G}_P(K)$.*

Remark 2.1.1. It might as well happen that two diagrams are connected by two different moves (see *e.g.* Figure 2.5), which will be considered as different edges in the graphs. On the other hand, moves coinciding up to a planar isotopy will be represented by a single edge.
There are a few immediate consequences of this definition; first of all the isomorphism class of the graphs $\mathcal{G}(K)$ and $\mathcal{G}_P(K)$ are knot invariants, and they are unchanged under mirroring of the knot. Also, Reidemeister's Theorem implies that, for each $K \in \mathcal{K}(S^3)$ the corresponding $\mathcal{R}$-graphs are connected.

It might seem strange to define invariants that are more complicated than the object we started with. However, beyond their intrinsic interest, the $\mathcal{R}$-graphs will allow us to produce several related simple numerical invariants.

To prove many of the local structure results of Section 2.2 for the graphs $\mathcal{G}(K)$ and $\mathcal{G}_P(K)$, we will need the diagram invariant introduced by Hass and Nowik in [52], whose properties are concisely recalled below. In the specialized form we are going to use it, this invariant takes values in the free abelian group generated by the formal variables $\{X_s, Y_s\}_{s\in\mathbb{Z}}$. We call an Ω_1^+ positive if the crossing (for an arbitrary choice of orientation) is positive, and negative otherwise; we will call a Ω_2 move *matched* if the two strands go in the same direction, and *unmatched* otherwise (see Figure 2.3). Note that Ω_T moves are always unmatched.

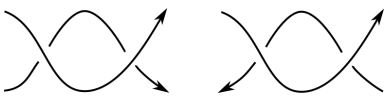

Figure 2.3: A matched and unmatched Ω_2 move (left and right respectively).

If two diagrams D and D' differ by a single Reidemeister move, the corresponding I_{lk}-invariants differ as shown below, for some $n, m, r \in \mathbb{Z}$.

- $I_{lk}(D') = I_{lk}(D) + X_0$ if the move is a positive Ω_1^+.
- $I_{lk}(D') = I_{lk}(D) + Y_0$ if the move is a negative Ω_1^+.
- $I_{lk}(D') = I_{lk}(D) + X_n + Y_{n+1}$ if the move is a matched Ω_2^+.
- $I_{lk}(D') = I_{lk}(D) + X_m + Y_m$ if the move is a unmatched Ω_2^+.
- $I_{lk}(D') = I_{lk}(D) + X_0 + Y_0$ if the move is a Ω_T^+.
- $I_{lk}(D') = I_{lk}(D) + \begin{cases} \pm(X_r - X_{r+1}) \\ \pm(Y_n - Y_{n+1}) \end{cases}$ if the move is a Ω_3.

The only other non-trivial invariants we are going to use are Arnold's *perestroika* invariants $St, J^{\pm}$, first defined in [3]. These are invariants of regular homotopy classes of immersions of S^1 in D^2 or S^2. They change in a controlled way under perestroikas, that is, the analogue of Reidemeister moves for immersions $S^1 \looparrowright D^2$ (or S^2), as shown in Figure 2.4. We will use them on the knot projections associated to the diagrams. Note that there is no analogue of Ω_1 moves for immersions, since performing it would change the *index* of the curve.

The invariant St changes by ± 1 under a triple point perestroika (which corresponds to a Ω_3 move in our setting), and is left unchanged under selftangency perestroikas (corresponding to Ω_2s and Ω_Ts). On the other hand, the invariant J^+ is unchanged under triple point perestroikas and changes by a fixed positive amount (conventionally 2), when a direct tangency perestroika is performed (that is a matched Ω_2^+). The invariant J^- behaves in similarly, but changes only for inverse selftangency perestroikas (that is an unmatched Ω_2^+ or Ω_T^+ in our case).

2.2 Local properties

Given a knot $K \in \mathcal{K}$ and $D \in \mathcal{D}(K)$, the Reidemeister graphs can be naturally endowed with the path metric. Note that the distance induced by this metric coincides with the minimal number of Reidemeister moves connecting two diagrams.

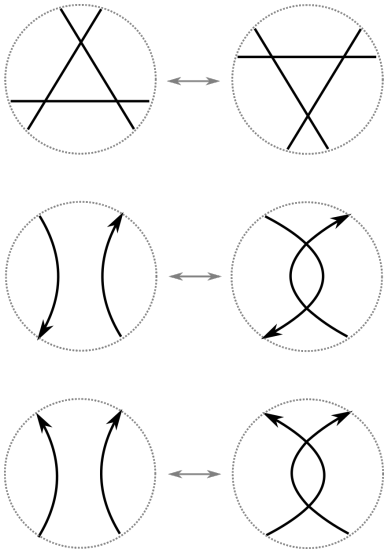

Figure 2.4: A triple point perestroika, followed by the two possible self-tangency perestroikas.

We denote by $S(D)$ the subgraph induced by the vertices having distance ≤ 1 from D, and more generally $S_R(D)$ will denote the subgraph spanned by the diagrams with distance $\leq R$ from D. As we will see in what follows, a lot of information about a diagram D can be extracted from $S(D)$.
The next results are aimed at understanding in detail the structure of small portions of the Reidemeister graph, in both the periodic and non-periodic cases.

We will find it convenient to denote by $\#\Omega_i^{\pm}(D)$ the number of Reidemeister i moves of type $\pm$ which can be applied to D.

This next result states that there are no *cosmetic Reidemeister moves*, meaning that a Reidemeister move necessarily changes the diagram, even up to planar isotopy.

Proposition 2.2.1. *The graphs $\mathcal{G}_P(K)$ and $\mathcal{G}(K)$ do not contain any self-edges.*

Proof. Since Ω_1 and Ω_2 moves change the crossing number, they can be immediately ruled out. The only possibility is then to have a Ω_3 move that, if performed, takes a diagram $D \in \mathcal{D}(K)$ to itself (up to planar isotopy). It is however easy to exclude this case as well using the Hass-Nowik I_{lk} invariant (or Arnold's St):

as recalled in the previous section this invariant changes in a non-trivial manner under Ω_3 moves. □

It is easy to realize that for a given knot, its $\mathcal{R}$-graph contains infinitely many multi-edges, of any order: just take n identical curls on the same arc for one diagram and $n+1$ on the other. Then there are $n+1$ edges connecting them, corresponding to the possible choices for adding another curl, as shown in the top part of Figure 2.5 for $n = 2$.
It is also possible to find multi-edges induced by Ω_2 moves, as shown in the middle and lower parts of Figure 2.5.

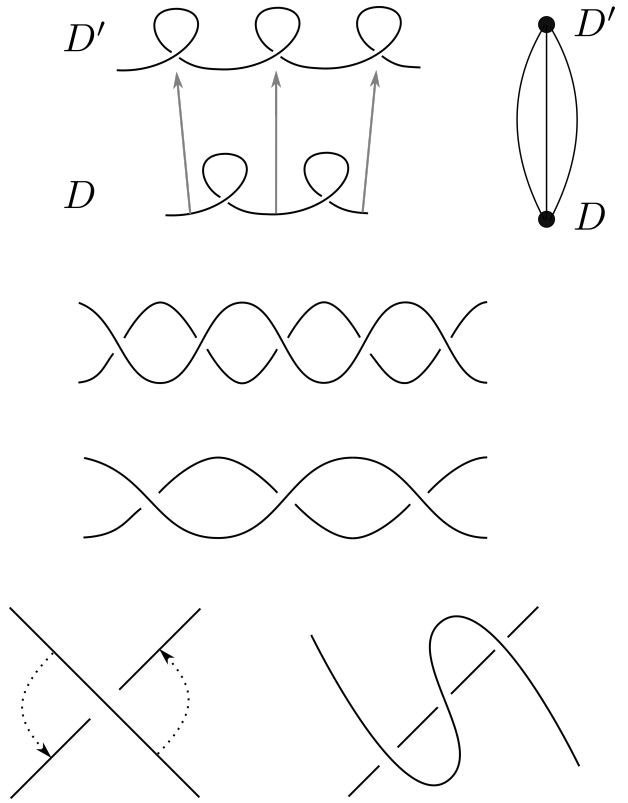

Figure 2.5: In the top part some curls on an arc inducing a multi-edge on the graph, together with the corresponding configuration. In the central part, a multi-edge induced by Ω_2 (or Ω_T) moves, and in the lower part a 2 multi-edge induced by Ω_2s.

In fact, using the configuration in the lower part of Figure 2.5, it is immediate to show that the only radius 1 ball not containing multi-edges is centred in

the crossingless diagram of the unknot. If the knot is periodic, one can also have multi-edges of the form shown in Figure 2.6. It is however easy to prove[2] that each

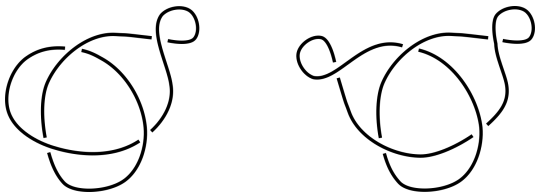

Figure 2.6: There are two inequivalent Ω_1 moves that take one diagram to the other. Note that, even if the diagrams are not periodic, they represent a periodic knot type.

multi-edge must be composed of moves of the same kind.

We will say that a graph contains a *triangle* if there are 3 distinct vertices, such that each vertex is at distance 1 from the other two. We want to analyse the shape of the cycles in $S(D)$, other than the multi-edges. It is easy to find a cycle of length 3, shown in Figure 2.7. Moreover, since this cycle can start from any unknotted portion of an arc, it is ubiquitous in all Reidemeister graphs. A

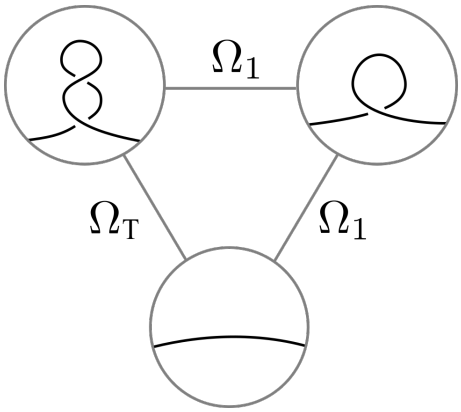

Figure 2.7: A triangle composed by $\Omega_T^{\pm}$-$\Omega_1^{\mp}$-$\Omega_1^{\mp}$.

similar and slightly more elaborate example involving a *higher tentacle* is shown in Figure 2.8. The following result will establish that in some sense these are the only possible cases. Moreover it will permit us to explore the main properties of

[2] *e.g.* using Arnold's invariants for Ω_2, Ω_3s, and I_{lk} for Ω_1s.

the graph. Its proof is roughly based on the following idea: the total sum of any diagram invariant has to vanish on a closed cycle. In most cases it will be sufficient to consider very simple diagram invariants, such as the crossing number.

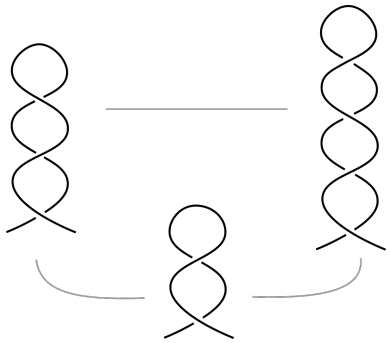

Figure 2.8: A triangle involving some tentacle configurations.

Theorem 2.2.2. *If K is a non-trivial knot, the only triangles in its Reidemeister graphs are of the form $\Omega_T^{\pm}$-$\Omega_1^{\mp}$-$\Omega_1^{\mp}$. If instead K is the unknot $\bigcirc$, there are some sporadic exceptions, shown in Figure 2.9, of cycles of the form $\Omega_2^{\pm}$-$\Omega_1^{\mp}$-$\Omega_1^{\mp}$.*

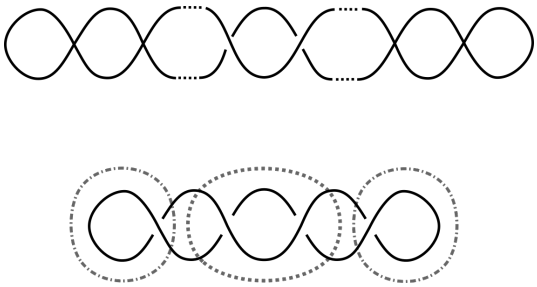

Figure 2.9: On the top, a diagram for the unknot obtained from the crossingless one by a $\Omega_{2/T}$ move followed by succesive Ω_1^+ moves creating crossings of any sign. On the bottom, an example of a triangle involving diagrams of this kind: performing the central Ω_2^- move or the two lateral Ω_1^-s produces the same diagram.

Proof. Suppose we have a length 3 cycle, connecting the diagrams D_0, D_1 and D_2. The total change of crossing number must be 0, hence we can immediately exclude most cases: a priori the only possible combinations (up to permutations) of 3 Reidemeister moves that could work are:

1. Ω_3-Ω_3-Ω_3
2. Ω_3-Ω_2-Ω_2
3. Ω_3-Ω_T-Ω_2
4. Ω_3-Ω_T-Ω_T
5. Ω_3-Ω_1-Ω_1
6. Ω_2-Ω_1-Ω_1
7. Ω_T-Ω_1-Ω_1

It is easy to exclude cases (1) to (4) using Arnold's St invariant: in any cycle (not containing Ω_1s) the number of Ω_3 moves must be even. Case (5) can instead be excluded using Hass-Nowik's invariant: the Ω_3 move contributes to I_{lk} with two consecutive terms (that is, of the form $A_n - A_{n+1}$ for $A = X$ or Y, and $n \in \mathbb{Z}$), while the Ω_1s can only add some terms of the form $\pm A_0$. Hence the total change in the sum can not be 0.

Finally we can focus on cases (6) and (7) and exclude the former. First notice that, in order to preserve the crossing number, a $\Omega_2^{\pm}$, must be followed by two $\Omega_1^{\mp}$. Moreover, using Hass-Nowik's invariant we can conclude that the crossings involved in the Ω_1 moves have different signs, and that the Ω_2 is unmatched.

Define the *self-intersection number* $SI(P)$ of a region P in the complement $S^2 \setminus D$, as the number of crossings in the boundary of P that connect P to itself. We can associate to each diagram D an unordered N-tuple $SI(D) = (SI(P_1), SI(P_2), \cdots, SI(P_N))$ where N is the number of regions in $S^2 \setminus D$.

Performing a Ω_1^- move always decreases the self-intersection number of a single region by 1, and leaves the self-intersection numbers of the other regions unchanged, see Figure 2.10.

On the other hand, a Ω_2^- move can change the self-intersection N-tuple in two different ways, depending on whether the regions denoted A and E in the lower part of Figure 2.11 coincide or not[3]. If A and E coincide, then the component

[3]The regions denoted by B and C are always distinct, otherwise the diagram would represent a two component link.

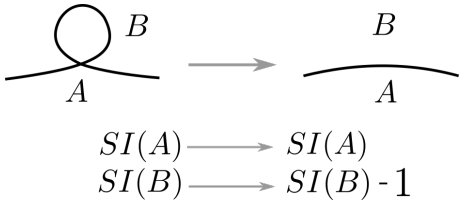

Figure 2.10: Undoing an Ω_1 move decreases $SI(B)$ by 1 and leaves $SI(A)$ unchanged.

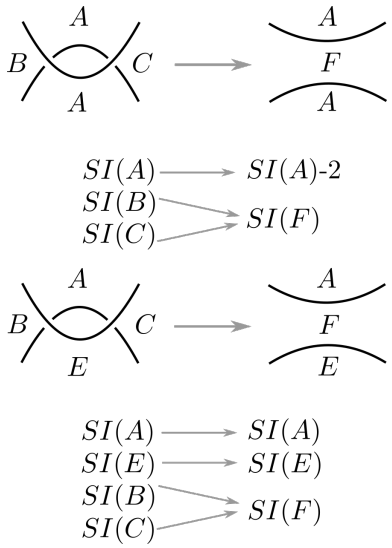

Figure 2.11: Changes in the self-intersection numbers for an Ω_2^- move.

$SI(A)$ of $SI(D)$ decreases by 2 when the move is performed (as in the upper part of Figure 2.11). In the other scenario, the only change in $SI(D)$ comes from the merging of the regions B and C; the new region formed has as self-intersection number greater or equal to $SI(B) + SI(C)$ (lower part of Figure 2.11).

Suppose now by contradiction that there exists a cycle of the form $\Omega_2^{\pm}$-$\Omega_1^{\mp}$-$\Omega_1^{\mp}$. That means we can obtain a diagram D' from D either by performing an Ω_2^- move or a sequence of 2 Ω_1^- moves on D and that the changes in $SI(D)$ must be the same. Now observe that, while the self-intersection number of at least one region decreases with two consecutive Ω_1^-s, if in the Ω_2 move the regions A and E are distinct, the sum of the self-intersections over all regions is increased or left unchanged. This fact allows us to exclude the case in which the Ω_2 move is as in the lower part of Figure 2.11.

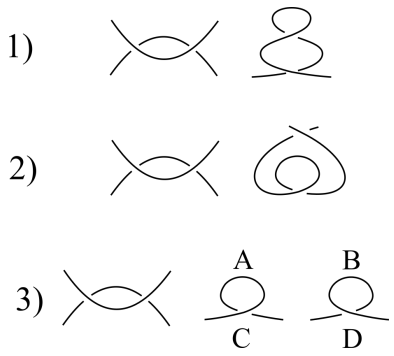

Figure 2.12: In each row we show the portions of D_0 involved in the Ω_* moves. In the first and second row, we assume that the curls undone by the Ω_1 moves do not appear both in the diagram, while in the third case they do. Letters in the latter row indicate the regions touched by the curls.

We will find it useful to divide the discussion in cases, depending on the mutual positions of the curls undone by the Ω_1^- moves. The relevant portions of the initial diagram D_0 are displayed in Figure 2.12 for each of these possibilities: in the first and second row we show the mutual positions the curls can have if they do not both appear in D_0; in other words, the 1-region undone by the second Ω_1 appears after undoing the first curl[4].

In the third row letters indicate the regions touched by the curls: these regions can either coincide or not.

In what follows, for each one of these cases we will either prove that the Ω_2^- needs to be a tentacle move (Figure 2.2), or exclude the configuration.

The first case in Figure 2.12 can be settled as follows: consider Figure 2.13; we can see that in the diagram D_2 there is a tentacle appearing. Since the diagrams D_1 and D_2 are equivalent by hypothesis, the tentacle in D_2 must appear somewhere in D_1. Moreover, since they coincide out of the portions of diagram drawn in the figure, the presence of a tentacle in D_1 *far away*[5] from the portions drawn would imply the existence of an identical tentacle somewhere in D_2, and we would still have one more tentacle in D_2 than in D_1.

A similar recursive argument applies if the tentacle appears by undoing the

[4]Recall that these two moves must have opposite signs.

[5]Here and in what follows, by *far away* we mean that the configuration is left untouched by the moves considered.

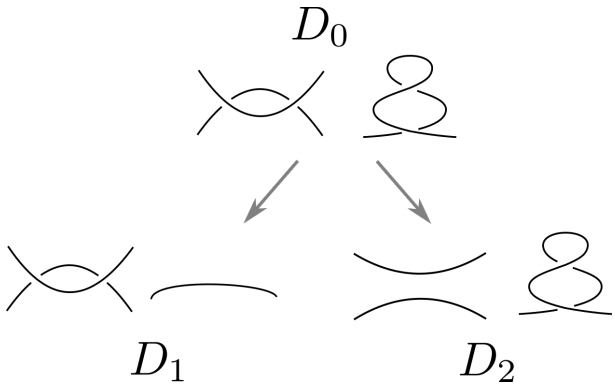

Figure 2.13: D_1 is the diagram obtained after performing the two Ω_1^- moves: together they cancel the tentacle appearing in D_0. D_2 is the result of undoing the Ω_2 move in the left-hand portion of the diagram in D_0.

Ω_1-moves, as in Figure 2.14. In fact, in each of the cases shown in Figure 2.14, there is a configuration in D_2 which does not appear in D_1, and the only way to have $D_1 = D_2$ is to find this configuration in D_1. Iterating this procedure, one sees that the two diagrams can not be equivalent.

It follows that the only way D_1 can be equivalent to D_2 is if the Ω_2 is in fact an Ω_T; thus the corresponding part of the diagram is a portion of a tentacle[6].

For the second case consider Figure 2.15: we apply the same argumentation of case 1). Since the diagrams D_1 and D_2 are equivalent the *heart shaped* configuration in D_2 must appear somewhere in D_1. Moreover, since the diagrams coincide out of the portions drawn in the figure, the presence of a heart in D_1 *far away* from the portions drawn would imply the existence of an identical heart somewhere in D_2, and we would still have one more heart in D_2 than in D_1. The same argument of case 1) (as in Figure 2.14) works if we assume that the heart appears after undoing two Ω_1 moves. It follows that the only possibility is the one depicted in Figure 2.16.

We can however prove that in this case D_1 and D_2 can not be equivalent diagrams, and thus exclude it. To this end, consider the blackboard framing of the projection: there are two possibilities to be considered, since we can draw the framing curve on either side of the diagram. Then, since we do not know how

[6]Note that if the portion of diagram involved in the Ω_2^- is attached to a piece whose projection is the same as a tentacle, but with *wrong* crossings, then the diagram does not fit in a triangle.

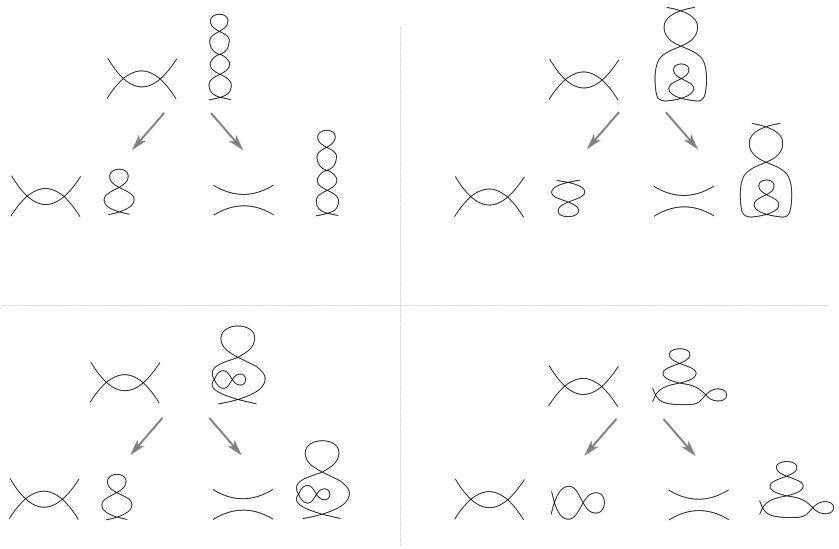

Figure 2.14: The only possible ways a tentacle can appear in case 1) after performing two Ω_1^- moves. In each of these cases we can exclude that the diagrams form a triangle by a recursive argument.

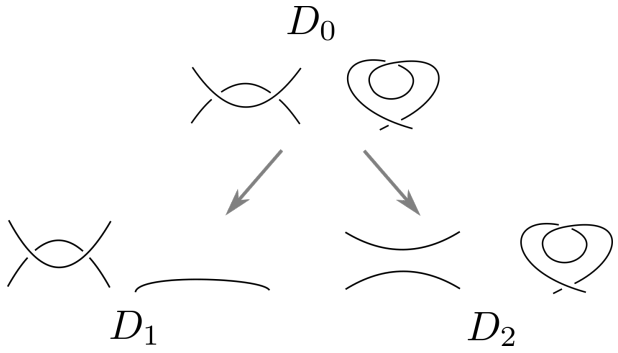

Figure 2.15: D_1 is the diagram we obtain after performing the two Ω_1^- moves: together they cancel the heart configuration appearing in D_0. D_2 is the result of undoing the Ω_2 move in the left-hand portion of diagram in D_0.

the portions of diagrams involving the moves are positioned with respect to each other, we need to consider four different cases, all shown in Figure 2.17. It is easy to argue that D_1 and D_2 can not be equivalent, since the number of curls having the blackboard framing *inside* is different in all four cases.

We are now left with case 3) from Figure 2.12. As usual, it is convenient to have in mind all the diagrams involved in the triangle, as in Figure 2.18.

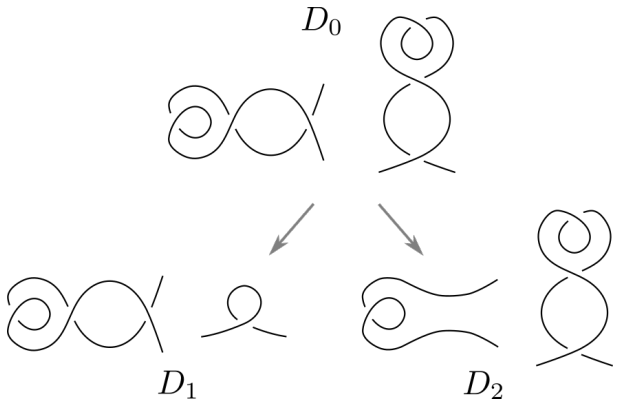

Figure 2.16: D_1 is the diagram we obtain after performing the two Ω_1^- moves: together they cancel the heart configuration appearing in D_0, leaving a curl. D_2 is the result of undoing the Ω_2 move in the left-hand portion of diagram in D_0.

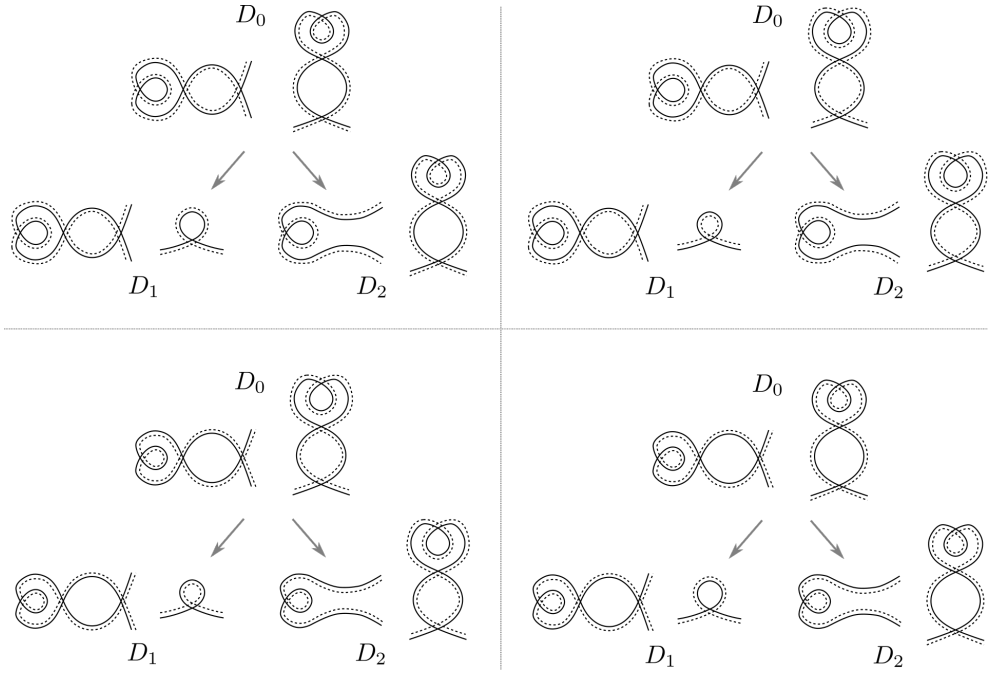

Figure 2.17: The four possible choices for the blackboard framing.

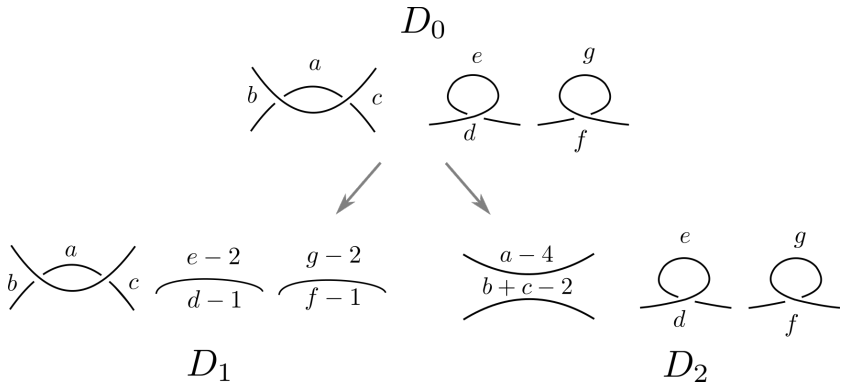

Figure 2.18: Lowercase letters indicate the number of edges in each region. Keep in mind that, even if in the picture all the regions are depicted as different, some of them might coincide.

From Figure 2.18 it is apparent that there are two more visible 1-regions in D_2 than in D_1: since by hypothesis the diagrams are equivalent, there must be two curls in D_1 as well. Suppose by contradiction that the Ω_2 is not a tentacle (that is $b, c \neq 1$). Then, the straight lines in D_1 left by undoing the Ω_1 moves must be part of two curls. If we assume (Figure 2.18) that the regions touching the curls in D_0 are different, this means that at least two among $d-1, e-2, f-1$ and $g-2$ must be equal to 1. Since the cases $(e, d) = (3, 2)$ and $(f, g) = (2, 3)$ are impossible, we are in one of the cases described in Figure 2.19.

Before dealing with the configurations described in Figure 2.19, we need to consider the cases in which some of the regions touching the curls coincide, keeping in mind that we are assuming that the Ω_2 is not a tentacle move. We have the following possibilities (capital letters denote regions, as in Figure 2.12):

I $A = B$ and $C = D$;

II $A = D$ and $B = C$;

III $A = B$ and $C \neq D$;

IV $C = D$ and $A \neq B$;

V $A = D$ and $B \neq C$;

VI $C = B$ and $A \neq D$.

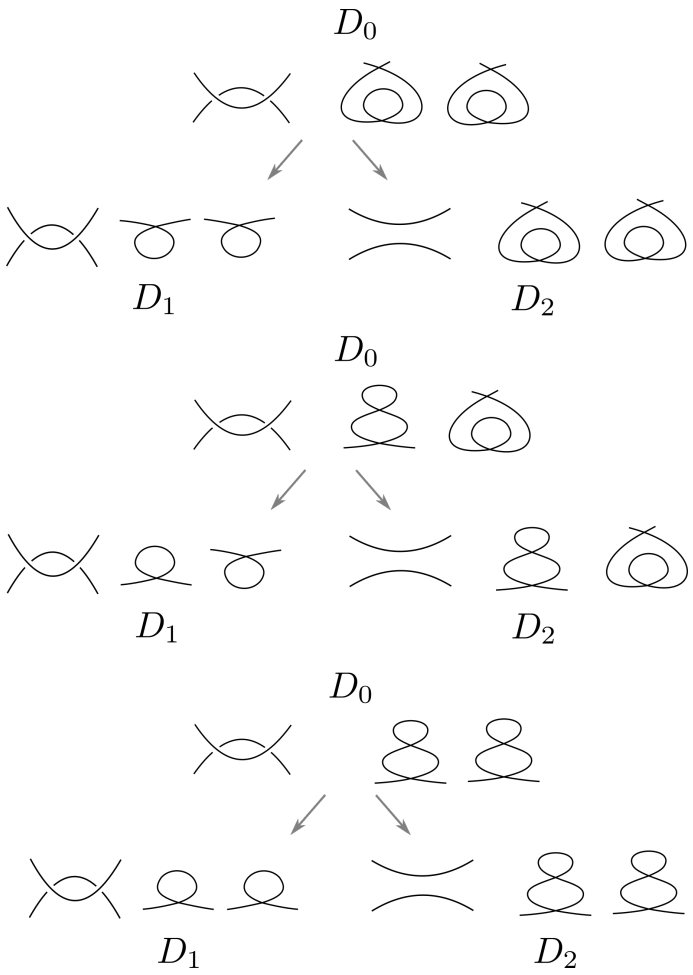

Figure 2.19: The three possible kinds of triangles, assuming that the regions touching the curls undone by the Ω_1 moves do not coincide.

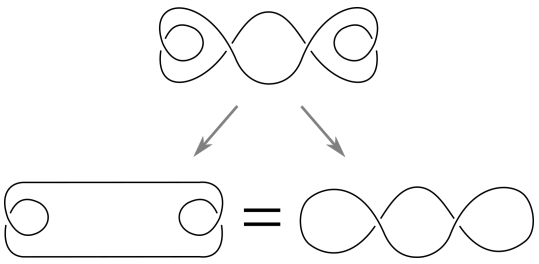

Figure 2.20: A triangle for the unknot fitting in the family described in the statement of the Theorem.

Note that the upper and lower regions left by undoing a curl can not be both 1-regions. Thus, cases I and II are straightforward to exclude, since if the regions coincided pairwise it would be impossible to recover two 1-regions from the straight lines left by undoing the starting curls. For the same reason, in the third case the only way to have two curls left after the Ω_1^- moves have been performed is to have a 2-region below each 1-region in D_0. Thus, case III fits in the bottom configuration described in Figure 2.19. Similarly, in case IV, we would necessarily have both the curls in D_0 lying inside a 4-region, forming an *heart* and fitting in the top case shown in Figure 2.19. The latter two cases are symmetric, and it is enough to discuss only the first one. Again, since it is impossible to have both the upper and lower region left by undoing a curl as 1-regions, it follows that the Ω_1^- moves must be performed in portions of diagrams identical to the ones drawn in the middle case of Figure 2.19.

Let's now discuss carefully Figure 2.19. Consider the configuration at the top of the figure: since the diagrams D_1 and D_2 are equivalent, the *heart* configurations in D_2 must appear somewhere in D_1. Moreover, since they coincide out of the portions drawn in the figure, and since using again a recursive argument we can exclude that they are created by undoing the curls in D_0, the only possibility is that these hearts are attached to the Ω_2-portion in D_1, as shown in Figure 2.20.

Note that even if in this case D_1 and D_2 turn out to be equivalent, the diagrams represent the trivial knot, and more precisely they fit in the family described in the statement of the Theorem.

Notice that this can only happen if we are working with diagrams on S^2; if we are working with planar diagrams instead, this configuration does not fit in a

triangle. Now, call *generalised tentacles* the configurations formed by two succesive Ω_1 moves made one on top of the other, as appearing in D_2 and D_0 on the bottom of Figure 2.19. If the crossings are such that the configurations form tentacles, then this implies (as in case 1) of Figure 2.12, that the Ω_2 is in fact a tentacle move.

Otherwise, by using a similar recursive argument as before, together with the fact that the upper and lower regions involved in the Ω_2 move coincide, we can exclude both the possibility that the configurations appear in D_1 by performing the Ω_1^- moves, and that they appear somewhere *far away* from the portions of diagram shown. Thus, we see that the only possibility for D_1 and D_2 to be equivalent occurs when the generalised tentacles are attached[7] to the Ω_2-portion of D_2, forming a diagram for the unknot fitting in the family described in the statement of the Theorem (see Figure 2.9). Notice that the triangle in $\mathcal{G}(\bigcirc)$ involving the heart configurations described before is a special case of this situation.

Finally, we are left with the middle configuration in Figure 2.19. As usual, since D_1 and D_2 are equivalent by hypothesis, the tentacle configuration in D_1 has to appear somewhere in D_2 as well. Assuming that the Ω_2 is not a tentacle move, since the diagrams coincide out of the portions drawn, using yet again a recursive argument we can exclude that the tentacle is created by undoing the curls in D_0; hence the only way to have a tentacle in D_1 is the one shown in Figure 2.21. We can however exclude this case as well by adding the blackboard framings. In Figure 2.22 two of the possible choices of framings are displayed: in both cases D_1 and D_2 are non-equivalent diagrams, since the framings do not coincide on the tentacles or in the 1-regions left. □

Remark 2.2.3. In what follows, unless otherwise specified, all the results will hold for every knot type with the exception of the unknot $\bigcirc$.

For each diagram $D \in \mathcal{D}(K)$, $S(D)$ consists of triangles having one vertex corresponding to D and two vertices corresponding to diagrams having distance 1 from D (note that these triangles are possibly attached to one another), and of edges emanating from D. Each of these might be a multi-edge. If we want to study the possible configurations in $S(D)$ involving triangles, by Theorem 2.2.2, we

[7]Or they are part of longer generalised tentacles attached to the Ω_2-portion of D_1.

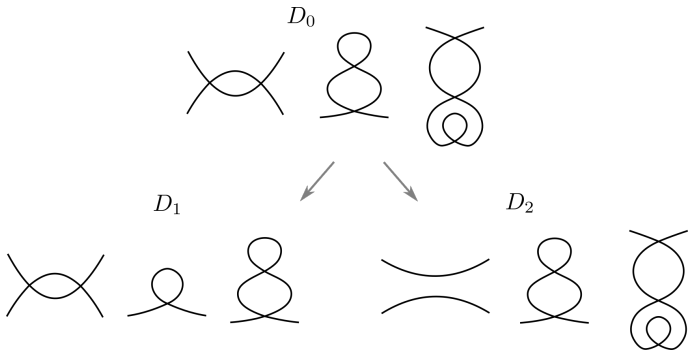

Figure 2.21: D_1 is the diagram we obtain after performing the two Ω_1^- moves: with the first one we cancel the curl inside the heart, while the other has the effect of decreasing the height of the left tentacle by 1. D_2 is the result of undoing the Ω_2 move in the left-hand portion of diagram in D_0.

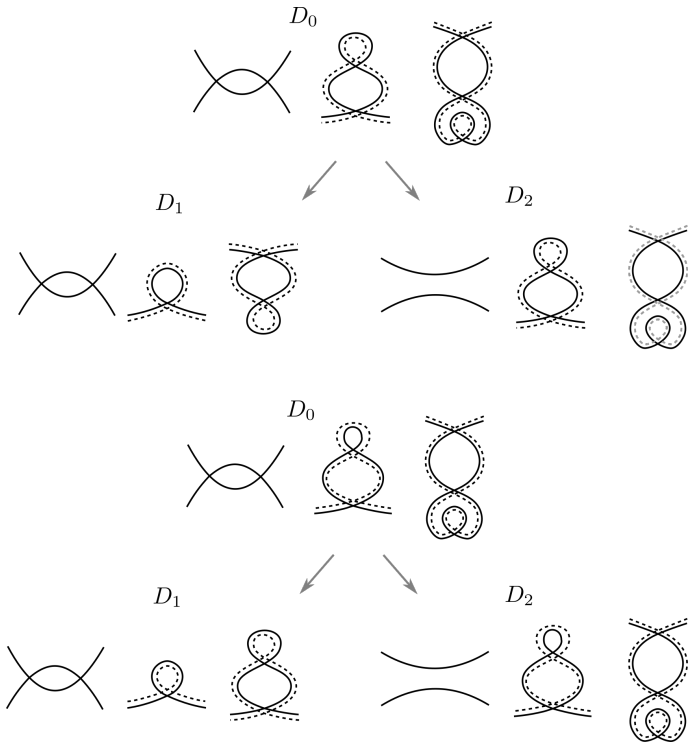

Figure 2.22: Two of the four possible choices of framing. The remaining two can be treated in the exact same way.

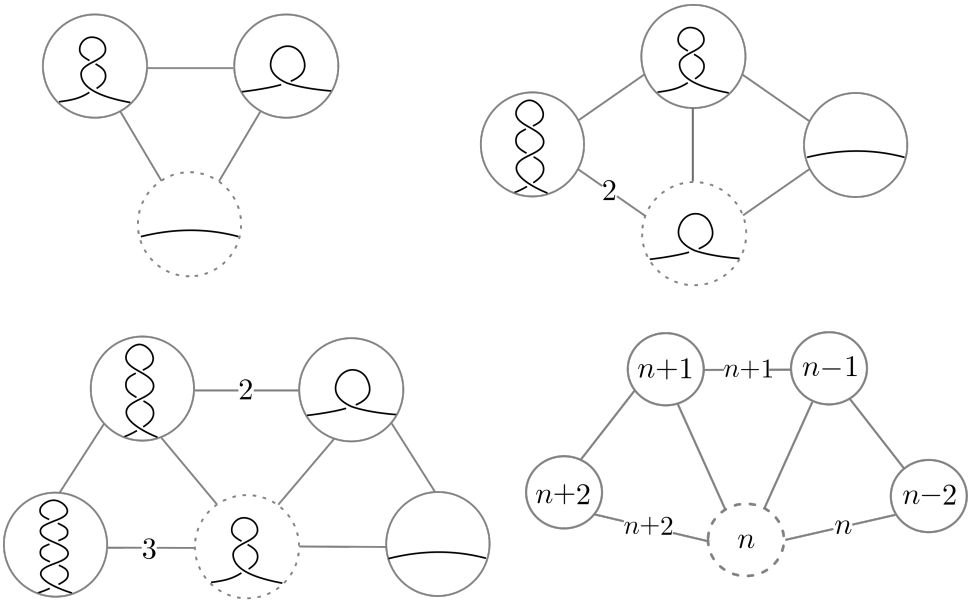

Figure 2.23: Some of the possible configurations in $S(D)$ involving at least one Ω_1 move (D is contained in the dotted circles). The top-left one is present in any $S(D)$, while the others can be found whenever there is a Ω_1^- (top-right), an height 1 tentacle (bottom-left), or a tentacle of height $n \geq 2$ (bottom-right). Numbered edges denote the valence of the corresponding multi-edge.

just need to restrict to those containing at least one Ω_1 move; various possibilities involving one or more curls/tentacles are shown in Figure 2.23 and 2.24.

So we have a complete description of the short paths that can appear in $\mathcal{G}(K)$; note that it makes less sense to pursue a systematic study of longer (≥ 3) cycles, since any pair of *distant* moves on a diagram produces a cycle of length 4. In the following we are going to examine more closely the properties and shapes of the various triangles that have been produced during the proof of Theorem 2.2.2. This technical analysis is going to be crucial in the proof of the results leading to Theorem 2.0.1.

Definition 2.2.4. *We will call a triangle* normal *if it is of the form described in Figure 2.7, meaning that all the Reidemeister moves are performed locally on the same arc.*

Lemma 2.2.5. *$p_1(D) = 0$ if and only if all the triangles in $S(D)$ are normal.*

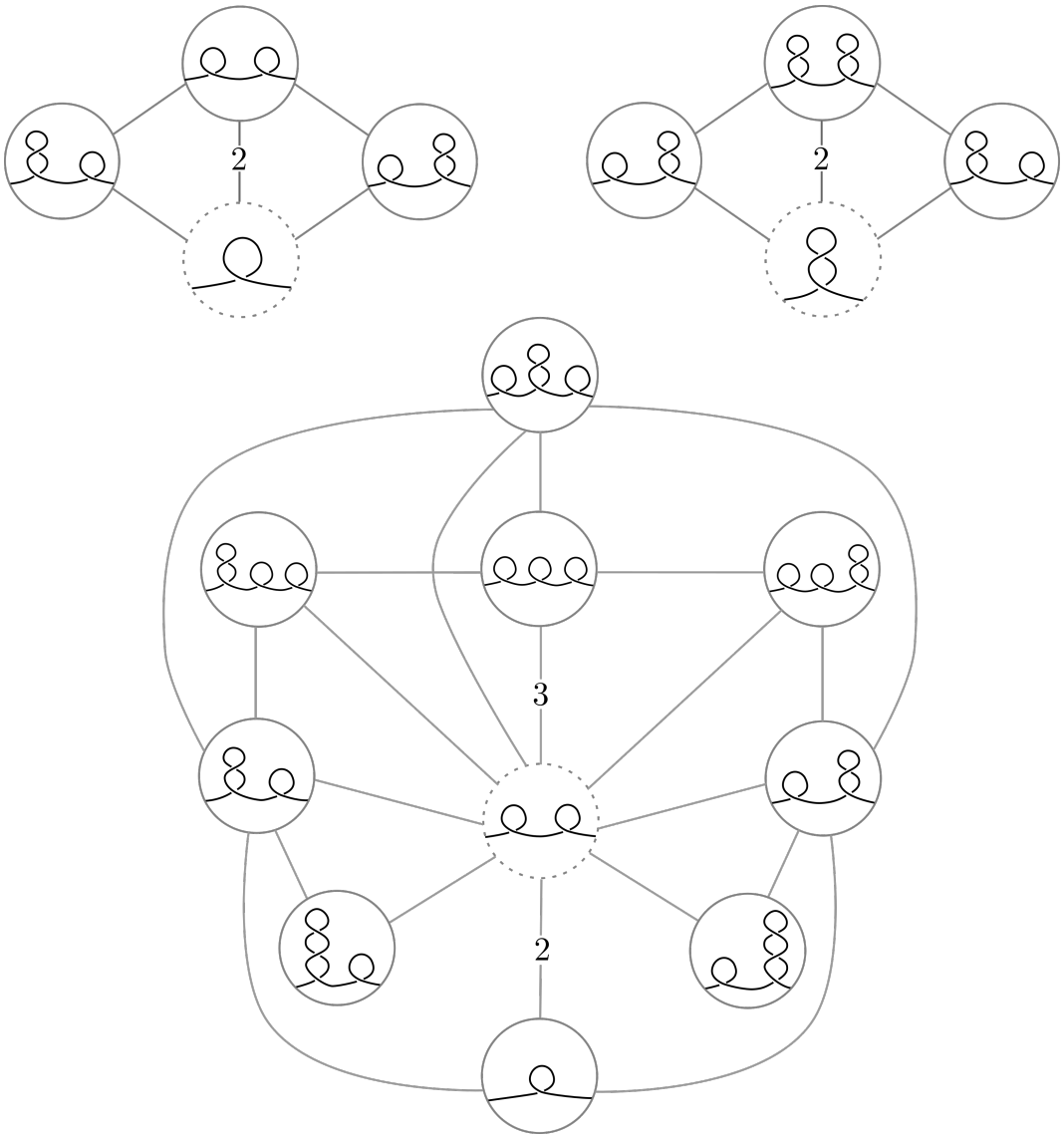

Figure 2.24: Other qualitatively different triangle configurations formed by Ω_T-Ω_1-Ω_1 can be found whenever there are multiple curls or height 1 tentacles on the same arc.

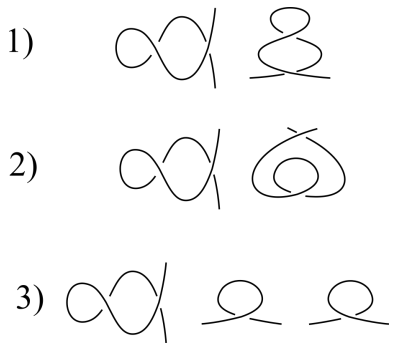

Figure 2.25: In each row the portions of D_0 involved in the Ω_* moves are shown. In the first and second row, we assume that the curls undone by the Ω_1 moves do not both appear in the diagram.

Proof. If $p_1(D) \neq 0$, then there are at least two triangles sharing a Ω_1^+ edge, as shown in the top-right part of Figure 2.23. This implies that there are at least two non-normal triangles, since one can perform the first Ω_1^+ move on either side of the pre-existing twirl, and complete this edge to a triangle by performing the successive Ω_1^+ and Ω_T^- on the pre-existing twirl.
Viceversa, suppose that $p_1(D) = 0$. Thanks to Theorem 2.2.2 we know that all triangles are made up by Ω_T-Ω_1-Ω_1; moreover, every Ω_1 and Ω_T is part of at least one triangle. We wish to understand all the possible configurations forming a triangle. To this end, we can use Figure 2.12, substituting[8] with Ω_T configurations the Ω_2s, as in Figure 2.25.

Since $p_1(D) = 0$, we can exclude the occurrence of cases 2) and 3) of Figure 2.25. In fact, in each of these triangles, the diagram with lower crossing number admits at least one 1-region. Let's suppose that there exists a non-normal triangle fitting in case 1) of Figure 2.25. By definition, this means that the moves are not performed on the same arc. Then, in the lower crossing number diagram, there is at least a 1-region (see Figure 2.26), contradicting the hypothesis $p_1(D) = 0$. □

Remark 2.2.6. If $p_1(D) \neq 0$, then more complicated triangles appear. We show an example of a non-normal triangle fitting in case 1) of Figure 2.12 in Figure 2.27.

In what follows we are going to analyse what happens in the remaining cases. In fact, case 2) of Figure 2.12 can be excluded as in the proof of Theorem 2.2.2.

[8]We can assume that the Ω_T move happens on the top of the tentacle.

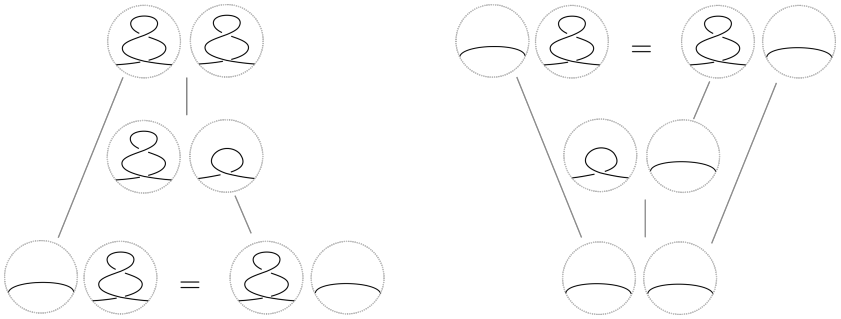

Figure 2.26: On the left, a non-normal triangle fitting in case 1). The diagrams with the lowest crossing number (on the bottom) are identified. On the right, a normal triangle fitting in case 1). Here the diagrams with the greatest crossing number are identified, and there is a Ω_T multi-edge.

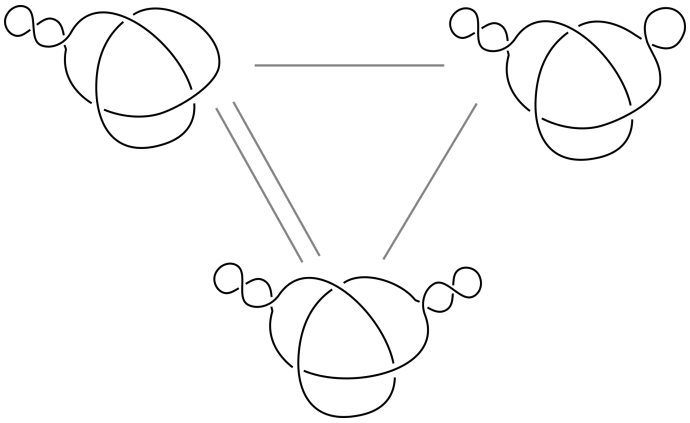

Figure 2.27: A triangle for a periodic knot fitting in case 1). The left and lower vertices are connected by a multi-edge.

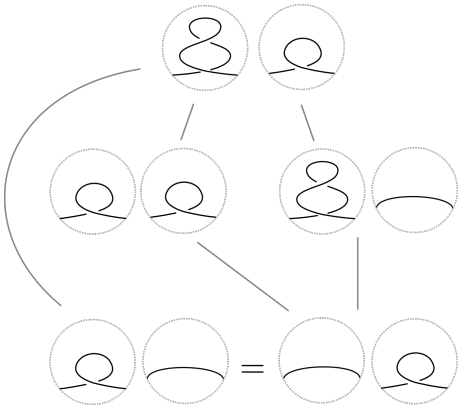

Figure 2.28: A non-normal triangle fitting in case $3a$). Notice that the diagrams with the lowest crossing number (on the bottom) are identified and present at least a curl.

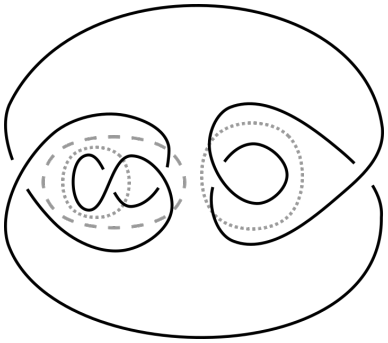

Figure 2.29: A triangle for a periodic (un)knot, fitting in case $3a$). Dotted circles enclose the Ω_1^-s, and the dashed one the Ω_T^-. This specific example was pointed out by M. Marengon.

It is convenient to divide the investigation on triangles fitting in case 3) of Figure 2.12 in two subcases (denoted by 3a and 3b respectively), differing in whether or not one of the Ω_1^- moves happens on the top part of the tentacle undone by the Ω_T. If it does, then we are in the situation described in Figure 2.28, and we notice that the diagram with the lowest crossing number contains at least one 1-region; an example of a non-normal triangle fitting in case $3a$) is shown in Figure 2.29.

Finally, if both the curls undone by the Ω_1 moves are not the top part of the tentacle, then the diagrams appear as in Figure 2.30.

Again, we can conclude that the diagram with the lowest crossing number presents a tentacle configuration. We show an example of a non-normal triangle

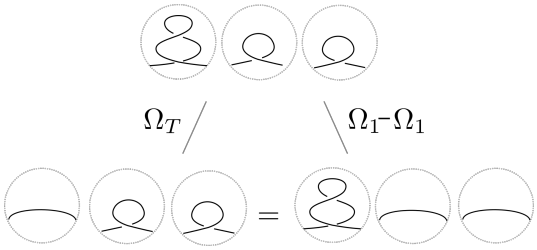

Figure 2.30: A non-normal triangle fitting in case 3*b*). Notice that the diagrams with the lowest crossing number (on the bottom) are identified, and present at least a tentacle configuration. See also Figure 2.31 for an explicit example.

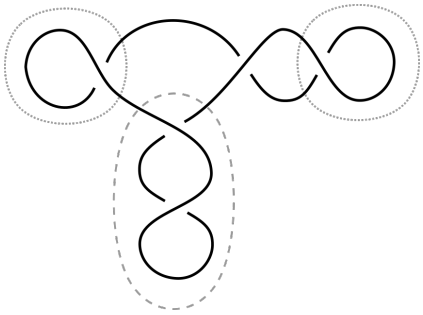

Figure 2.31: A triangle for a periodic (un)knot, fitting in case 3*b*).

fitting in case 3*b*) in Figure 2.31. In all the non-normal cases above two diagrams are identified, and this implies either the existence of a periodicity for the knot, or that the moves happen on the same edge, involving adjacent curls or tentacles.

Lemma 2.2.7. *Given any knot diagram D, there exists an arc on D such that performing either a Ω_1^+ or a Ω_T^+ belonging to a normal triangle, the resulting diagrams are non-periodic. Moreover, if we perform another Ω_T^+ on the top of the tentacle created, the diagram obtained and all of the diagrams in its radius* 1 *ball are non-periodic.*

Proof. This follows from the fact that the height h tentacle configurations are permuted by any symmetry of the diagram, so if there's only one the diagram can not be periodic. So, just take any diagram D; if $p_1(D) = 0$, then performing any Ω_1^+ or the Ω_T^+ it is paired with will produce a non-periodic diagram. If instead D contains at least one curl, choose the one which appears on the top of the highest tentacle, and perform there the Ω_1^+/Ω_T^+ pair (with appropriate signs). Since

the new diagram will have only one tentacle of maximal height we can conclude. Finally, if we further increase the length of the tentacle, we are sure that we are at least at distance 2 from any periodic diagram. □

Unlike the Gordian graph, the Reidemeister graphs are locally finite, even though the valence is not uniformly bounded (Remark 2.2.9). The first invariant we can extract from them is in some sense a measure of the minimal complexity of the diagrams of K:

Definition 2.2.8. *Let $v(D)$ denote the valence of the vertex D. The* diagram complexity *of a knot K is*

$$\delta(K) = \min_{D \in \mathcal{D}(K)} v(D).$$

If $v(D) = \delta(K)$ we say that D is a minimum. *We also define $\#\delta(K)$ as the number of minima of $\mathcal{G}(K)$; if a knot type K is such that $\#\delta(K) = 1$, we call K* simple. *Both δ and $\#\delta$ are $\mathbb{N}$-valued knot invariants. There is of course an identical definition for $\mathcal{G}_P(K)$; we denote by δ_P and $\#\delta_P$ the corresponding invariants.*

Remark 2.2.9. We will postpone the proof that $\#\delta(K)$ is in fact well defined to Lemma 2.2.13. Note that the diagram complexity is not a function of the crossing number, as one might naively think. In Remark 2.2.22 we are going to provide some examples of this phenomenon. It is however true that, for a fixed knot type K, the valence becomes arbitrarily high as the crossing number of the diagrams representing K increases.

Given a non-periodic diagram $D \in \mathcal{D}(K)$, one can enumerate the possible Reidemeister moves on D, in order to compute

$$v(D) = \#\Omega_1^{\pm}(D) + \#\Omega_T^{\pm}(D) + \#\Omega_2^{\pm}(D) + \#\Omega_3(D).$$

We start by counting the possible number of Ω_1^+ and Ω_T^+. For each arc in D we can perform 4 Ω_1^+ moves, as shown in Figure 2.32, and the same holds for Ω_T^+.

When working with $\mathcal{G}_P(K)$, so diagrams on the plane, we must put a bit of care in counting Ω_2^+ moves, since the number of such possible moves depends on whether we are in the *external* polygon or not. If a polygon $P \in D^2 \setminus D$ has k

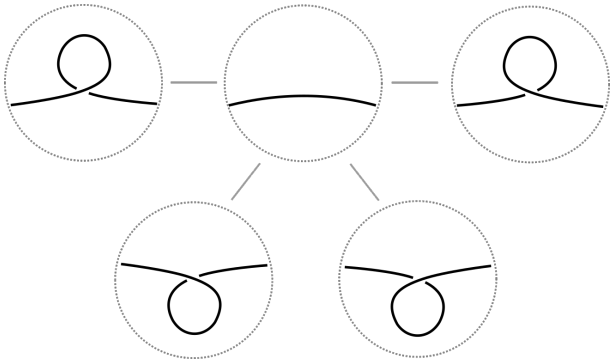

Figure 2.32: The possible Ω_1^+ moves that can be performed on each arc.

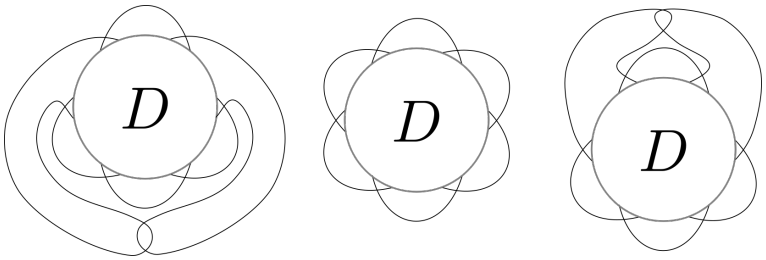

Figure 2.33: The two non equivalent possibilities for a Ω_2 move in the external zone.

edges, there are $2\binom{k}{2} = k(k-1)$ possible[9] Ω_2^+ moves we can perform in it (the factor of 2 comes from the two possible choices of which arc passes over the other). In the external zone however we need to double the previous quantity, since there are two cases to be considered, as shown in Figure 2.33. So if we denote by k_{ext} the number of edges of the external zone, we have an extra contribution of $k_{ext}(k_{ext}-1)$. This extra term does not appear when working with diagrams on the 2-sphere, as there is no preferential polygon.

Adding all up, we end with this rather unpleasant equation for the valence of a non-periodic planar diagram. Note that multi-edges do not create issues in the sum, as they are counted separately.

[9]In the present discussion we find it convenient to blur a bit the distinction between Ω_2 and Ω_T, since we are only interested in the total count.

$$v(D) = 8\alpha(D) + \sum_{k\geq 2} p_k(D)k(k-1) + k_{ext}(k_{ext}-1) + \\ +\#\Omega_3(D) + \#\Omega_2^-(D) + \#\Omega_T^-(D) + \#\Omega_1^-(D) \tag{2.2}$$

It follows from Equation (2.2) that the valence of any diagram is bounded from above by quantities depending only on the knot projection:

$$v(D) \leq 8\alpha(D) + p_1(D) + p_2(D) + p_3(D) + 2\sum_{k\geq 2} p_k(D)k(k-1). \tag{2.3}$$

Equation (2.3) is obtained by giving an upper bound on the possible Ω^- and Ω_3 moves in terms of the number of edges of the regions interested by the moves (*i.e.* on the number of 1, 2 and 3-regions for Ω_1^-, $\Omega_2^- + \Omega_T^-$ and Ω_3 moves respectively).

Looking at Equation (2.2) we can obtain a lower bound as well, which allows to say that the valence grows at least linearly with the crossing number. Define $P(D)$, the maximal period of a non-trivial diagram D, as the maximal order of a finite group acting on the sphere (or the plane), preserving the diagram setwise[10]. Recall that if K is not the unknot, then K admits finitely many orders of periodicity (see [41, Thm. 3]).

Lemma 2.2.10. *If D is a non-trivial knot diagram with periodicity $P(D)$ (where $P(D) = 1$ if D is non-periodic) then*

$$v(D) \geq \frac{8\alpha(D)}{P(D)}. \tag{2.4}$$

This follows easily by observing that each fundamental domain for the periodic action must contain at least one arc.

Of course if D is non-periodic, the lower bound

$$v(D) \geq 8\alpha(D) + \sum_{k\geq 2} p_k(D)k(k-1) + k_{ext}(k_{ext}-1) \tag{2.5}$$

holds as well.

Proposition 2.2.11. *The minimal valence δ detects the unknot $\bigcirc$.*

[10]We need to exclude the trivial diagram of the unknot to ensure that $P(D)$ is in fact finite.

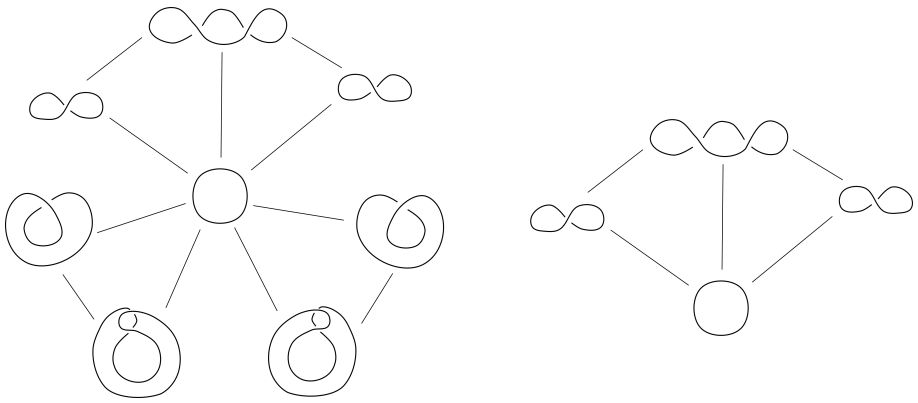

Figure 2.34: The ball $S(\bigcirc)$ in the planar (left) and S^2 graphs (right).

Proof. $\delta(\bigcirc) = 3$, as shown in Figure 2.34, while if $K \neq \bigcirc$, then for every diagram D representing K we have $v(D) \geq 4$, since each fundamental domain for a periodic action must contain at least one arc (as in the proof of Lemma 2.2.10), and for every arc there are at least 4 (two Ω_T^+ and two Ω_1^+) possible moves. □

Lemma 2.2.12. *For each knot K, the number of vertices in $\mathcal{G}_P(K)$ or $\mathcal{G}(K)$ whose valence is bounded by a constant is finite.*

Proof. This follows immediately from the fact that there are only finitely many diagrams of a knot with crossing number bounded by a constant, finitely many periods for each knot, and by Equation (2.4) the valence is bounded from below by a linear function in $cr(D)$. □

In particular, choosing $\delta(K)$ as the constant in the previous Lemma, we get:

Corollary 2.2.13. *$\#\delta(K)$ is well defined.*

Following [65], we call a diagram $D \in \mathcal{D}(K)$ *hard* if $\#\Omega_1^-(D) = \#\Omega_2^-(D) = \#\Omega_T^-(D) = \#\Omega_3(D) = 0$.

We can refine (2.2) for hard diagrams:

Corollary 2.2.14. *If D is a hard diagram of a non-periodic knot K, then*

$$v_S(D) = 8\alpha(D) + \sum_{k>1} k(k-1)p_k(D).$$

The analogous result for $\mathcal{G}_P(K)$ is obtained by adding $k_{ext}(k_{ext} - 1)$.

In [65] Kauffman and Lambropoulou exhibit an infinite family of hard unknots. Using their result, it is not difficult to argue that every knot admits (infinitely many) hard diagrams. Take any diagram $D \in \mathcal{D}(K)$, and choose a (non-trivial) hard diagram U of the unknot. If D is not hard, choose a Ω_i^- or Ω_3 move and perform a diagram connected sum with U to "kill it" as in Figure 2.35. Generally,

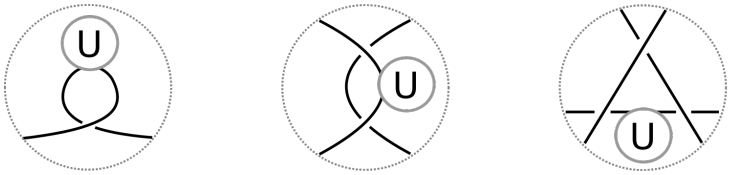

Figure 2.35: How to kill Reidemeister moves.

hard diagrams of non-periodic knots are interesting from the $\mathcal{R}$-graphs viewpoint, since for them the valence is completely determined by the knot projection, rather than by the diagram. In particular this implies that given a hard diagram, it will have minimal valence among all the diagrams obtained from it by changing any number of crossings[11].

Remark 2.2.15. It is possible to compute the valence of the two trefoil knots of Figure 1.5 in $\mathcal{G}_P(3_1)$. Taking into account the periodicities of the two diagrams (it is of order 3 for the first and 2 for the other), one gets that (as planar diagrams) the first has valence 24 and the second 32, so they are set apart in $\mathcal{G}_P(3_1)$. The valence in $\mathcal{G}(3_1)$ instead is 12.

In order to facilitate the proof of Theorem 2.0.1, understanding how the valence of a diagram can change under the various Reidemeister moves is crucial.

It is of course impossible to *a priori* compute the difference of the valence between two vertices at distance 1, since this value depends on the crossings and specific configurations in the diagrams involved. It is however possible to pinpoint a quite good bound by accounting for the number of edges of the regions interested by the Reidemeister move.

[11] This is no longer true if one of the diagrams obtained by changing some crossings in a hard one is periodic.

This last task is a quite tedious exercise; in the following we denote by[12] $\varepsilon_{j,i}$ and $\varepsilon_{j,3}$ the difference in the number of Reidemeister moves of type Ω_i^- and Ω_3 respectively that can be performed on two diagrams differing by a single Reidemeister move Ω_j^+, with $i, j \in \{1, T, 2\}$.
If $D' = \Omega_1^+(D)$, then:

- $\varepsilon_{1,1} = \#\Omega_1^-(D') - \#\Omega_1^-(D) \in \{0, 1\}$;
- $\varepsilon_{1,T} + \varepsilon_{1,2} = \big(\#\Omega_T^-(D') - \#\Omega_T^-(D)\big) + \big(\#\Omega_2^-(D') - \#\Omega_2^-(D)\big) \in \{-2, 0, 1\}$[13];
- $\varepsilon_{1,3} = \#\Omega_3^-(D') - \#\Omega_3^-(D) \in \{-4, \dots, 4\}$.

We denote the sum of the ε contributions in each case as $\sum_i \varepsilon_{1,i}$; these count the part of the valence of a diagram that is not completely determined by the knot projection. In particular, we have that

$$-6 \leq \sum_{i \in \{1,2,T,3\}} \varepsilon_{1,i} \leq 6. \tag{2.6}$$

Proposition 2.2.16. *If K is a non-periodic knot and $D' \in \mathcal{D}(K)$ is obtained from D by adding a curl (*i.e. *performing a Ω_1^+ move, as in the upper part of Figure 2.36) then $v(D') > v(D)$. More precisely, if the move is* internal*, that is the two zones involved are not the external one, then:*

$$v(D') = v(D) + 8 + 4a + 2b + \sum_j \varepsilon_{1,j}. \tag{2.7}$$

If the zone with a edges is external:

$$v(D') = v(D) + 2 + 8a + 2b + \sum_j \varepsilon_{1,j}. \tag{2.8}$$

And finally if the zone with b edges is external:

$$v(D') = v(D) + 6 + 4a + 4b + \sum_j \varepsilon_{1,j}. \tag{2.9}$$

Moreover, we have $\sum_j \varepsilon_{1,j} \in \{-6, \dots, 6\}$. Thus, performing an Ω_1^+ move always increases the valence.

[12] We suppress the dependency of the $\varepsilon_{j,i}$ from the diagrams in the notation for aesthetic reasons.

[13] Here we consider the sum $\varepsilon_{1,T} + \varepsilon_{1,2}$ since performing an Ω_1^+ move at the top of a pre-existing tentacle may decrease the number of Ω_T moves, changing them in Ω_2 moves.

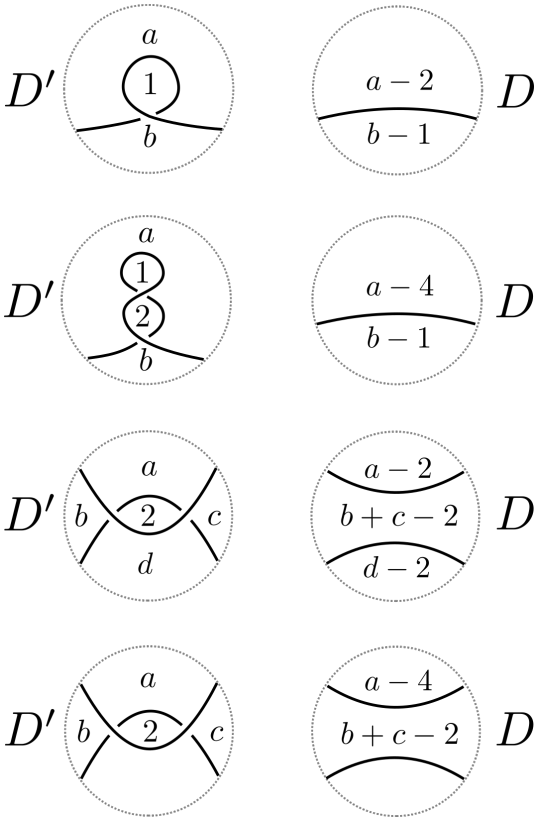

Figure 2.36: The four possible configurations considered in Propositions 2.2.16 to 2.2.19.

Proof. After performing a Ω_1^+ move, the number of arcs in D' increases by 2, that is $\alpha(D') = \alpha(D)+2$. Moreover, assuming that $a, b, a-2, b-1$ are pairwise distinct, we have the following changes in the p_ks:

- $p_a(D') = p_a(D) + 1$
- $p_{a-2}(D') = p_{a-2}(D) - 1$
- $p_b(D') = p_b(D) + 1$
- $p_{b-1}(D') = p_{b-1}(D) - 1$

Adding all up, and keeping in mind Equation (2.2), we obtain

$$v(D') - v(D) = 8 \cdot 2 + a(a-1) - (a-2)(a-3)+$$

$$+b(b-1)-(b-1)(b-2)+\sum_j \varepsilon_{1,j}.$$

That is precisely

$$v(D') = v(D) + 8 + 4a + 2b + \sum_j \varepsilon_{1,j}.$$

Notice that even if $a, b, a-2, b-1$ are not pairwise distinct, the same computation holds. All other Ω_j^- moves (that do not depend solely on the knot projection) add up to $\sum_j \varepsilon_{1,j}$.
To obtain Equations (2.8) and (2.9) it is enough to add the contribution of the external region, which is $a(a-1)-(a-2)(a-3) = 4a-6$ in the first case, and $b(b-1)-(b-1)(b-2) = 2b-2$ in the second. □

The proof is identical in the other cases considered below, and we are going to omit it.

Proposition 2.2.17. *Let $D, D' \in \mathcal{D}(K)$ be two non-periodic diagrams differing by a Ω_T creating a tentacle of length 1 as in the upper-middle part of Figure 2.36. Then, if the zones involved are not external:*

$$v(D') = v(D) + 12 + 8a + 2b + \sum_j \varepsilon_{T,j}. \tag{2.10}$$

If the zone with a edges is external:

$$v(D') = v(D) - 8 + 16a + 2b + \sum_j \varepsilon_{T,j}. \tag{2.11}$$

And finally if the zone with b edges is external:

$$v(D') = v(D) + 10 + 8a + 4b + \sum_j \varepsilon_{T,j}. \tag{2.12}$$

Proposition 2.2.18. *If two non-periodic diagrams $D, D' \in \mathcal{D}(K)$ differ by a Ω_2 move in which the regions with a and d edges do not coincide, as in the middle part of Figure 2.36, then if the move is internal:*

$$v(D') = v(D) + 16 + 4(a+b+c+d) - 2bc + \sum_j \varepsilon_{2,j}. \tag{2.13}$$

Proposition 2.2.19. *If two non-periodic diagrams $D, D' \in \mathcal{D}(K)$ differ by a Ω_2 move in which the regions with a and d edges coincide, as in the lower part of Figure 2.36, then if the move is internal:*

$$v(D') = v(D) + 8 + 4(2a + b + c) - 2bc + \sum_j \varepsilon_{2,j}. \tag{2.14}$$

Remark 2.2.20. A Ω_T creating a tentacle of length greater than 1 is a special case of 2.2.19 in which $c = 2$. Thus, in this case we obtain

$$v(D') = v(D) + 8 + 4(2a + b + 2) - 4b + \sum_j \varepsilon_i =$$

$$= v(D) + 16 + 8a + \sum_j \varepsilon_{T,j}.$$

It is worth to remark that, when dealing with $\mathcal{G}(K)$, the change of the valence is determined by Equations (2.7), (2.10) and (2.13) in the respective cases.

Remark 2.2.21. We will find useful to divide the valence of every vertex in two parts, namely the positive valence $v^+(D)$ and the negative valence $v^-(D)$. The positive valence is defined as the number of edges emanating from D which correspond to Ω^+_* moves, where $* \in \{1, 2, T\}$. Note that $v^+(D)$ only depends on the projection of D. If we wish to consider only the positive valence, Equations (2.7), (2.10), (2.13) and (2.14) can be rewritten as:

$$v^+(D') = v^+(D) + 8 + 4a + 2b \tag{2.15}$$

$$v^+(D') = v^+(D) + 12 + 8a + 2b \tag{2.16}$$

$$v^+(D') = v^+(D) + 16 + 4(a + b + c + d) - 2bc \tag{2.17}$$

$$v^+(D') = v^+(D) + 8 + 4(2a + b + c) - 2bc \tag{2.18}$$

Remark 2.2.22. Proposition 2.2.17 suggests how to produce examples of knots in which the minimal complexity is not realised by a diagram minimising the crossing number. From Equation (2.13) it is apparent that if b and/or c are sufficiently big, then the diagram D' (with higher crossing number than D) obtained by performing a Ω^+_2 move, will have a lower valence. An easy example of this phenomenon is given in Figure 2.37. This is the twist knot with 17 crossings; note that the

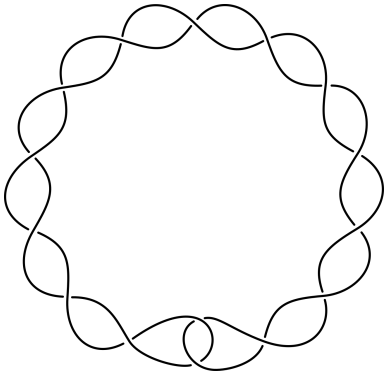

Figure 2.37: By performing a Ω_2^+ move in the central (or external) region, we obtain a diagram with lower valence.

example shown is also alternating, reduced and non-periodic. When the internal (and external) region has more than 12 faces, performing a Ω_2^+ move decreases the valence, according to Equation (2.13) (with $a = d = 4$ and $b = c = 8$).

In particular, any knot in which all diagrams realizing the crossing number have many regions with a sufficiently high number of edges provides an example where the minimal valence is not realised in the diagram with minimal crossing number.

We prove here some facts that are going to be useful in the next sections. First of all we show that the graph can *distinguish* between the different Reidemeister moves. This means that by looking at a neighbourhood of an edge of $\mathcal{G}(K)$, we can tell which Reidemeister move it represents; furthermore this will provide a way to read the crossing number of a diagram D from the combinatorial structure of $S(D)$.

Theorem 2.2.23. *The S^2-graph distinguishes the Reidemeister moves, and detects the crossing number of a diagram. More precisely, the information contained in the (unlabelled) S^2-graph is sufficient to recover the labelled graph (*i.e. *the graph where each edge is labelled according to the Reidemeister move it represents) and consequently to compute the crossing number of the diagram corresponding to each vertex.*

Proof. In the interest of clarity we are going to start by examining the non-periodic case. Fix a diagram $D \in \mathcal{D}(K)$ for a non-periodic knot K. The combinatorics

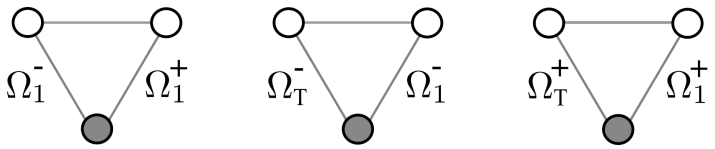

Figure 2.38: The grey dots represent the diagram D we start from.

of $S(D)$ will allow us to distinguish the various moves; recall that we are not considering the case of the unknot (Remark 2.2.3).

Since by Theorem 2.2.2 all Ω_1 moves are paired with at least one Ω_T move in a triangle, it is easy to argue that the graph can tell apart the two sets of moves $M_1 = \{\Omega_1^\pm, \Omega_T^\pm\}$ and $M_2 = \{\Omega_2^\pm, \Omega_3\}$.

To further separate the elements of M_1 we can thus restrict to triangles in $S(D)$. Choose an edge emanating from a vertex D, which is part of a triangle. There are 3 possibilities, shown in Figure 2.38.

From this, using the fact that an Ω_1^+ move always increases the valence (Proposition 2.2.16) and that every $\Omega_T^\pm$ is the result of two Ω_1^+, it is easy to argue that $\mathcal{G}(K)$ can tell apart the elements in M_1. Indeed, if only one of the two moves decreases the valence, then they are both Ω_1s, and the one which decreases it is the Ω_1^-. If both moves decrease the valence, then the one that decreases it most is the Ω_T^-, and the other is a Ω_1^-. Lastly, if both moves increase the valence, then the one that increases it most is a $\Omega_T^\pm$, and the other is a Ω_1^+.

Now, since the number of Ω_1^+ moves is a multiple of the arc number of the diagram (cf. Figure 2.32), the crossing number $cr(D)$ corresponds to $\frac{1}{8}\#\Omega_1^+(D)$. Hence, since we can distinguish and count such moves, we can read the crossing number of a diagram from $S(D)$.

Using this information we can tell apart the elements of M_2 as well and conclude: the only remaining moves are $\Omega_2^\pm$s and Ω_3s, all of which are not part of a triangle. These appear as edges connected only to the center of $S(D)$. We can distinguish between them by counting the crossing number of the vertices they connect D to; one then just needs to recall that Ω_3 moves do not increase it, while Ω_2 increase or decrease it by 2. Hence it follows that we can distinguish among Ω_2^+,Ω_2^- and Ω_3 moves as well.

In all the previous discussion, in order to determine $cr(D)$, we only used the fact that all diagrams in $S(D)$ were non-periodic; this fact will allow us to compute it in the periodic case as well.

If K is periodic we can not use directly the various equations relating the valence of two neighbouring vertices, since one could be periodic.

Instead of trying to directly detect from the structure of the graph whether a diagram is periodic, we can use Lemma 2.2.7 to bypass most complications. For every vertex D, define the generalized triangle number $n_{tr}(D) = \#\Omega_1^{\pm}(D) + \#\Omega_T^{\pm}(D)$. This quantity is computable from the graph, since by Theorem 2.2.2 it coincides with the number of edges emanating from D which are part of at least one triangle. By Lemma 2.2.7, at least two diagrams appearing in a triangle, reached by a Ω_1^+ and a Ω_T^+ respectively will be non-periodic, and we claim that such diagrams maximise n_{tr} among all the diagrams reached by edges starting from D that are part of at least one triangle. Let $a_h(D)$ denote the number of (maximal) height h-tentacles in D, and define

$$n(D) = p_1(D) + \sum_{h \geq 1} h a_h(D).$$

Note that $n(D)$ is equal to the sum $\Omega_1^-(D) + \Omega_T^-(D)$ when D is not periodic. Then, for the diagrams D'' and D' in Lemma 2.2.7, the following equalities hold:

$$n_{tr}(D'') = 16cr(D'') + n(D'') = 16(cr(D) + 2) + n(D) + 2$$

$$n_{tr}(D'_1) = 16cr(D') + n(D') = 16(cr(D) + 1) + n(D) + 1$$

This follows since we are performing the curls on the top of a tentacle (or on any arc, if there are no curls in D), and this fact ensures that the number of Ω_*^- moves is equal to $n(D) + 1$ when $* = 1$ and to $n(D) + 2$ when $* = T$. On the other hand, for any diagram D_T^+ and D_1^+ reached from D by a Ω_T^+ move and a Ω_1^+ respectively, the following inequalities hold:

$$n_{tr}(D_T^+) \leq 16(cr(D) + 2) + n(D) + 2$$

$$n_{tr}(D_1^+) \leq 16(cr(D) + 1) + n(D) + 1$$

The presence of periodicity in D_1^+ or D_T^+ can only decrease the value of n_{tr}, and

the same holds if the moves are not performed (with the appropriate sign) on the top of a pre-existing tentacle. In other words these moves maximise $\#\Omega_1^- + \#\Omega_T^-$. If we consider moves that decrease the crossing number, disregarding the possible periodicities, the numbers n_{tr} we obtain have no chance of being greater than $n_{tr}(D'')$. So, choose the diagrams in $S(D)$ maximising this quantity; they correspond to vertices reached by Ω_T^+ moves. Consider all the edges that form triangles with them: these have to correspond to diagrams reached by Ω_1^+ moves. Choose between them one maximising n_{tr}. Notice that D is non-periodic if and only if $n_{tr}(D) = n_{tr}(D') - 17$. Now, choose D''' in $S(D')$ forming a triangle with D'', with $S(D''')$ totally non-periodic[14], and such that it maximises n_{tr} in $S(D')$. We know that such a diagram exist by Lemma 2.2.7, and we can check the hypothesis on the non-periodicity of $S(D''')$ thanks to the above criteria. Then, we can recover $cr(D''')$, and obtain $cr(D)$ as $cr(D''') - 3$.

Hence, using the crossing number as in the non-periodic case, we can tell apart the various types of moves, and we are done. □

This last result will allow us to say *perform a $\Omega_i^\pm$ move on a diagram* in a way that is meaningful also at the level of the graph. In other words, we just proved that the $\mathcal{R}$-graphs intrinsically contain the same amount of information as the same graphs with edges decorated according to which $\Omega_i^\pm$ move we are performing.

By the previous result we know that the crossing number of a diagram can be read by looking at $S(D)$. Thus if a knot is non-periodic, taking the minimum of $\frac{1}{8}\#\Omega_1^+$ among all vertices of the corresponding Reidemeister graphs gives back $cr(K)$, the crossing number of the knot. For periodic knots, this procedure produces a slightly different invariant, which can be regarded as crossing number up to periodicities. More precisely define

$$\widehat{cr}(K) = \frac{1}{8} \min_{D \in \mathcal{D}(K)} \#\Omega_1^+(D).$$

$\widehat{cr}(K) = cr(K)$ if K is non-periodic, while in general $\widehat{cr}(K) \leq cr(D)$. As an example, we have $\widehat{cr}(3_1) = \frac{1}{2}$.

[14]We say that a diagram D is *totally non-periodic* if it is non-periodic and if $S(D)$ does not contain any periodic diagram.

Note that a similar consideration for the other kinds of moves does not yield useful invariants: it is possible to show that the minimal number of Ω_2^+ moves is simply related to the combinatorics of the number of regions in the complement of the diagram on D^2 or S^2, and the minimal number of Ω_2^- and Ω_3 moves one can perform within a knot type is always 0 (as can be seen by "killing" all the Ω_3 moves with a Ω_1 in the region with 3 edges, similarly to what was done in Figure 2.35). Nonetheless one might obtain some meaningful invariants by restricting diagrams not minimising the valence.

The knowledge of the crossing number from the graph also implies that we can use Coward and Lackenby's result [28] to give some upper bounds on the path distance between two diagrams.

2.3 Global properties

This section is devoted to the analysis of some global properties of the $\mathcal{R}$-graphs. We begin by proving that each $\mathcal{R}$-graph is not hyperbolic[15].

Proposition 2.3.1. *The $\mathcal{R}$-graphs are not hyperbolic.*

Proof. Choose a non-periodic diagram $D \in \mathcal{D}(K)$ not containing 1-regions, an arc on D, and a polygon P having this arc as a face. We can embed isometrically the rank 2 lattice graph as follows: to the pair $(a, b) \in \mathbb{Z}^2$ associate the configuration on the arc composed by a positive curls in the region P if $a > 0$, and in the other region touching the arc if $a < 0$; do the same for b, this time with negative crossings on the right of the previous ones. An example is shown in Figure 2.39. The fact that the embeddings are isometric follows *e.g.* from the analysis of the I_{lk} invariants of the diagrams: $I_{lk}(D_{a,b}) = I_{lk}(D) + aX_0 + bY_0$, where $D_{a,b}$ is the diagram corresponding to the element (a, b).

□

Proposition 2.3.2. *The Reidemeister graphs $\mathcal{G}_P(K)$ and $\mathcal{G}(K)$ are not planar.*

[15] For a definition of *hyperbolic metric space* see *e.g.* [121], Section 2.

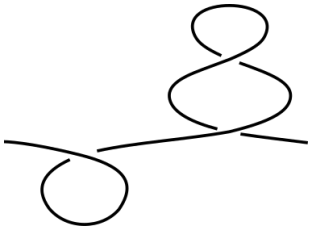

Figure 2.39: This configuration represents $(-1, 2) \in \mathbb{Z}^2$.

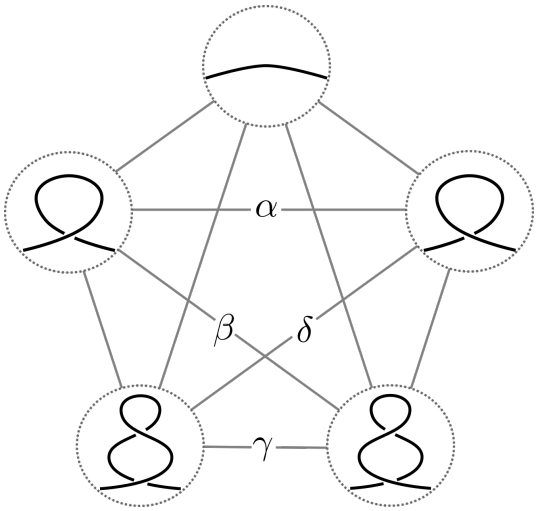

Figure 2.40: A local embedding of K_5 as a minor of any $\mathcal{G}(K)$.

Proof. We are going to prove that for every knot K we can find a K_5 minor[16] contained in each $\mathcal{R}$-graph of K. This is achieved by considering the local construction shown in Figure 2.40. The edges denoted with a Greek letter are length 2 paths; as shown in Figure 2.41, these can be obtained by putting alongside the two moves, and then resolving either one.

□

[16] As is customary, K_n denotes the complete graph on n vertices.

Figure 2.41: The path corresponding to the β edge in Figure 2.40.

In graph theory, it is customary to consider *coarse* properties of a (infinite and locally finite) graph. One way to do this is to study the quasi-isometry class of the graph, often through related invariants.

A *ray* of a locally finite graph G, is a semi-infinite simple path in G; two rays $r_1, r_2 \subset G$ are regarded as equivalent if there exists a third ray r_3, containing infinitely many vertices of both r_1 and r_2.
An *end* is an equivalence class of rays, and it is called *thick* if it contains infinitely many pairwise disjoint rays.

Proposition 2.3.3. *Each S^2-Reidemeister graph has only one thick end.*

Proof. It is immediate to show (*e.g.* using paths as those in Figure 2.42 or tentacle configurations) that there are infinitely many disjoint rays in $\mathcal{G}_P(K)$ and $\mathcal{G}(K)$ for each choice of $K \in \mathcal{K}$. To show that there is only one end, we will prove that removing any ball with arbitrary radius does not disconnect the graphs into two pieces, each containing infinitely many vertices. This in turn would immediately imply that there is only one equivalence class of rays in the graph.
Consider a diagram $D \in \mathcal{D}(K)$ for a knot K, and the radius R ball $S_R(D)$ in $\mathcal{G}(K)$ (or equivalently in $\mathcal{G}_P(K)$). Call H the maximal height among the tentacles of the diagrams contained in $S_R(D)$, and take any two diagrams $D_0, D_1 \in \mathcal{D}(K)$ which do not belong to $S_{R+H+1}(D)$; we need to find a path in $\mathcal{G}(K) \setminus S_R(D)$ connecting D_0 to D_1. Choose an arc on D_0 and on D_1, and create on each a tentacle of height greater than H. These two new diagrams D_0' and D_1' can be connected through moves that avoid the newly created tentacles[17], and this path γ from D_0' to D_1' will not intersect $S_R(D)$, thanks to the hypothesis on H. Attaching to the ends of γ the two paths $\widehat{\gamma}_i$ from D_i to D_i', induced by the creation of the tentacles, gives the desired path from D_0 to D_1. Note that the hypothesis on the height of the tentacle allow us to say that the paths $\widehat{\gamma}_i$ do not intersect $S_R(D)$, and $S_{R+H+1}(D) \setminus S_R(D)$ contains only finitely many vertices. □

The S^2-Reidemeister graphs contain only one end, but infinitely many disjoint rays, hence by Halin's grid Theorem [51], each must contain a subdivision of the planar hexagonal tiling.

[17] Remember that we are working on S^2.

Remark 2.3.4. One might find reasonable to assume that the graphs $\mathcal{G}_P(K)$ and $\mathcal{G}(K)$ are quasi-isometric; it is however easy to see that the *natural* map[18] $\mathcal{G}_P(K) \hookrightarrow \mathcal{G}(K)$ between the two graphs fails to be a quasi-isometry. This can be seen from Figure 2.33: the two diagrams on the left and right can have arbitrarily large distance in $\mathcal{G}_P(K)$, but are identified in $\mathcal{G}(K)$.

These graphs also exhibit a fractal behaviour, which can be observed *e.g.* by considering sequences of Ω_1 moves as in Figure 2.42. The corresponding subgraph

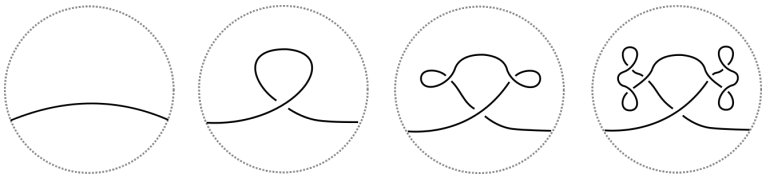

Figure 2.42: The fractal behaviour of $\mathcal{G}(K)$.

can be embedded (infinitely many times) in each $\mathcal{R}$-graph for any knot K.

The $\mathcal{R}$-graphs can be filtered in several ways; the easiest one is to consider the filtration induced by the distance from the vertices with minimal valence.

Given a knot K, denote by $\mathcal{F}_m(K)$ the subgraph spanned by those vertices whose distance from the minimal diagrams of K is $\leq m$, and denote by $\#\mathcal{F}_m(K)$ the number of vertices it contains.

We can extract some numerical invariants from this filtration on $\mathcal{G}(K)$:

Definition 2.3.5. *Define*

$$f_K : \mathbb{N} \longrightarrow \mathbb{N}$$

$$f_K(m) = \#\mathcal{F}_m(K),$$

and

$$M(K) = \min_{m \geq \delta(K)} \{\pi_0(\mathcal{F}_m(K)) = \mathbb{Z}\}.$$

In other words, $M(K)$ measures the minimal distance between the diagrams of minimal complexity in $\mathcal{G}(K)$. In particular, $M(K) = 0$ if and only if a knot type is simple.

[18] Where we map a planar diagram D to its equivalence class in $\mathcal{G}(K)$.

Recalling the proof of Lemma 2.2.12, we can also define another filtration on $\mathcal{G}(K)$:

Definition 2.3.6. *Let $\widetilde{\mathcal{F}}_K$ be the filtration of $\mathcal{G}(K)$ whose m-level consists of the vertices of $\mathcal{G}(K)$ with valence less or equal to m. Let also*

$$g_K : \mathbb{N} \longrightarrow \mathbb{N}$$

be defined as the associated counting function

$$g_K(m) = \#\{D \in \mathcal{G}(K) \mid v(D) \leq m\}.$$

Clearly $g_K(m) = 0 \; \forall m < \delta(K)$, and $g_K(\delta(K)) = \#\delta(K)$.

Both these filtrations $\mathcal{F}$ and $\widetilde{\mathcal{F}}$, together with the associated integer valued counting functions f_K and g_K are knot invariants, and it is not hard to show that they both distinguish the unknot. Moreover one can consider the homology groups of the various level sets and obtain yet other knot invariants.

In [91] Miyazawa computes the homology groups of the *Reidemeister complex*, which he denotes by $M(K : P_5, 1)$, in the case of oriented diagrams with a minimal generating set of Reidemeister moves. Along these lines we can define a slightly different version of Reidemeister complex, denoted by $\mathcal{CG}(K)$ and defined as follows: an oriented n-simplex $\Delta_n = \langle D_0, \ldots, D_n \rangle$ is given by a string of $n+1$ distinct diagrams such that[19] $d(D_i, D_j) = 1 - \delta_{i,j}$, considered up to even permutations of the indices.

Define $C_n(\mathcal{CG}(K))$ as the free abelian group generated by n-simplices, with the obvious boundary operator induced by simplicial homology:

$$\partial(\langle D_0, \ldots, D_n \rangle) = \sum_{i=0}^{n} (-1)^i \langle D_0, \ldots, \widehat{D_j}, \ldots, D_n \rangle. \tag{2.19}$$

From this perspective, $\mathcal{G}(K)$ is the 1-skeleton of $\mathcal{CG}(K)$. Miyazawa proved that $H_0(M(K : P_5, 1); \mathbb{Z}) = \mathbb{Z}$ (which follows from Reidemeister's Theorem), and that $H_n(M(K : P_5, 1); \mathbb{Z}) = 0$ for every $n \geq 2$ and $K \in \mathcal{K}$.
Our situation is slightly different; with the methods developed in Section 2.1 we can easily establish the triviality of $H_n(\mathcal{CG}(K); \mathbb{Z})$ for $n \geq 3$:

[19] Here $\delta_{i,j}$ denotes Kronecker's delta function, and d is the path distance.

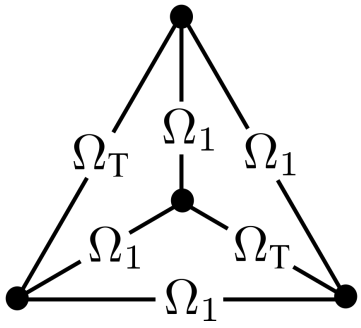

Figure 2.43: The only tetrahedron with compatible faces. There is no way of coherently orienting the signs on the edges of its faces.

Proposition 2.3.7. *For any knot K we have $H_n(\mathcal{CG}(K);\mathbb{Z}) = 0$ for $n \geq 3$ (in both the planar and S^2 case).*

Proof. Assume there exists a tetrahedron Δ_3 in $\mathcal{CG}(K)$; then it follows from Theorem 2.2.2 that all faces have to be made up triples $\Omega_T^{\pm}$-$\Omega_1^{\mp}$-$\Omega_1^{\mp}$. Up to symmetries, there is only one possibility to be considered, shown in Figure 2.43. However this can be excluded as well, by taking into account the signs of the moves composing the tetrahedron. In particular this shows that there are no simplices of dimension $n \geq 3$, hence all the corresponding homology groups vanish. □

In particular it follows that $\mathcal{CG}(K)$ is just $\mathcal{G}(K)$ with all triangles capped by 2-simplices. It is not hard to prove that $H_1(\mathcal{CG}(K);\mathbb{Z})$ contains an infinitely generated free abelian group, as any pair of distant Ω_3-Ω_2 moves does not bound any union of 2-simplices.

2.4 Completeness of the S^2-graph invariant

This section is devoted to the proof of Theorem 2.0.1 (recalled below). The proof will rely solely on results from Section 2.2, and exploits rather large portions of the graph.

Theorem. *The S^2-Reidemeister graph is a complete knot invariant up to mirroring. That is $\mathcal{G}(K) \equiv \mathcal{G}(K')$ iff $K' = K$ or K_{mir}.*

We will prove the Theorem by breaking it down in smaller parts, which are the content of the following Propositions.

Suppose we have a knot $K \in \mathcal{K}$, and that $D \in \mathcal{D}(K)$ is any diagram. Write $P(D) = (p_1(D), \dots, p_m(D))$ where m is the greatest coefficient with a non-zero entry (or equivalently the maximal number of sides among the regions in the complement of D in S^2).

Proposition 2.4.1. *The S^2-graph of a knot determines $P(D)$ for each vertex D such that all diagrams in $S(D)$ are non-periodic and $p_1(D) = 0$.*

Proof. Thanks to Lemma 2.2.5 we know that if a diagram D does not contain any curls, then all the triangles in $S(D)$ which admit D as the vertex with lower crossing number are normal. Moreover, since there are $8cr(D)$ Ω_1^+ moves and Ω_T^+ moves, we can conclude that in $S(D)$ there are exactly $8cr(D)$ triangles. For each Ω_1^+ move, choose the corresponding Ω_T^+ move; call D' and D'' respectively the diagrams obtained by performing these Ω_1^+ and Ω_T^+ moves on D. By Equations (2.15) and (2.16), the difference of the positive valences is

$$v^+(D'') - v^+(D') = 4a + 20,$$

where a is the number of edges of the region in which the tentacle and the curl will appear.

If we do the same for all possible Ω_1^+ moves applicable to D, we get a set of numbers $\{n_i'\}_{i \in \{0,\dots,\#\Omega_1^+(D)\}}$; define a new set $\{n_i\}_{i \in \{0,\dots,\#\Omega_1^+(D)\}}$, where $n_i = \frac{n_i' - 20}{4}$. Each region with a sides contributes to this new list with exactly[20] $2a$ entries equal to a. It is thus immediate to show that we can compute each $p_a(D)$ from $S(D)$. □

However the knowledge of $P(D)$ on a subset of vertices does not immediately guarantee the completeness of $\mathcal{G}(K)$. A priori there might be two distinct knots (up to mirroring), whose diagrams have the same number and types of Reidemeister moves, and such that their complement has the same number of regions. We first need to detect the structure of D as a 4-valent graph on S^2.

[20] Corresponding to the two possible Ω_1^+ moves performed with the curl contained in the region on one of its edges.

Proposition 2.4.2. *The S^2-graph recognises the projections of the knot corresponding to diagrams without* 1*-regions.*

Proof. Let us deal only with non-periodic knots for the moment, and come back to the periodic case afterwards.

Choose a vertex $D \in \mathcal{D}(K)$ with $p_1(D) = 0$. This is possible by Theorem 2.2.23, since the condition $p_1(D) = 0$ is equivalent to the absence of Ω_1^- moves emanating from D.

To obtain the structure of D as a graph, we need to be able to tell which regions are adjacent to one another in S^2, or in other words, we want to determine the dual graph of the projection.

We need to look for this information outside of $S(D)$; begin by assuming for the moment that D only has one region R with a certain number k of edges (that is, $p_k(D) = 1$), and k is such that there are no regions with $k \pm l$ sides, for any $l \leq L$ where L is a suitably big integer.

To determine the number of edges of the regions adjacent to R, perform a Ω_1^+ move on one edge of[21] R, so that the curl is contained in the interior of R. We can then compute the number of edges of the other region involved in the move as follows. The Ω_1^+ move is associated to a unique Ω_T^+ move, connecting D with a diagram D'' with which they form a triangle. By counting the difference of the positive valences between D' and D'' and by using Equations (2.15) and (2.16) we can compute the number of edges of R. Once we have that, the difference in the positive valence between D and D' gives us the number of edges of the other region involved. Moreover, note that knowing the number of edges in these two regions is enough to compute $P(D')$ from $P(D)$.

Repeating for all edges[22] in R we get the number of sides of each region which shares an edge with R.

From this last paragraph it follows that if we could find a diagram of K such that, with the exception of regions with one side, all the regions have a different

[21] This is in fact well defined on the graph, since the valence of the diagrams obtained in this fashion will be different from any other obtainable by making a Ω_1^+ anywhere else.

[22] Thanks to the hypothesis on R, we can recognise from the graph all the Ω_1^+ which create a curl in R.

and sufficiently spaced number of sides, then we could infer how they are globally *patched together* to form the corresponding 4-valent graph.

There is an easy way to achieve such a configuration in a controlled way. Start with a diagram D with $p_1(D) = 0$, and perform a Ω_1^+ move; again by the previous line of thought[23] we can tell that the move has been made with the curl contained in a region with a edges, which is adjacent to a region with b edges (as in the top of Figure 2.36).

Call D_1 the diagram obtained; we can recover $P(D_1)$ from $P(D)$, since we know the number of edges of the regions involved. There are only two possible choices to perform another Ω_1^+ move on this new diagram, in such a way that a Ω_1-multi-edge with valence 2 is created (given by performing an identical Ω_1^+ move on the left or right of the previous one). We can repeat this process $N_1 \gg 0$ times, obtaining a new diagram D_{N_1} with only one region with $a + 2N_1$ edges, and a region with $b + N_1$ edges, and such that there is only one multi-edge of order N_1, and exactly N_1 regions with 1 edge. Notice again that at each step we can recover $P(D_i)$ form $P(D_{i-1})$, since at each step we already know the number of edges of one region involved, and from the difference in the positive valence between D_{i-1} and D_i we can recover the second one. Eventually, we are able to compute $P(D_{N_1})$.

Now we have a more complicated diagram with two distinguished adjacent regions; we can then iterate the process: choose another edge of the first region[24] and make N_2 identical Ω_1s, with $N_1 \gg N_2 \gg 0$, in such a way that the curls are contained in the first region. Again, the first step is well defined, since such Ω_1^+ moves are the only ones that reach diagrams whose positive valence is increased by approximately $8N_1$ and do not increase the multiplicity of the multi-edge. From the second step on, the lack of periodicity (see Remark 2.2.6) ensures that making a curl close to the previous one is the only way to create a Ω_1^+-multi-edge. We still can recover $P(D_i)$ at every step.

We can fill up every edge of the region who once had a edges in the same fashion, and then move to another region. If at each step we start making curls on an edge

[23]Since triangles in $S(D)$ are normal, we can compute $P(D)$ by considering the difference in the valence between diagrams reached by triangles. Moreover, by considering one triangle at the time, and using the differences in the positive valences between D'' and D', and between D' and D, we can compute the number of edges involved in the corresponding Ω_1^+.

[24]Such that it is not on the top of the Ω_1^+s we just made.

bounding two regions whose number of edges is different enough[25], and if we keep track of the number of curls added, we are sure that the moves are well defined on the graph and that we can compute the n-tuples.

Notice that we need to choose the numbers N_i incredibly big and suitably distant, with $N_i \gg N_{i+1}$ in order to avoid confusion and ultimately get a diagram $\widetilde{D}$ such that it has region sequence of the form

$$P(\widetilde{D}) = (N, 0, \ldots, 0, 1, 0 \ldots, 0, 1, 0, \ldots),$$

where $N = \sum_i N_i$, and the minimal gap between two non-zero entries is $\gg 0$. Call a diagram with these properties *sparse*.

If the number of edges of the various regions are sufficiently spaced, then the previous claim applies[26], and we can explicitly see which regions are adjacent to one another. However thus far we have only determined the dual graph to the knot projection as an *abstract graph*; we need a bit more work to find out the specific planar embedding of the dual, in order to get back the projection of D_0. It is well known that an abstract finite planar graph G, together with a *rotational system*, uniquely determines an embedding of G and thus G^*, which is the diagram projection we want. A local rotational system for a vertex $v \in G$ is just a choice of a cyclic order for the edges emanating from v. A rotational system for G is such a choice for each $v \in G$, and it is said to be *coherent* if all the local systems are coherently oriented[27].

Choose a region R in the sparse diagram $\widetilde{D}$ and suppose that R is bounded by r edges. Choose a Ω_2^+ move that: creates a new bigon and a new 4-region, and increases the number of edges of two regions adjacent to R by 2; one example is shown in the top-right part of Figure 2.44. Notice that this choice is well defined on the graph thanks to the sparseness of $\widetilde{D}$. Indeed, we know the numbers r_i of edges of all the regions adjacent to R, and the Ω_2^+-moves of that kind are the

[25] This can be achieved by moving through adjacent regions. Notice that every time an edge is filled with N_i curls, we can "remember" the number of edges of the regions involved, and the number of curls made.

[26] Notice that even if the $p_1(\widetilde{D}) \neq 0$, the previous claim applies anyway, thanks to the sparseness of $\widetilde{D}$ and to the fact that the only 1-regions in $\widetilde{D}$ are the ones created by the construction.

[27] That is, given any two adjacent region in the (embedded) dual of G, the orientations induced on the common edges do not coincide, as in Figure 2.45.

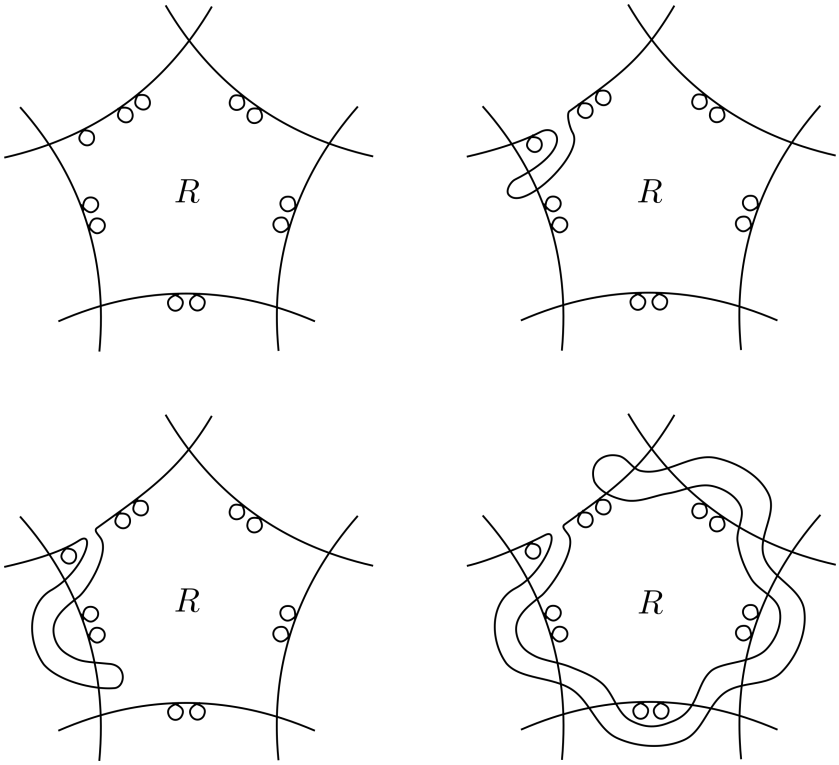

Figure 2.44: The choice of a local orientation system for the dual. By the previous construction the curls on the arcs can be on either side of an edge.

only ones that change the positive valence by a value of $56 + 4r_j + 4r_i - 4r$ (as in Equation (2.17)).

Then there are only two choices for a second Ω_2^+ move that: creates a new bigon adjacent to R leaving all the 1-regions on the edge on the left of the newly created bigon, eliminates one bigon adjacent to one of the two regions whose vertices increased in the previous move (let us call this region M), and replaces it with a quadrilateral. Again, thanks to the sparseness of $\widetilde{D}$ we can identify such a move on the graph, by considering the valence of the diagram reached. In fact, we can identify all the Ω_2 moves creating a new bigon adjacent to R and eliminating the other bigon, since these are the only ones changing the valence by [28] $40 + 4r - 2n_1r_j + 2(n_1 + 2)(n_1 - 2)$ (as in Equation (2.17)) where n_1 is the number of 1-regions on the left of the newly created bigon. In order to detect the

[28]The following expression is valid if the 1-regions are inside R. To consider the other case it is enough to change every n_1 in the expression with $2n_1$.

correct Ω_2 moves it is sufficient to choose the one minimising the coefficient of r_j in the previous expression[29]. These two options correspond to the possible choices of over/under passing for the first Ω_2^+ move in Figure 2.44. These moves might also decrease by a lot the number of edges of M (according to how many curls are contained on the edge between R and M). Now we can repeat the process following[30] Figure 2.44, until we get back to the first region that had its edges increased by 2 in the first move (but was not M). Keeping track of the various regions encountered during this process allows to reconstruct a local orientation system about the vertex corresponding to R in the dual graph. Since we know the numbers r_i of edges of all the regions adjacent to R, and thanks to the sparseness of the diagram, this construction works even if two distinct edges of R are shared with the same region.
Again, this sequence of Ω_2^+ is only well-defined up to a choice of over/under passing at each step, but this indeterminacy does not affect the result.

Finally, in order to get a proper orientation system for the dual, we need to be able to have a coherent way of orienting these local rotational systems we obtained. The process is shown in Figure 2.45. Once we have made the first Ω_2^+ move of Figure 2.44 (and thus chosen a clockwise or counterclockwise orientation), there are only 2 other Ω_2^+ moves that increase the number of regions with 3 sides by one and change the valence by approximately[31] $4q - 2m$. This move will also increase by 2 the number of edges of the region denoted by Q; we are going to choose the only cyclic orientation based at the vertex in the dual, corresponding to the region M, that has Q after R. Repeating this process for all regions produces a well-defined and coherent orientation system for each vertex in the dual graph, hence uniquely determines the embedding of the dual and consequently the knot projection.

Now suppose we have a periodic knot type K; in order to repeat the previous strategy we need to be able, for each $D \in \mathcal{D}(K)$ with $p_1(D) = 0$, to find in a controlled way a sparse diagram $D' \in \mathcal{D}(K)$, and a sufficiently large ball, centred

[29] We can do that thanks to the sparseness of the diagram.

[30] We only need to follow moves that do not *separate* curls lying on the same edge in different regions, and we can do that again using the difference in the valence together with the sparseness of the initial diagram.

[31] Lower case letters denote the number of edges in the corresponding regions.

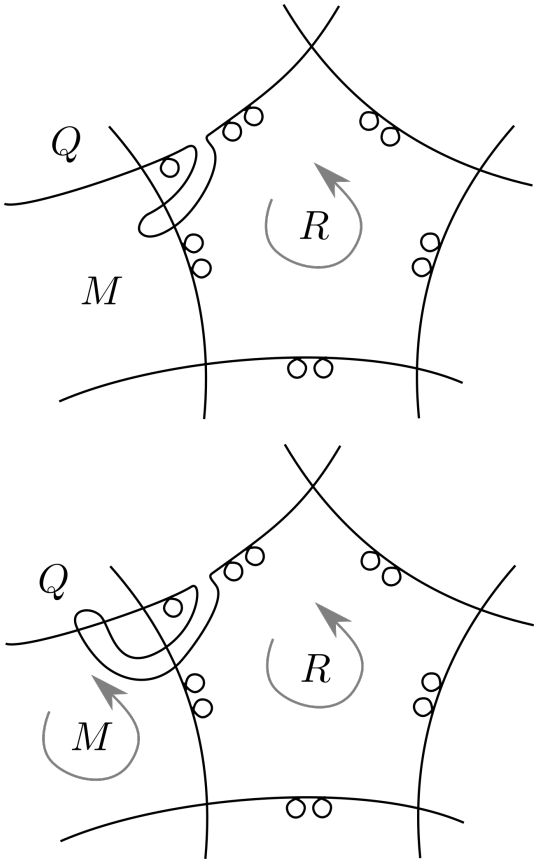

Figure 2.45: How to choose a coherent cyclic ordering for the orientation system.

in D', such that all diagrams in this ball are non-periodic. Since we can verify whether a diagram is periodic[32], by changing the order of the Ω_1^+ multi-edges appearing in the previous construction, and/or their valence, we can achieve a sparse configuration with these properties. □

To conclude the proof, we only need to be able to say that the only possible knots sharing all projections without curls are mirrors of one another.

Proposition 2.4.3. *The S^2-graph $\mathcal{G}(K)$ detects some diagrams of K up to mirroring.*

Proof. Suppose we have two knots K and K' sharing the same graph. Take a vertex D of $\mathcal{G}(K)$ such that $\#\Omega_1^-(D) = 0$. The corresponding vertex D' in the

[32] As explained in the proof of Theorem 2.2.23.

isomorphic graph $\mathcal{G}(K')$ will have the same knot projection as D by the previous Proposition. Hence if $K \neq K'$ the diagrams must differ in at least one crossing. If they differ in *all* crossings, then K' is the mirror of K, and we are done. Otherwise there must be a pair of crossings that up to mirroring looks like the pair in the top part of Figure 2.46 in D and D'.

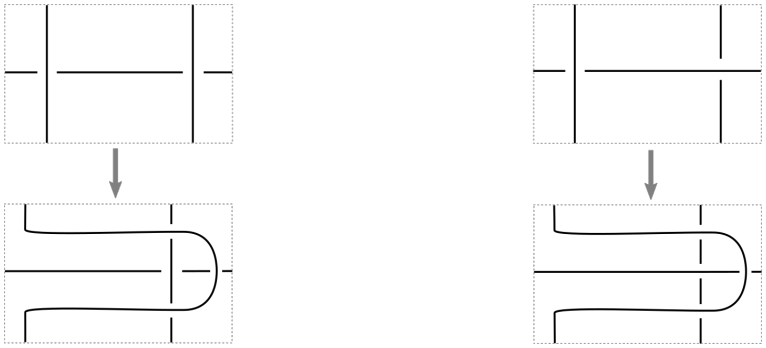

Figure 2.46: The two paths in $\mathcal{G}(K)$ and $\mathcal{G}(K')$. The grey arrows denote the sequence of Ω_2^+-Ω_3-Ω_2^- moves connecting the two diagrams.

Now, perform the sequence of Ω_2^+-Ω_3-Ω_2^- moves that takes the upper diagrams in Figure 2.46, and ends in the lower ones. Note that these paths are well defined, since all the diagrams involved respect the condition $p_1 = 0$; thus we are able to actually determine the effect of these moves on the projections by the previous Proposition. Consider Figure 2.47; there are two distinct sequences of Ω_2^+-Ω_3 (differing by the choice of over/under passing for the first Ω_2^+ move) starting from the diagram on the top-left of Figure 2.47 and ending in two different diagrams sharing the same projection. On the other hand, there is only one way to perform an Ω_2^+ from the diagram on the top-right of the Figure in order to be able to complete the sequence with an Ω_3 and obtain a diagram with the same projection as the other two. Again, these moves are all well defined thanks to Proposition 2.4.2.

Hence the two graphs can not coincide, since there is a path in one of the graphs which is not present in the other one, and we can conclude. □

The three previous propositions together with Proposition 2.2.11 can be easily seen to imply Theorem 2.0.1, but as a matter of fact the result proved is even

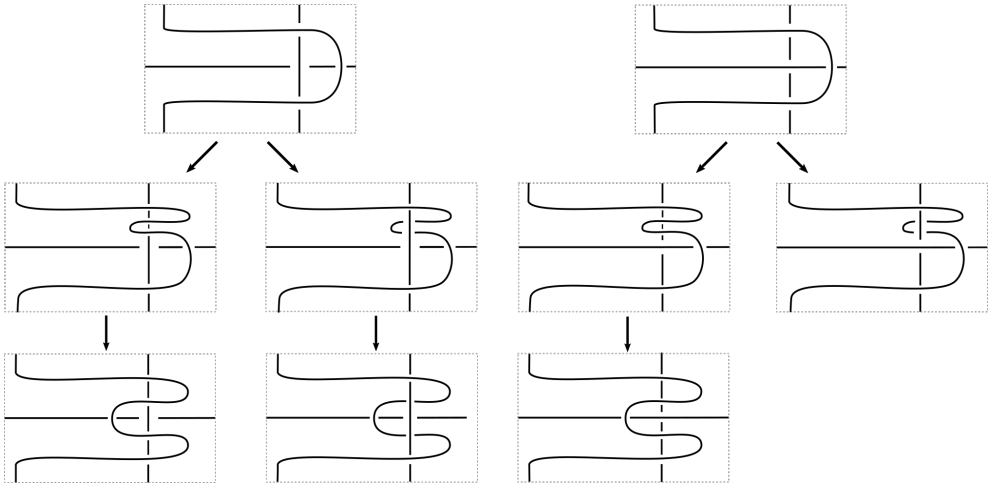

Figure 2.47: The two paths in $\mathcal{G}(K)$ and $\mathcal{G}(K')$. The top/middle arrows denote a Ω_2^+ and Ω_3 move respectively.

stronger, since it allows to recover the actual diagrams[33] represented by some specific vertex of the graph, and not only its knot type. From the proof of Proposition 2.4.2 we are actually obtaining an embedding for the graph which is dual to the knot projection corresponding to the diagram D_0. Hence, this proves that we can actually get back the shape of any diagram not containing any region with 1 edge (in the non-periodic case).

This next result follows directly from the proofs of the previous three Propositions:

Corollary 2.4.4. *Let K be a knot. For every vertex $D \in \mathcal{G}(K)$ there exists an integer $R > 0$ such that $S_R(D)$ is* characterizing*, meaning that this graph can only appear in $\mathcal{G}(K)$. Moreover, in the non-periodic case, R is computable.*

A similar argument should guarantee the completeness of the planar $\mathcal{R}$-graphs, even though the whole process is complicated by the fact that the presence of the external region does not allow a straightforward adjustment of Proposition 2.4.1.

[33]For knots $K \neq \bigcirc$.

2.5 The blown-up Gordian graph

We can unify the Gordian and Reidemeister graphs in a single object, by a sort of *blowup* construction; just replace each vertex of the Gordian graph with the corresponding $\mathcal{G}(K)$. The edges between two knots in the Gordian graph can be split into edges between the diagrams realising the crossing changes.

Definition 2.5.1. *Define the* blown-up Gordian graphs $\mathcal{G}_P^*$ *and* $\mathcal{G}^*$ *respectively, as the graphs whose vertices are knot diagrams in the plane (respectively in* S^2*) up to the corresponding notion of diagram isotopy; there is an edge between two vertices if and only if they are connected by a single Reidemeister move or a crossing change.*

As in the previous setting, the valence of each vertex is finite. For non-periodic diagrams we have

$$v_*(D) = v(D) + cr(D),$$

where $v_*(D)$ denotes the valence of D in $\mathcal{G}_P^*$, and $v(D)$ is the valence of D in the corresponding $\mathcal{R}$-graph. For non-periodic diagrams we only get an inequality.

Note that $\mathcal{G}^*$ admits an order 2 automorphism, induced by changing all crossing of each diagram, *i.e.* taking the mirror image. The only fixed points of this automorphism are the diagrams of amphichiral knots which are equivalent to their mirror up to planar isotopy.

Remark 2.5.2. There are embeddings of $\mathcal{G}_P(K) \hookrightarrow \mathcal{G}_P^*$ and $\mathcal{G}(K) \hookrightarrow \mathcal{G}^*$ for each $K \in \mathcal{K}$, and there are many crossing-change edges in both $\mathcal{G}_P^*$ and $\mathcal{G}^*$ connecting two diagrams representing the same knot type; according to the *cosmetic crossing conjecture* ([69, Problem 1.58]) all these should correspond to nugatory crossings. It would be interesting to explore the possible applications of these graphs to the conjecture.

If we look at the ball of radius 1 in $\mathcal{G}^*$ about a diagram D, we find all the length 3 paths of Theorem 2.2.2, together with a new configuration, shown in Figure 2.48. The fact that the only new triangle[34] appearing is actually this one, follows easily by considering Arnold's and Hass-Nowik's invariants, together with crossing number and writhe, as in Theorem 2.2.2. More precisely, using these invariants we can

[34]That is, triangles that contain at least one crossing change.

restrict to cycles of the form Ω_1-Ω_1-C, where the Ω_1s create crossings of opposite sign, and C denotes a crossing change. Then, with the same line of thought as in Theorem 2.2.2, we can prove that the curls must lie in the same region by taking in account the self-touching number. It follows that the regions under the two curls have the same number of edges. However, we are not able to prove that the crossing change happens exactly on the curls.

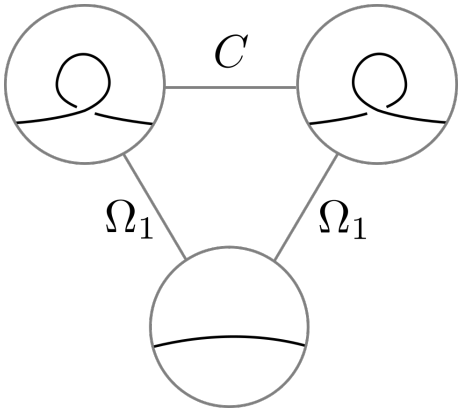

Figure 2.48: The only other possible length 3 path in $\mathcal{G}^*$ which is not a path in any $\mathcal{G}(K)$.

By extending the proof of Theorem 2.2.23 to the blown-up graph it is possible to prove the analogous result; namely that $\mathcal{G}^*$ detects the crossing changes and Reidemeister moves.

Chapter 3

Grid diagrams and type II topoisomerases

As anticipated in Section 1.5, the blown-up Gordian graph provides a purely topological and discretised framework that can be used to quantify the intensity of crossing changes-mediated passages between different knot types.

The same construction can be done when replacing classical knot diagrams with *grid diagrams* [99], Reidemeister moves by *Cromwell moves*, and crossing changes by interleaving commutations. As we will see in what follows, grid diagrams are a combinatorial version of classical knot diagrams. Thanks to their definition and properties, by using grid diagrams we are able to define a meaningful notion of local geometry, crucial to test the hooked juxtaposition hypothesis (recall Section 1.2 and Section 1.4).

Grid diagrams with their relatively simple mathematical formalism provide a convenient way to generate and model projections of various knotted conformations. In what follows, we show how to model topoisomerase-mediated passages actions on double-stranded DNA segments using the formalism of grid diagrams. We show that our grid diagram-based approach captures the essence of the preferential unknotting mechanism, based on topoisomerase selectivity of hooked DNA juxtapositions as acting sites. Our model provides an important, new, and computationally convenient framework for investigating entanglement in biopolymers.

All the results in this chapter are joint with Daniele Celoria, Heather Harrington, Dorothy Buck and Andrzej Stasiak [8].

3.1 Introducing grid diagrams

Grid diagrams are a special kind of knot diagram that provide an easy, combinatorial way to represent knots and links in S^3. First introduced by Cromwell in [29], these objects are widely used in knot theory, thanks to their convenient combinatorial features [99] and for their deep connections with some aspects of the topology of 3-manifolds [36]. Grid diagrams can be defined using the concept of *arc presentations* [29], or intrinsically, as in what follows.

Definition 3.1.1. *A grid diagram is a $n \times n$ grid G, together with two sets of n markings, denoted by $\mathbb{X} = \{X_0, \dots, X_{n-1}\}$ and $\mathbb{O} = \{O_0, \dots, O_{n-1}\}$. Each row and each column of the grid contains exactly one X and one O marking. An oriented link diagram can be retrieved from a grid diagram by connecting the X with the O in each row and column (with the convention that orientation goes from Os to Xs). In the crossings we let the vertical strand always pass over the horizontal one. The size of the grid is a natural number $n \geq 2$, called the* grid number *of G.*

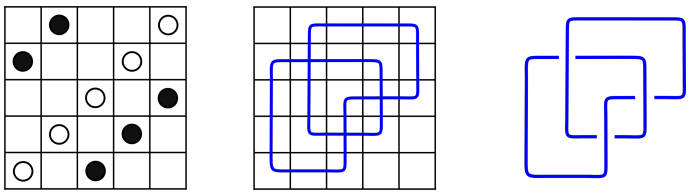

Figure 3.1: A grid diagram representing the trefoil knot. Here the black circles represent the O-markings and the white circles the Xs. It follows that $\sigma_{\mathbb{X}} = (0, 1, 2, 3, 4)$ and $\sigma_{\mathbb{O}} = (3, 4, 0, 1, 2)$

An example of a grid diagram representing the trefoil knot is shown in Figure 3.1. A grid diagram can be described by two permutations $\sigma_{\mathbb{O}}$ and $\sigma_{\mathbb{X}}$. If there is an O-marking in the intersection of the i^{th} column and the j^{th} row, then $\sigma_{\mathbb{O}}$ maps i to j. The number of disjoint cycles into which the permutation $\sigma_{\mathbb{X}} \cdot \sigma_{\mathbb{O}}^{-1}$ splits is the number of components of the corresponding link diagram [99].

Theorem 3.1.2. *Any link L can be represented by a grid diagram.*

Theorem 3.1.2 can be proven using arc presentations [29], or directly, by approximating L with a PL-embedding admitting a projection with only horizontal and vertical segments. After modifying every crossing in which the horizontal arc is over passing as displayed in Figure 3.2, and by moving the link such that different segments are not collinear, we obtain a grid diagram representing L (for more details, see [99], Chapter 3). The minimum of the grid numbers among all grids representing a link L is called the *grid number of* L.

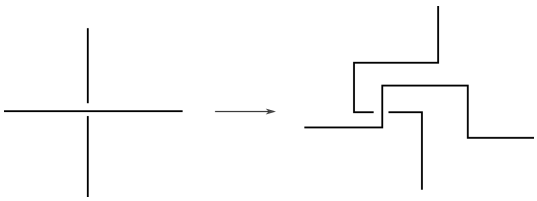

Figure 3.2: Correcting a crossing to fit a grid presentation.

Remark 3.1.3. Note that even if Theorem 3.1.2 implies that any knotted configuration can be represented by a grid diagram, the constraints imposed by the over/underpassing convention of Definition 3.1.1 undermines the possibility to establish a simple, uniform mapping with lattice walks. In other words, there is no easy meaningful to define a 1-1 correspondence between knots in the cubic lattice and grid diagrams.

As for classical knot diagrams, there is a finite set of local moves that relate any two grids representing the same knot type. These moves are collectively known as *Cromwell moves*. Cromwell moves come into two different kinds, called *commutations* and *stabilisations*. While commutations leave the size of the grid invariant, stabilisations change it by ± 1. A detailed description of these moves can be found in [99], Chapter 3. Thus, any ambient isotopy between two knot types K_0 and K_1 can be described by moves between grid diagrams representing K_0 and K_1, in analogy with Reidemeister's theorem (see again [99], Chapter 3 for a proof of this statement). We are however interested in another kind of moves, called *interleaving commutations*, shown in Figure 3.3.

Definition 3.1.4. *Fix two consecutive columns (or rows) in a grid diagram G, and suppose that these are such that their corresponding intervals intersect non-trivially, but neither is contained in the other. Let G' be obtained by swapping these two columns (or rows). We say that the grid diagrams G and G' are related by an* interleaving commutation. *Note that interleaving commutations do not change the size of the grid.*

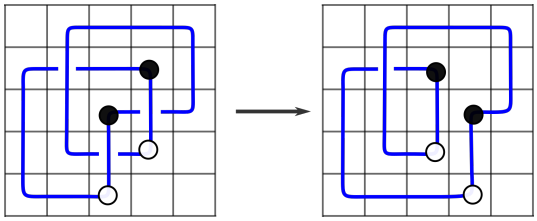

Figure 3.3: An interleaving commutation between two grid diagrams.

When two grid diagrams G and G' are related by an interleaving commutation, their corresponding knot types K and K' are related by a crossing change [Ch.3, [99]].

Thus, as for classical knot diagrams, we can model the configuration space of knots as an infinite graph, whose vertices consists of grid diagrams, and edges represent either interleaving commutations or single Cromwell moves. Since our main interest is on the action of type II topoisomerases, we can consider a simpler object.

Call $\mathbb{G}$ the graph whose vertices are grid diagrams, and edges represent single interleaving commutation. Interleaving commutations leave the size of the grid unchanged. Thus, $\mathbb{G}$ splits into the disjoint union $\mathbb{G} = \bigsqcup_{n\in\mathbb{N}} \mathbb{G}_n$, where each $\mathbb{G}_n$ is the finite graph whose vertices are size n grid diagrams. Note that the grid number provides a measure of complexity for grid diagrams, and that a grid diagram of size n can be seen as corresponding to an equilateral polymer chain with $2n$ statistical segments (see, *e.g.* [67]). For example, grid diagrams in grid number 5 can be used to estimate the behaviour under random strand passages of a polymer having the length of ~ 10 statistical segments, which, in the case of DNA molecules, would

correspond to $\sim$ 3-kb[1]. For the same reason grid diagrams in grid number 15 can be seen as corresponding to DNA molecules of length $\sim$ 10-kb, for which knotting probabilities and simplification rates under type II topoisomerases are available experimentally [106].

3.1.1 Uniformity of sampling

Consider the set of grid diagrams of size N (*i.e.* vertices of $\mathbb{G}_N$), for some $N >> 0$, and denote by K_N the set of knot types represented by those grids. Each element in $\mathbb{G}_N$ is uniquely determined by a pair of N-permutations, which we assume can be randomly sampled using python's `random()` function. In this context, uniformity of our sampling population means that a given knot type $K \in K_N$ will be sampled with probability $\#\{G \in \mathbb{G}_N \text{ representing } K\}/\#\{ \text{ vertices } \in \mathbb{G}_N\}$. This is equivalent to asking that the set of pairs of permutations P giving us grids in the set $S = \{G \in \mathbb{G}_N | G \text{ represents } K\}$ is sampled with probability $\#\{P \text{ yelding a grid in } S\}$/total number of pairs of permutations. This is indeed the case if we are considering the uniform probability on the set of pairs of permutations, which is equivalent to requiring that the `random()` function is indeed random. Hence, grid diagrams uniformly sample the ensemble of possible conformational states of a knotted curve (*i.e.* they are ergodic). Note that this does not imply that we are sampling uniformly in the set of knots in the cubic lattice or in the set of equilateral polymers (see also Remark 3.1.3).

3.1.2 Recovering local geometry

In addition to their combinatorial definition, a further advantage of grid diagrams is that they allow to encode some information on the local geometry of the knot.

The portion of a diagram involved in an interleaving commutation can assume different shapes, some of which might be seen as corresponding to the projection of a hooked juxtaposition, see Figure 3.4.

In particular, we say that a strand passage happens at a hooked juxtaposition when both the horizontal arcs emanating from the innermost markings in the two

[1] A *kilobase*, written "kb", is a measure of length for DNA molecules, and it corresponds to $1,000$ base pairs.

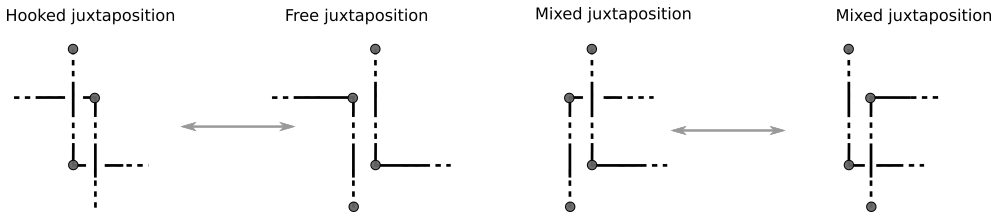

Figure 3.4: The portion of a diagram involved in an interleaving commutation may assume several different shapes, depending on the directions of the arcs emanating from the innermost markings in the two consecutive columns. When each one of those horizontal arcs intersects one of the interleaving vertical arcs in a crossing, we call the portion of the diagram involved a *hooked juxtaposition*. Note that when this happens, the area delimited by the two portions of the diagram between the two consecutive crossings forms a rectangle. In this rectangle, one of the edges length is always 1. The other edge has length $1 \leq l \leq n-3$, where n is the grid number. Hooked juxtapositions are transformed into *free* juxtapositions by an interleaving commutation. We call juxtapositions which are neither hooked nor free *mixed*.

consecutive columns intersect one of the interleaving vertical arcs. In this case, the interleaving commutation is such that the area delimited by two portions of the diagram between the interleaving columns (or rows) forms a simple rectangle, as shown in Figure 3.4 and Figure 3.5.

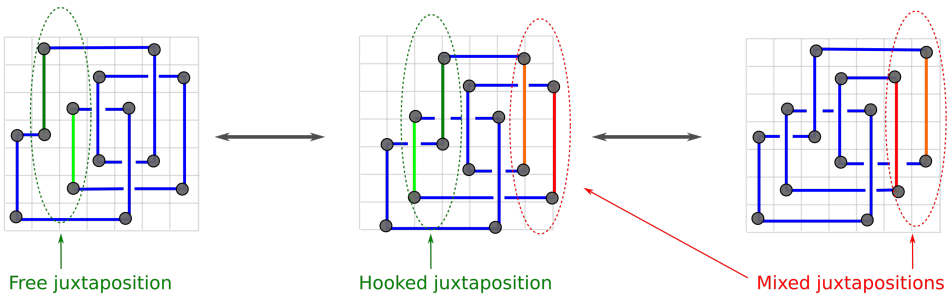

Figure 3.5: On the diagram in the centre of the figure, enclosed in a circle, a strongly hooked-juxtaposition is shown. Performing a interleaving commutation there transforms the 5_2 twist knot into the trivial knot. This exchange transforms the hooked juxtaposition into a *free* one.

We can then define a measure of how much a juxtaposition is hooked using the area of such a rectangle as parameter: the larger the parameter value, the less

the configuration is hooked. We call *strongly hooked* the smallest juxtapositions, *i.e.* those with unitary area (see Figure 3.5).

3.1.3 A new model: the graph of grids

The graph $\mathbb{G}$ provides a discrete and computationally convenient representation of the configuration space of a knotted DNA molecule undergoing the action of type II topoisomerases. Using this model, we can investigate the effect of geometric selection of sites by these enzymes.

3.2 Methods

Consider the graph $\mathbb{G}_n$ for some integer n. The *strand passages-mediated flux* (or *knot interconversion flux*) from a knot K_1 to a knot K_2 is the union of the directed edges in $\mathbb{G}_n$ connecting grid diagrams representing K_1 to grids representing K_2. Our first objective is to quantify the intensity of the knot interconversion fluxes for small crossing number knots[2] in the graphs $\mathbb{G}_n$, with $5 \leq n \leq 19$.

To do that, we use a code in Python written in Sage [116]. Recall that a pair of permutations on n-elements $\sigma_{\mathbb{X}}$ and $\sigma_{\mathbb{O}}$, represents a grid diagram for a link whenever $\sigma_{\mathbb{X}}(i) \neq \sigma_{\mathbb{O}}(i)$ for all $i = 0, \cdots, n-1$. Moreover, by checking the number of cycles in $\sigma_{\mathbb{X}} \cdot \sigma_{\mathbb{O}}^{-1}$, we can tell whether it represents a grid diagram for a knot. Theoretically, it is possible to exactly enumerate all the size n grids whose underlying diagrams represent knots. This can be done by listing all the pairs of permutation on n-elements, and then keeping only those corresponding to knot diagrams. However, since there are $1/2(n((n-1)!))^2$ different configurations in grid number n [53], exact enumeration becomes quickly unfeasible for computational reasons.

Our program proceeds by enumerating all grid diagrams of size n for $5 \leq n \leq 7$, and by randomly sampling a set of grid diagrams of size n for $8 \leq n \leq 19$. Since grid diagrams are encoded by a pair of permutations, uniformity of sampling is

[2] In our work we only consider knots with crossing number ≤ 8, since these are more relevant from the biological point of view.

automatically built-in our model, and only relies on Python's extensively tested `random()` function (recall Section 3.1.1). We emphasise again that, as discussed in Section 3.1.1 and Remark 3.1.3, the uniformity of sampling mentioned here is not equivalent to uniformity of sampling in the configuration space of lattice configurations. To determine the underlying knot type of each configuration we use a combination of knot invariants (specifically, the Alexander and Jones polynomials, the determinant and the signature [105]). We then perform every possible interleaving commutation on each configuration, and we compute the knot type of the resulting grid. For each n, the data is summarised in the *unbiased adjacency matrix* U^n, whose entry $u^n_{i,j}$ is the number of observed passages from the i^{th} to the j^{th} knot type.

In analogy with the investigations performed in [82] and [81] we test the effect of geometrical selection of sites (see Figure 3.5) on the unknotting function of type II topoisomerases. To do that, on the same sets of configurations considered before, we restrict our attention to passages happening at hooked juxtapositions. More specifically, for each grid number n, and for every $1 \leq A \leq n-3$ we only count those passages happening at hooked juxtapositions with rectangle area $\leq A$. Again, the data is collected in the *hooked adjacency matrix* H^n_A. Our code and the full set of data are available online at [6].

In [6], each file contains the data relative to a specific grid number n. For each grid number $9 \leq n \leq 19$ we sampled a total of $16,000$ configurations (*i.e.* $16,000$ vertices in $\mathbb{G}_n$). In each file, for each iteration, we write:

- the grid number n;
- the total number of configurations considered (*e.g.* the number of sampled configurations plus the number of configurations reached through strand passages);
- the number of sampled configurations;
- the distribution of knot types in the sample;

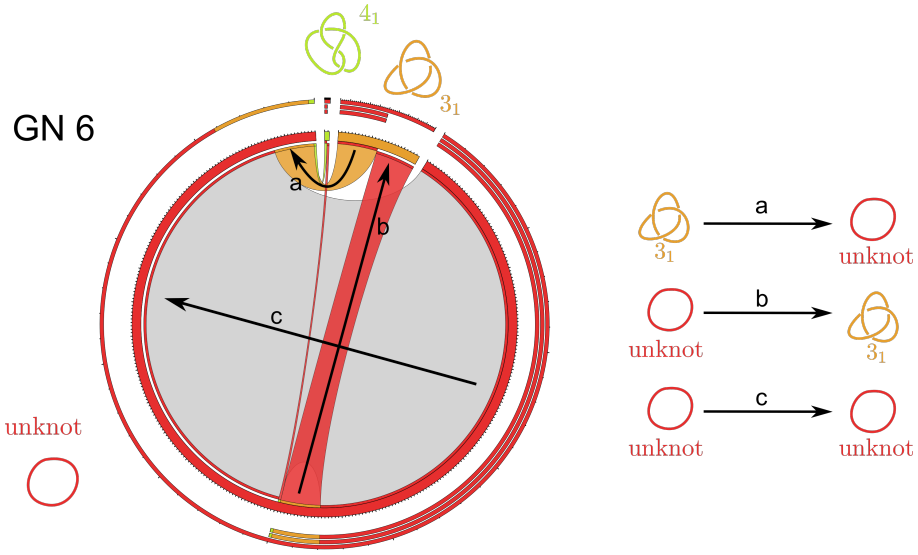

Figure 3.6: For each grid number n, the data contained in the unbiased and hooked adjacency matrices is visualised using circos plots [75]. The figure shows, as an example, the case of unbiased strand passages for grid number 6. In the plot, the three layers of thin external arcs, progressing from inside to outside, represent outgoing, incoming, and total fluxes involving a given knot type, respectively. These external arcs are segmented to indicate how the respective fluxes were redistributed. The thickness of the (interior) chords connecting different knot types reflects the fraction of outgoing and incoming knot interconversion fluxes between given types of knots. The chords representing knot interconversion fluxes are coloured as the knot type that these fluxes originate from, with the exception of chords starting and ending in the same knot type, which are in gray. These correspond to the fluxes resulting from strand passages not changing the knot type. The bases of the chords representing outgoing fluxes are coloured according to the knot type that a given flux leads to. The bases of chords representing incoming fluxes are left white. The length of the various thick arcs around the circumference, coloured as the corresponding knot diagrams, indicates the sum of fluxes outgoing from and incoming to a given knot type.

- the distribution of knot types with respect to the total number of configurations considered;
- a list of adjacency tables, starting from the unbiased one U^n, followed by the hooked ones H^n_A. The hooked adjacency tables are ordered from less to more hooked.

3.3 Geometric selection of sites results in topological simplification

The data contained in the unbiased and hooked adjacency matrices is visualised using circos plots [75], see Figure 3.6.

3.3.1 The configuration space of grid diagrams

There are a total of $1,859,118$ different grid configurations with grid number $n \leq 7$, of which $1,773,114$ are unknotted, $78,296$ are (left or right handed) trefoils, $6,014$ are figure eight knots, 798 are 5_1 torus knots, 882 are 5_2 twist knots, and only 14 of them are 8_{19} knots. As an example, the unbiased adjacency table of knots with $n = 6$ is visualised in the leftmost circos plot on Figure 3.8 (B, i). We observe that, in agreement with previous works [40, 57], most ($\sim 91.7\%$) of the strand passages occurring in unknotted diagrams do not change the topology of these diagrams and, of those passages that change the topology, $\sim 94.5\%$ transform the unknot into the trefoil.

The circos plots summarising the sampling in grid number $n = 9$ and $n = 16$ are shown in Figure 3.8 (B, *ii* and *iii*). It is immediately apparent how the knot-type fauna becomes more variegated as the grid number increases, with considerably higher occurrence of complex knots, and strand passage-mediated fluxes become more visible. In the exact enumeration of unbiased strand passages, the number of diagrams passing from the i^{th} knot type to the j^{th} knot type is obviously equal to those passing from the j^{th} to the i^{th}. In higher grid numbers, we have to ensure that the sampling method enables us to describe the system at equilibrium. As mentioned in Section 1.2, the specific nature of grid diagrams (recall Section 3.1.1) allows us to easily perform uniform sampling, and thus to achieve detailed and global balance[3] effortlessly. This can be seen from the circos plots of Figure 3.8 (B, *ii* and *iii*), in which the sizes of the arcs representing incoming and outgoing

[3]Saying that the system is at global balance means that the fraction of DNA molecules forming any given knot type reaches its equilibrium level and the relative occurrence probability will not show a tendency to increase or decrease, although one may observe some fluctuations. Detailed balance means that the interconversion fluxes between any two types of knots are the same in both directions when observed over a sufficiently long time.

fluxes of each pair of knot types correspond almost exactly.

3.3.2 Evolution of the configuration space of knots

It is well known [114, 127] that for closed polymers, the probability that a configuration is unknotted decreases as the length of the polymer increases. The same behaviour can be observed for grid diagrams. Figures 3.8 and 3.7 show how the configuration spaces of a knotted molecule evolve as the complexity given by the grid number increases.

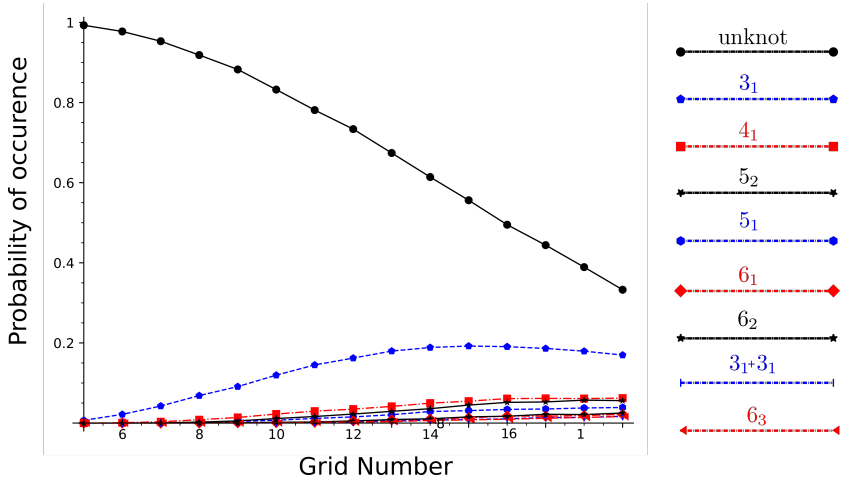

Figure 3.7: The curves give the occurrence probabilities of knots with minimal crossing number up to 6, plotted as a function of the grid number. The occurrence probability of a given knot type is defined as the ratio between the configurations representing that knot type and the total number of configurations. We consider also the composite knots obtained as the connected sum of two trefoils. Note that with grid diagrams knotting is stimulated as compared to 3-dimensional situations [64]. In our case, the population of nontrivial knots starts to exceed 50% at $n = 17$, and every knot with minimal crossing number ≤ 13 can be represented by grids of size ≤ 12 [22]. This in particular implies that for grid number 15 (thus, for grids that can be seen as corresponding to DNA molecules of length $\sim$ 10-kb, as mentioned in Section 3.1) the probability that a configuration is knotted is much higher than the knotting probability found experimentally [106]. This clear limitation in our model turns out not to be problematic for our results, since we are mostly interested in transition probabilities and in knot reduction rates.

The probability that a configuration of a given knot type is converted into another knot type is called *transition probability*. Note that as n increases, the probability of occurrence of unknotted conformations appears to decrease monotonically, and therefore, the transition probabilities toward *simpler* knot types also decrease monotonically, as shown in Figure 3.9. For example, the probability of passing from a trefoil diagram to an unknot passes from an initial value of almost 1 to about 0.4 as the grid size increases from 5 to 19. Unsurprisingly, for every grid number, among all the unknotting number 1 knots, the transition probability towards the unknot is consistently higher for the trefoil. One may be tempted to sort knot types connected through a single crossing change to another knot, in terms of the amount of observed strand passages towards the knot types in question, as discussed in [40] (there, they refer to this concept as *interface area* between knot spaces). In our setting, we can formalize the heuristic notion of knot closeness between two given knot types K_1 and K_2 as the ratio of the occurrences of intersegmental passages between K_1 and K_2 over the total number of intersegmental passages between any two knot types. As an example, the data discussed above suggest that the trefoil is the closest knot type to the trivial knot. The observation that these properties are maintained as the grid number increases, coupled with the fact that our results are topological in nature (hence, independent of any geometric or physical feature of the model), indicates that these are intrinsic features of the various knot types. Figure 3.7 shows how the knot fractions change as the grid number increases.

We observe that the trend is qualitatively similar to the case of equilibrated polygonal chains embedded in the 3-space (see, *e.g.* Figure 2 of [64]). However, in our 2-dimensional grid diagrams, knotting is stimulated as compared to 3-dimensional situations [64]. In our case, the population of nontrivial knots starts to exceed 50% at $n = 17$, and every knot with minimal crossing number ≤ 13 can be represented by grids of size ≤ 12 [22]. This highlights a further advantage of our framework. Namely, we are able to account for complex knot types while working with configurations of relatively small size.

3.3.3 Topological simplification through geometric selection of sites and the knotting reduction factor

By comparing the biased and unbiased matrices, we quantified the changes in the intensity of simplification fluxes. In particular, we show how adding geometrical selection of sites increases the probability that a random strand passages results in knot simplification, for every starting knot type, and in each grid number considered. The extent of this knotting diminution, also known as *knot reduction factor*, was measured experimentally for intersegmental passages mediated by the type II topoisomerase, topoisomerase IV [106], and for several simulated systems [82, 81, 20, 40]. More formally, the *knot reduction factor* is defined as the ratio of the number of passages from 3_1 to 0_1 over the number of passages from 0_1 to 3_1.

The experimentally observed reduction of trefoil knot concentration was approximately 90-fold for 7-kb DNA circles and approximately 50-fold for 10-kb DNA circles [106]. The knotted population seen in the experiments for 10-kb DNA circles divides into approximately 3% trefoils and 97% unknots. A similar ratio in our model can be found in the range $5 \leq n \leq 7$.

In $n = 6$, U^6 shows that there are 6240 passages from configurations representing the trefoil knot to configurations representing the unknot and viceversa. When we restrict to passages happening at strongly hooked juxtapositions, we see 1220 passages from trefoils to unknots and only 80 from unknots to trefoils. Thus, the knot reduction factor is in this case > 15. Note this knotting reduction can be considered strong, but it is still substantially smaller than the ones observed experimentally [106]. Our observed knot reduction factors in the range $5 \leq n \leq 7$ are then comparable with those observed in DNA of 7-10kb. This is apparently in contradiction with the discussion in Section 3.1 on how the size of grid diagrams compares to the length of equilateral polygons. Indeed, while the transition probabilities between different knot types computed for grids of size n are similar to those computed for equilateral polygons of length $2n$ (this can be seen for example by comparing Figure 3.8, grid number 16, and [40], Table 1) the knot reduction factor strongly depends on the amount of knotted configurations in the system. This explains why the best agreement with experimentally computed reduction

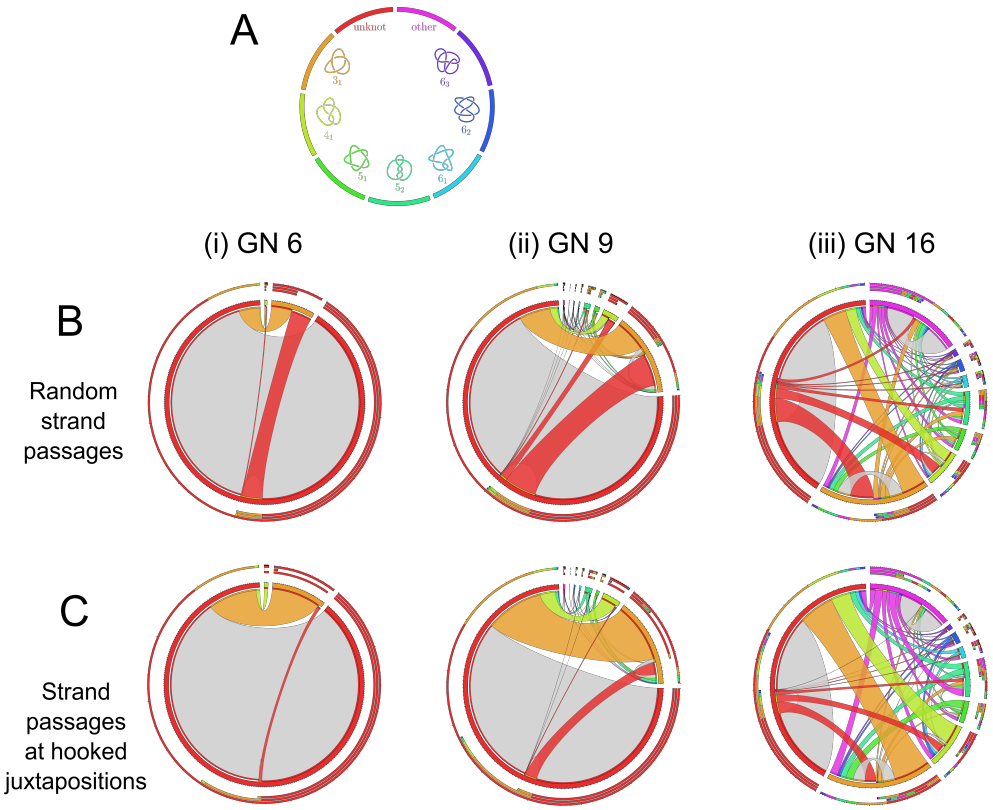

Figure 3.8: (A) Knot types are colour-coded according to this plot. (B)-(C) The figure shows the data contained in the unbiased and strongly hooked adjacency matrices for grid number 6, 9 and 16. As the system's complexity increases, more complicated knots appear. In the plots representing fluxes resulting from unbiased strand passages (B) the incoming and outgoing fluxes connecting any pair of knots are of the same intensity. This indicates that the generated set of grid diagrams represents the topological equilibrium. When the same set of grid diagrams undergoes intersegmental passages involving only strongly hooked juxtaposition the interconversion-fluxes towards the unknot are much more intense than the opposite fluxes. This effect is especially strong for smaller grid number.

factor is found in the range $5 \leq n \leq 7$.

In experiments performed by Rybenkov et al. [106], 7-kb-long DNA circles showed a knotting reduction factor nearly two times higher than 10-kb-long DNA circles. The inverse relation between the knotting reduction factor and the size of circular DNA molecules stems naturally from the mechanism proposed in [18], in

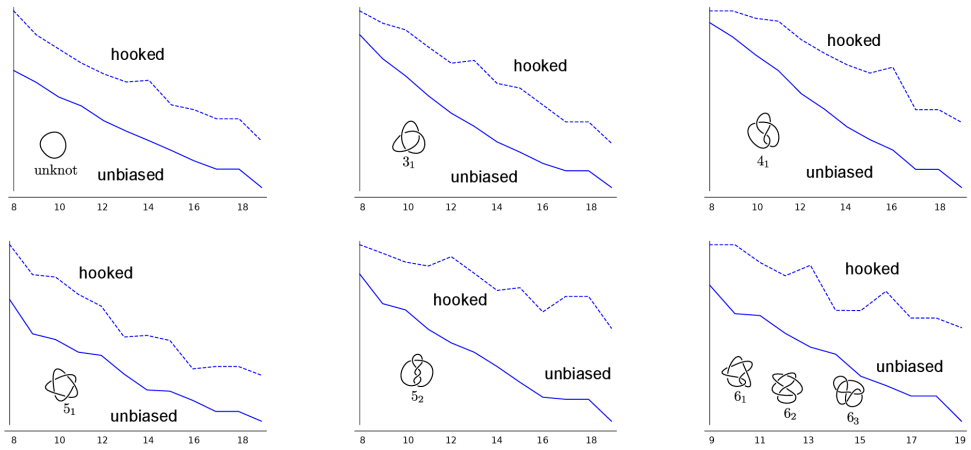

Figure 3.9: The plots show the transition probabilities of each knot type towards *simpler* knots, as a function of the grid number. In each plot, the dotted line refers to strand passages happening at strongly hooked juxtaposition, while for the other we consider unbiased interleaving commutations. In the case of the unknot, the 3_1 and the 4_1 we consider only the unknotting probabilities. For the 5_1 and the 5_2 we consider passages towards the 3_1, the 4_1 and the unknot. Finally, for 6 crossings knots, we plot the transition probabilities towards knots with lower *length over diameter ratio* [63] (thus, for the 6_1 we consider only passages towards knots with crossing number less than or equal to 5, while for the 6_2 and the 6_3 we consider also passages towards the 6_1 and towards the 6_1 and 6_2 respectively).

which a higher ratio between the bending rigidity and the size of DNA molecules corresponds to a higher type II topoisomerase-mediated knot reduction factor. This effect was confirmed in simulation studies using polygonal knots in the lattice model [82, 81]. As our model is essentially a 2-dimensional model, it is of interest to analyse how knot reduction factor changes with the grid size. For grid diagrams with $n = 5$ (where there are only 10 different grids forming the trefoil knot), the knotting reduction factor connected to intersegmental passages at hooked juxtapositions was infinite, meaning that all the passages happening at strongly hooked juxtapositions result in topological simplification. On the other hand, all passages occurring at strongly hooked juxtapositions in unknotted diagrams did not result in a change of topology. As already mentioned, for grid number 6, the knotting reduction factor is approximately 15. Analysis of diagrams in grid number 7 show that the selection of sites results in a knotting reduction factor of about 8. The

same decreasing trend is observed for higher grid numbers. Therefore, we can conclude that planar grid diagrams adequately capture the experimental observation that knotting reduction by type II topoisomerases is strongest when acting on short DNA molecules [106].

Earlier studies [20] showed that, when restricting to passages happening at hooked juxtapositions, the more the juxtapositions are hooked, the larger the corresponding knotting reduction factor. In analogy with [20], we investigated how the knot reduction factor changes as the size of the rectangle area enclosed by the interleaving strands in hooked juxtapositions is decreased. Unsurprisingly, and as shown in Figure 3.10), the knot reduction factor increases as the area of the rectangle decreases.

Further, we tested how the effect of those biases change as the size of the grids increases. In agreement with experimental data [106], the unknotting power of geometrical selection of sites is less evident for high grid number diagrams (see Figure 3.8 and Figure 3.9).

3.3.4 Conclusions

Our simulations agree with both experimental data [106] and with previous computations [40, 82, 20] *etc*, thus further validating the hooked juxtaposition hypothesis [18]. We demonstrated that grid diagrams provide a new and compelling tool to investigate statistical and probabilistic properties of knotted polymers.

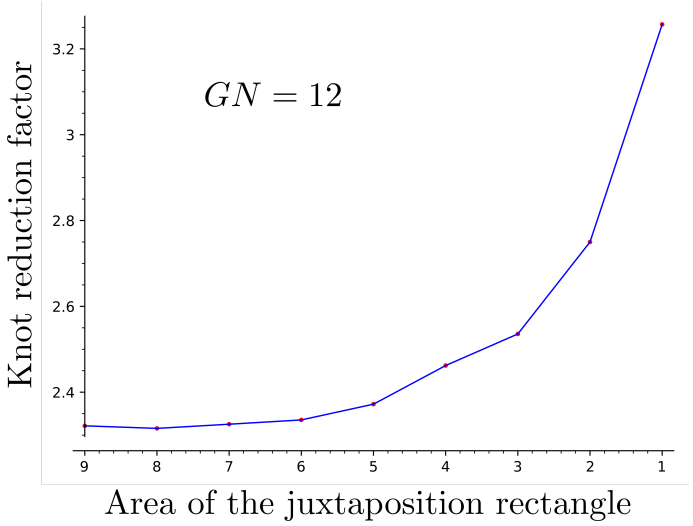

Figure 3.10: The plot displayed shows the knot reduction factor in $\mathbb{G}_{12}$, plotted as a function of the rectangle area A enclosed by the interleaving strands in hooked juxtaposition. For each $1 \leq A \leq 9$, we only consider strand passages happening at hooked juxtapositions with rectangles of size $\leq A$. It is apparent how decreasing such area increases the knot reduction factor.

Part II

Knotoids and Protein Entanglement

Chapter 4

Introduction to Part II

In nature, proteins often appear in rather complex configurations, and understanding their geometry and topology is a challenging problem. In the last 25 years the existence of non trivial entanglement in proteins has been investigated. The first example of a knot in a protein dates back to 1994 [87], and from there, many more have been identified [115, 14].

More precisely, proteins are long chains of amino acids that fold into specific conformations, that can sometimes form open ended knots. Despite the fraction of knotted proteins being fairly small [30], and even if the presence of knots in proteins is known to slow the folding process [85, 112], the knotted domains of some families of proteins have been conserved through evolution [113, 101, 83, 123]. While studies seem to suggest that knots provide advantages to some proteins [31, 108], the purpose of the presence of knots in proteins is still an open and interesting question in biology. Thus, understanding topological features of knotted proteins is an important step in investigating the effect of the presence of knots to the structure and function of proteins.

Since proteins consist of long polymeric chains, they can be modelled as open polygonal curves. For this reason, investigating entanglement phenomena on linear biopolymers entails the problem of characterising knottiness in open curves. In fact, the formalism used for proper knots does not apply to this context, since any open arc in $\mathbb{R}^3$ can be transformed into a straight segment by an ambient isotopy. One possible way to deal with it is to *virtually close* the open chain to form a proper knot. However, since there is no canonical way to close an open

curve, the downside of this approach is that the choice made when closing the open chain deeply affects the knot types obtained (a detailed discussion on this topic can be found in [90, 119]). A common (and relatively unbiased) method for closing protein chains is the following one. Consider the chain as lying in the centre of a large enough 2-sphere. By randomly choosing different points in the 2-sphere and by subsequently joining each one of them to the endpoints of the chain [87, 89] it is possible to perform several different closures. A *distribution* of knots in S^2 is then obtained by computing the knot type of each one of these random closures.

A more subtle classification of knottiness in proteins has been recently achieved with analogous methods using the concept of *knotoids* [120]. Indeed, knotoids were recently introduced by V.Turaev [120] as a generalisation of knots in S^3. Knotoids' main purpose is to deal with the problem of classifying knottiness for open curves. They are defined as equivalence classes of diagrams of oriented arcs in S^2 up to an appropriate set of moves and isotopies. More formally, we have the following definition.

Definition 4.0.1. *A* knotoid diagram *in S^2 is a generic immersion of the interval $[0, 1]$ in S^2 with finitely many transverse double points endowed with over/under-crossing data. The images of the points* 0 *and* 1 *are distinct from the other points and from each other. The* endpoints *of a knotoid diagram are called the* tail *and the* head *respectively, and denoted by v_0 and v_1. Knotoid diagrams are oriented from the tail to the head, see Figure 5.2. A* knotoid *is an equivalence class of knotoid diagrams on the sphere considered up to isotopies of S^2 and the three classical Reidemeister moves, performed away from the endpoints.*

Some examples of knotoids are shown in Figure 5.2.

In the past few years, knotoids have been used to classify entanglement in proteins [48, 46, 33, 30]. As in the case of the virtual closure, in the knotoids approach a protein is represented as an open-ended polygonal chain. This open curve is then studied by considering all of its planar projections, and each projection is then analysed as a knotoid. In this way, the topology of the curve is characterised by a *distribution* of knotoid types, also called the *spectrum* of the

curve. The knotoid classification for knotted proteins is available in the online database KnotProt [30].

4.1 Knotoid invariants

It should be clear that in order to be able to characterise entanglement in proteins using knotoids, it is crucial to efficiently and reliably distinguish between inequivalent knotoids. Several invariants for knotoids have been adapted from classical knot theory, such as various versions of knotoid polynomial [120, 49, 48], and there are several well defined maps that associate a classical knot to a knotoid [120, 49, 74]. Often, non-equivalent knotoids share the same image under these maps, and it is possible to exhibit examples of non-equivalent knotoids with the same polynomials.

Our first effort on this direction is to use a double branched cover construction to define a new class of powerful knotoid invariants.

As described in Chapter 5, by using double branched covers, we prove that there is a 1-1 correspondence between the set of knotoids, taken up to certain symmetries called *rotation* and *reversion*, and knots with a *strong inversion*, taken up to conjugacy. All these terms are going to be formally defined in Chapter 5.

Theorem 4.1.1. *There is a* 1-1 *correspondence between unoriented knotoids, up to rotation, and knots K with a strong inversion τ, up to conjugacy.*

By exploiting properties of knot symmetries we have the following corollary of Theorem 4.1.1.

Corollary 4.1.2. *Given any torus knot K_t there is exactly* 1 *knotoid associated to it, up to rotation and reversion. Given any strongly invertible hyperbolic knot K_h there are either* 1 *or* 2 *knotoids associated to it up to reversion and rotation, depending on whether or not K_h is periodic with period* 2*. In general, given any strongly invertible knot K there are only finitely many knotoids associated to it.*

This correspondence allows us to study knotoids through tools and invariants coming from knot theory. In particular, concepts from geometrisation generalise

to knotoids, allowing us to characterise reversibility and other properties in the hyperbolic case.

Theorem 4.1.3. *A hyperbolic, oriented knotoid $k \in \mathbb{K}(S^2)$ is reversible if and only if its double branched cover has cyclic period 2. Analogously, it is equivalent to the reverse of its rotation if and only if its double branched cover has free period 2.*

Theorem 4.1.4. *A hyperbolic knotoid is never rotatable.*

As a consequence of these results we obtain the following.

Corollary 4.1.5. *Given any strongly invertible hyperbolic knot K there are exactly 4 oriented knotoids associated to it. Moreover, one of the following holds.*

- *If K has cyclic period 2, these are two inequivalent reversible knotoids k^1, k^2 and their rotations $k^1_{\boldsymbol{rot}}$, $k^2_{\boldsymbol{rot}}$;*
- *If K has free period 2, these are two inequivalent knotoids k^1, k^2 (each equivalent to the reverse of its rotation) and their reverses $-k^1$, $-k^2$;*
- *If K does not have period 2, these are a knotoid k, its reverse $-k$, its rotation $k_{\boldsymbol{rot}}$ and its reverse rotation $-k_{\boldsymbol{rot}}$.*

As there is an algorithm to decide whether two hyperbolic knots are equivalent [86, 76], and since there is an algorithm to decide whether two involutions of a hyperbolic knot complement are conjugate (see *e.g.* Theorems 8.2 and 8.3 of [77]), Theorem 4.1.1 implies the following stronger result.

Theorem 4.1.6. *Given two hyperbolic knotoids k_1 and k_2, there is an algorithm to determine whether k_1 and k_2 are equivalent as oriented knotoids.*

Finally, with our construction we are able to distinguish the trivial, crossingless knotoid among all the others.

All the results discussed in Chapter 5 are joint with my advisors Marc Lackenby, Heather Harrington and Dorothy Buck [5]. The invariants we define have been fundamental in the completion of the current knotoid classification due to Goundaroulis [47].

4.2 Application to the study of protein's topology

As mentioned earlier, by tracing the coordinates of its amino acids, each protein can be modelled as an open curve in space. To classify its entanglement, the curve representing the protein is thought of as living inside a surrounding 2-sphere. Each point on this enclosing sphere defines a planar projection of the open curve, yielding a knotoid diagram. In this way we can associate to any given protein a distribution of knotoids on the 2-sphere, called the *knotoid distribution*, somehow describing its global entanglement. Since considering all possible projections of a curve is not computationally feasible, it is necessary to rely on random sampling of a finite number of projections to construct an *approximated* knotoid distribution.

The *dominant* knotoid of a protein is defined as the most common knotoid type found in the approximated distribution, and computing it provides a first step in the classification of entanglement for proteins. However, the same dominant knotoid is shared by proteins having extremely different characteristics, ranging from length to their biological function [30]. As one might expect, the knotoid distribution contains far more information on the topology and geometry of a protein than the dominant type.

In Chapter 6, we study the relation between pairs of knotoids that are obtained from projections that differ from one another only by a small perturbation. Indeed, small perturbations in the choice of the direction of projections can either leave the corresponding knotoid type unchanged (*i.e.* by changing the knotoid diagram by isotopies of S^2) or have the effect of performing a sequence of local moves called *forbidden moves* (see Figure 5.1) on the knotoid diagram. Thus, when the approximated distribution provides an accurate description of the knotoid distribution, a pair of different knotoids whose projections are related by a small perturbation will at most differ by a single forbidden move.

Since forbidden moves are *unknotting operation*, we are able to define a distance between knotoids called the *forbidden move distance*.

Definition. *Given two knotoids k_1 and k_2, their* forbidden move-distance *or f-distance $d_f(k_1, k_2)$ is the minimal number of forbidden moves, across all representatives of k_1 and k_2, needed to transform k_1 into k_2.*

In the first part of our investigation we exploit the theoretical framework developed in Chapter 5 to compute the f-distance for knotoids with low crossing number.

More precisely, we characterise forbidden moves between knotoids in terms of topological operations between the associated θ-curves and strongly invertible knots.

Theorem 4.2.1. *Consider two equivalence classes of of knotoids k_1 and k_2 up to rotation and reversion. The following are equivalent:*

- *k_1 and k_2 differ by a single forbidden move;*
- *their corresponding θ-curves $t_{\approx}(k_1)$ and $t_{\approx}(k_2)$ differ by a strand passage of the edge e_0 over either e_+ or e_-;*
- *their corresponding strongly invertible knots $\gamma_{S_{\approx}}(k_1)$ and $\gamma_{S_{\approx}}(k_2)$ differ by an equivariant band surgery.*

By understanding the topological relations between neighbouring knotoids, we are able to determine the optimal sample size of projections needed to well approximate the knotoid distribution associated to a protein, both in terms of computational speed and accuracy. Moreover, using the mathematical tools we developed, we propose a new numerical measure associated to the knotoid distribution, which can distinguish between deeply and shallow knotted proteins, without requiring any of the established computationally expensive methods [33]. Finally, we test our results by doing statistical analysis on a specific set of knotted proteins.

All the results discussed in Chapter 6 are joint with Dimos Goundaroulis [9].

Chapter 5

Knotoid invariants from Double Branched Cover

All the results in this chapter are joint with my advisors Marc Lackenby, Heather Harrington and Dorothy Buck [5].

5.1 Preliminaries on knotoids

The aim of this section is to give some preliminary facts on knotoids. Note that allowing the strand adjacent to an endpoint to pass over/under a transversal strand as shown in Figure 5.1 produces a trivial theory. Namely, any knotoid diagram can be transformed into the trivial, crossingless one by a finite sequence of forbidden moves. We will denote by 0_1 the equivalence class of the trivial knotoid diagram.

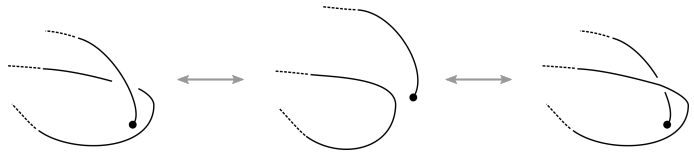

Figure 5.1: Forbidden moves between knotoid diagrams. Performing a forbidden move on a knotoid diagram usually results in a change of the knotoid type. Moreover, these moves define an *unknotting operation*, meaning that any knotoid diagram can be transformed into the trivial one by a finite sequence of forbidden moves. As we will see in Chapter 6, this fact allows us to define a notion of distance between knotoids.

Just as in the case of knots, knotoids admit natural involutive operations such

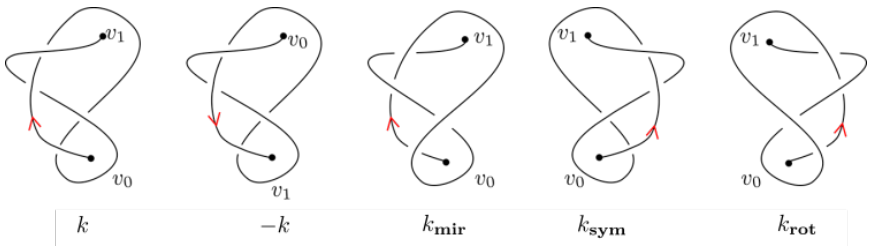

Figure 5.2: From left to right, a knotoid k, its reverse $-k$, its mirror reflection $k_{\mathbf{mir}}$, its symmetric $k_{\mathbf{sym}}$ and its rotation $k_{\mathbf{rot}}$.

as mirror reflection and reversion. In addition, it is possible to define two further modifications for knotoids called *symmetry* and *rotation*, see Figure 5.2. As for knots, reversion has the effect of changing the orientation of a knotoid, and mirror reflection transforms a knotoid into a knotoid represented by the same diagrams with all the crossings changed. Symmetry instead reflects a knotoid diagram with respect to the line in D^2 passing through the endpoints. The last involution, the rotation, is defined as the composition of symmetry and mirror reflection. We will often consider knotoids up to some of these involution, and we will call *reversible* and *rotatable* knotoids equivalent to their reversion and rotation, respectively.

As it happens for knot diagrams (recall Remark 1.3.1), we might choose D^2 instead of S^2 as the ambient space for knotoid diagrams. Two knotoid diagrams in D^2 are said to be *equivalent* if they are related by planar isotopies and a finite sequence of Reidemeister moves, performed away from the endpoints. We will call those equivalence classes of arc diagrams *planar knotoids*, and we will denote by 0_1^{pl} the equivalence class in D^2 of the crossingless knotoid diagram. To distinguish between the two objects, we will denote by $\mathbb{K}(S^2)$ and $\mathbb{K}(D^2)$ the sets of spherical and planar knotoids, respectively. We can define the map

$$\iota : \mathbb{K}(D^2) \longrightarrow \mathbb{K}(S^2)$$

induced by the inclusion $D^2 \hookrightarrow S^2 = D^2 \cup \infty$. The map ι is surjective but not injective. Indeed, the knotoids in Figure 5.3 are equivalent in S^2 but not in D^2.

There are several well defined maps that associate a classical knot to a knotoid [120, 49, 74]. As an example, given a knotoid diagram we can construct a knot diagram by connecting the endpoints with an arc, declared to go under (respectively

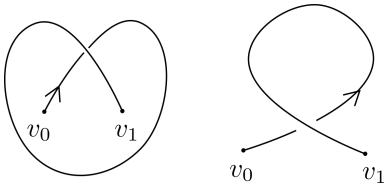

Figure 5.3: The diagrams in the picture represent inequivalent planar knotoids, but they share the same image in $\mathbb{K}(S^2)$ under the map ι. Indeed, they are distinguished by the loop arrow polynomial (see Section 5.1.1), but they are both equivalent to the trivial knotoid 0_1 as elements of $\mathbb{K}(S^2)$. To see this, just pass the twirl on the right diagram *up to infinity* in S^2.

over) each strand it meets during the connection. We call the resulting knots the *underpass closure* and the *overpass closure* of the knotoid [49]. It is not hard to prove [120, 49] that the knot type obtained does not depend on the choice of the starting knotoid diagram. Thus, these operations induce well defined maps

$$\omega_{\pm} : \mathbb{K}(S^2) \longrightarrow \mathcal{K}(S^3).$$

It is often the case that non-equivalent knotoids share the same image under these maps, as it can be appreciated from the knotoids in Figure 5.4. In Section 5.3 we are going to present a more subtle way to associate a knot to a knotoid, which allows for a finer classification.

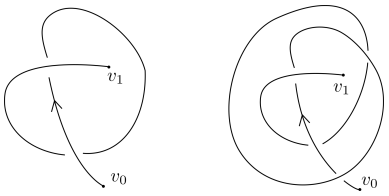

Figure 5.4: The images under ω_- of the two knotoids in the figure are both the trefoil knot, and the images under ω_+ are both the trivial knot, but the knotoids are not equivalent.

Every knot $K \subset S^3$ arises as the image under $\omega_{\pm}$ of a knotoid diagram. Indeed, choose any diagram representing K, and cut out an arc that does not contain any crossings, or that contains only crossings which are overcrossings (respectively undercrossings). This results in creating a knotoid diagram, whose image under ω_+ (respectively ω_-) is the starting knot K. It is important to note that different

choices of arcs in K may result in non-equivalent knotoid diagrams. However, choosing the arc to be crossingless induces a well defined injective map α from the set of knots in S^3 to $\mathbb{K}(S^2)$ [120, 49].

Definition 5.1.1. *Knotoids in $\mathbb{K}(S^2)$ that are contained in the image of α are called* knot-type knotoids. *Equivalently, a knotoid is a knot-type knotoid if and only if it admits a diagram in which the endpoints lie in the same region. As an example, both the knotoids in Figure 5.3 are knot-type knotoids. The other knotoids are called proper knotoids.*

Remark 5.1.2. There is a 1-1 correspondence between knot-type knotoids and classical knots, induced by the operation of *closing* the endpoints [120, 49]. In particular, for knot-type knotoids symmetry and mirror reflection coincide [120], and every knot-type knotoid is rotatable.

5.1.1 Knotoid polynomials

Several invariants for knotoids have been adapted from classical knot theory, such as various versions of knotoid polynomials [120, 49, 47].

As an example, the *bracket polynomial* of oriented knotoids in $\mathbb{K}(S^2)$ or in $\mathbb{K}(D^2)$ [120] is defined by extending the state expansion of the bracket polynomial of knots. The definition can be given in terms of a skein relation, with the appropriate normalisations, as for the bracket polynomial of knots. A normalisation of the bracket polynomial of knotoids gives rise to a knotoid invariant generalising the Jones polynomial of knots (after a change of variable).

The *arrow polynomial* [49] is defined using an *oriented state expansion* of the bracket polynomial, generalising what was previously done for virtual knots [35]. The arrow polynomial is sufficient to distinguish spherical knotoids with low crossing number [47]. As for the bracket polynomial, the arrow polynomial can be defined recursively using skein relations and a specific set of rules.

It is often hard to distinguish non-equivalent planar knotoids which represent the same class in $\mathbb{K}(S^2)$. Important developments in this direction have been

carried on in [48], where the *loop arrow polynomial* is defined. Together with the invariants coming from our double branched cover construction (see Section 5.3), the arrow polynomial is enough to distinguish low crossing number planar knotoids [47].

5.1.2 Multiplication of knotoids

In [120] an analogue for the connected sum of knots is defined: the multiplication of knotoids. Note that each endpoint of a knotoid diagram k in S^2 admits a neighbourhood D such that k intersects it in exactly one arc (a radius) of D. Such a neighbourhood is called a *regular neighbourhood* of the endpoint. Given two diagrams in S^2 representing the knotoids k_1 and k_2, equipped with a regular neighbourhood D_1 for the head of k_1 and D_2 for the tail of k_2, the *product knotoid* $k = k_1 \cdot k_2$ is defined as the equivalence class in $\mathbb{K}(S^2)$ of the diagram obtained by gluing $S^2 \backslash \text{int}(D_1)$ to $S^2 \backslash \text{int}(D_2)$ through an orientation-reversing homeomorphism $\partial D_1 \longrightarrow \partial D_2$ mapping the only point in $\partial D_1 \cap k_1$ to the only point in $\partial D_2 \cap k_2$. Note that this operation is not commutative [[120], Section 4].

Definition 5.1.3. *A knotoid k in $\mathbb{K}(S^2)$ is called* prime *if it is not the trivial knotoid and $k = k_1 \cdot k_2$ implies that either k_1 or k_2 is the trivial knotoid.*

Knotoids which are neither trivial nor prime are called *composite*. This multiplication operation has been extensively studied in [120], where the following result on prime decomposition is proven.

Theorem 5.1.4 (Theorem 4.2, [120])**.** *Every knotoid k in $\mathbb{K}(S^2)$ expands as a product of prime knotoids.*

Moreover, the expansion as a product is unique up to the identity

$$k \cdot K = K \cdot k$$

where K is a knot-type knotoid, and the multiplication operation turns $\mathbb{K}(S^2)$ into a semigroup.

Remark 5.1.5. Since the surface in which the diagram of $k = k_1 \cdot k_2$ lies is the 2-sphere obtained as the connected sum between the 2-spheres containing the diagrams of k_1 and k_2, the operation of multiplication is well defined in $\mathbb{K}(S^2)$ but not in $\mathbb{K}(D^2)$. A diagram in the plane for k can be obtained by drawing the tail of k_2 in the *external* region of the diagram, as shown in Figure 5.5.

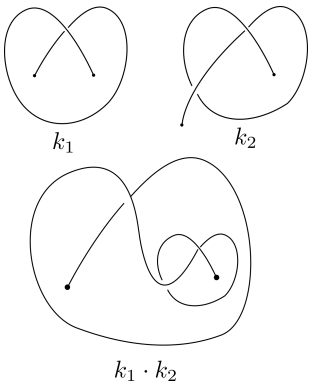

Figure 5.5: On the bottom line, a diagram representing the product $k_1 \cdot k_2$ of the knotoids in the upper line.

Note that the orientation is required in order to define the multiplication operation. In particular, given a knotoid $k \in \mathbb{K}(S^2)$, the following relations hold.

- $k_1 \cdot k_2 = -(-k_2 \cdot -k_1)$
- $-k_1 \cdot k_2 = -(-k_2 \cdot k_1)$
- $k_1 \cdot -k_2 = -(k_2 \cdot -k_1)$
- $k_2 \cdot k_1 = -(-k_1 \cdot -k_2)$

We will sometimes find it useful to consider knotoids up to orientation reversing. To this end, we will call $\mathbb{K}(S^2)/_\sim$ and $\mathbb{K}(D^2)/_\sim$ the sets of unoriented knotoids in the sphere and in the plane, respectively. Note that, in general, the products $k_1 \cdot k_2$, $-k_1 \cdot k_2$, $k_1 \cdot -k_2$ and $k_2 \cdot k_1$ represent different elements in $\mathbb{K}(S^2)/_\sim$, *i.e.* they are not equivalent as unoriented knotoids.

5.2 Knotoids as embedded arcs

As described in [49], it is possible to give a 3-dimensional definition of planar and spherical knotoids, as embedded arcs in D^3, up to a particular isotopy notion.

Consider a knotoid diagram k in D^2, and identify the plane of the diagram with $D^2 \times \{0\} \subset D^3$, where D^3 is seen as $D^2 \times I$, where I is the interval $[-1, 1]$. We can embed k in D^3 by pushing the overpasses of the diagram into the upper half-space, and the underpasses into the lower one. The endpoints v_0 and v_1 of k are attached to two lines $t \times I, h \times I$ perpendicular to $D^2 \times \{0\}$.

Two embedded arcs in D^3 with endpoints lying on these two lines are said to be *line isotopic* if there is a smooth ambient isotopy of the pair $(D^3, t \times I \cup h \times I)$ taking one curve to the other, endpoints to endpoints, and leaving each one of the special lines invariant. Conversely, an embedded curve in D^3 whose projection on $D^2 \times \{0\}$ is generic (plus the additional data of over and under passings) defines a knotoid diagram (see Figure 5.6).

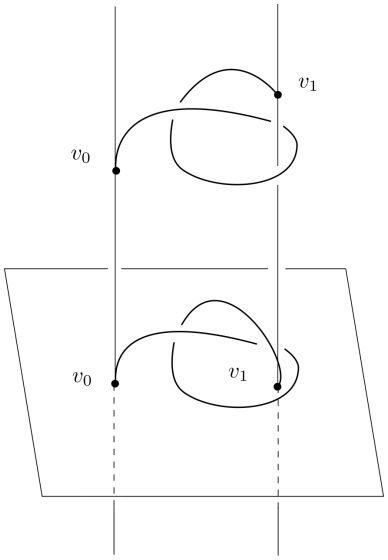

Figure 5.6: On the top, the curve in D^3 obtained from the knotoid diagram on the bottom.

There is a 1-1 correspondence (see [49], Theorem 2.1 and Corollary 2.2) between

the set $\mathbb{K}(D^2)$ of oriented knotoids in D^2 and the set of line-isotopy classes of smooth oriented arcs in D^3, with endpoints attached to two lines perpendicular to $D^2 \times \{0\}$.

Remark 5.2.1. The notion of line isotopy between open arcs is explored also in [72], where *rail knotoids* are introduced. As for line isotopy classes of embedded arcs, rail knotoids corresponds bijectively with planar knotoids. Moreover, the rail knotoid approach is related to the study of genus 2 handlebodies.

Remark 5.2.2. There is an easy way to visualise rotation of knotoids in this setting. Indeed, consider a knotoid k and its rotation $k_{\mathbf{rot}}$. If we view the knotoids as embedded arcs in D^3 with endpoints in $t \times I, h \times I$, then they differ from each other by applying a rotation through an angle π along a horizontal line going through $t \times I$ and $h \times I$.

Similarly, given a knotoid k in $\mathbb{K}(S^2)$ we can construct an embedded arc in $S^2 \times I$ with the same procedure. Now the endpoints are attached to two lines perpendicular to the sphere $S^2 \times \{pt\}$. Theorem 2.1 and Corollary 2.2 in [49] extend naturally to this setting.

Consider a knotoid as an embedded curve in $S^2 \times I$, with endpoints attached to the two special lines. We can compactify the manifold by collapsing $S^2 \times \partial I$ to two points, obtaining an embedded curve in S^3 with endpoints lying on an unknotted circle, as in Figure 5.7.

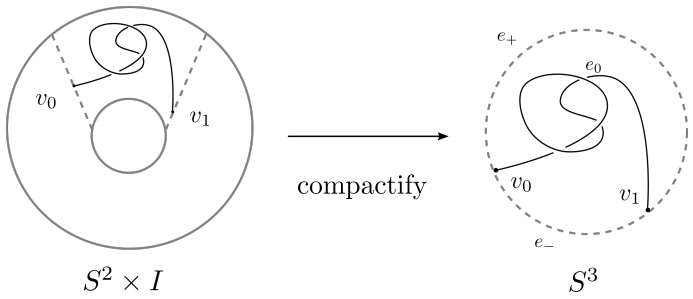

Figure 5.7: On the left, a knotoid seen as an embedded curve in $S^2 \times I$, with endpoints lying on the dotted lines. By collapsing $S^2 \times \partial I$ to two points, we obtain an embedded arc in S^3, with endpoints lying on a dotted circle (the projection of the dotted lines).

The union of the embedded curve with this unknotted circle is a θ-curve.

Definition 5.2.3. *A labelled θ-curve is a graph embedded in S^3 with 2 vertices, v_0 and v_1, and 3 edges, e_+, e_- and e_0, each of which joins v_0 to v_1. The curves $e_0 \cup e_-$, $e_- \cup e_+$ and $e_0 \cup e_+$ are called the* constituent knots *of the θ-curve. We will call two labelled θ-curves isotopic if they are related by an ambient isotopy preserving the labels of the vertices and the edges. A θ-curve is called simple if its constituent knot $e_- \cup e_+$ is the trivial knot.*

Thus, we can associate a simple labelled θ-curve to a knotoid $k \in \mathbb{K}(S^2)$, whose vertices are the endpoints of k and with $e_0 = k$. We label the remaining edges of the θ-curve in the following way (see Figure 5.8). The edge containing the image of $S^2 \times \{1\}$ under the collapsing map is labelled e_+. The edge containing the image of $S^2 \times \{-1\}$ is labelled e_-. We will call the unknotted circle $e_- \cup e_+$ the *preferred constituent unknot* of the θ-curve.

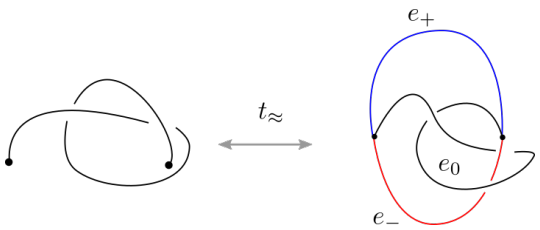

Figure 5.8: A knotoid and its associated simple θ-curve. The constituent knot $e_- \cup e_+$ (the blue&red circle) is the trivial knot.

It is shown in [120] that this construction induces a well defined map t between the set of oriented knotoids $\mathbb{K}(S^2)$ and the set Θ^s of isotopy classes of simple labelled θ-curves. Moreover, Θ^s endowed with the vertex-multiplication operation (for a definition of the vertex-multiplication operation see *e.g.* [120], Section 5, and see Figure 5.13 for an example) is a semigroup, and the following theorem holds.

Theorem 5.2.4 (Theorem 6.2 in [120])**.** *The map $t : \mathbb{K}(S^2) \longrightarrow \Theta^s$ is a semigroup isomorphism.*

The inverse map t^{-1} associates a knotoid in $\mathbb{K}(S^2)$ to a labelled simple θ-curve in the following way. Any element θ of Θ^s can be isotoped to lie in $D^3 \subset S^3$, with the edge e_+ contained in the upper half-space, and e_- in the lower one, in such a way that they both project to a same arc a in D^2 connecting v_0 to v_1. We say that

the θ-curve is in *standard position*. The projection of the edge e_0 to D^2 defines the associated knotoid (see [120] for more details).

It should be clear that the θ-curves associated to a knotoid and its reverse differ by exchanging the labels of the vertices. Consider now a knotoid k and its rotation $k_{\mathbf{rot}}$. Their θ-curves differ from each other simply by swapping the labels on the e_- and e_+ edges, and leaving all other labels unchanged. To see this, arrange the θ-curve $t(k)$ in standard position, and swap the labels e_- and e_+. Then, we can isotope the θ-curve in a way that reinstates e_+ as lying above the horizontal plane and e_- as lying below it. After projecting, we get the knotoid $k_{\mathbf{rot}}$. Thus, swapping the labels of the edges e_- and e_+ takes the θ-curve $t(k)$ to $t(k_{\mathbf{rot}})$, see Figure 5.9.

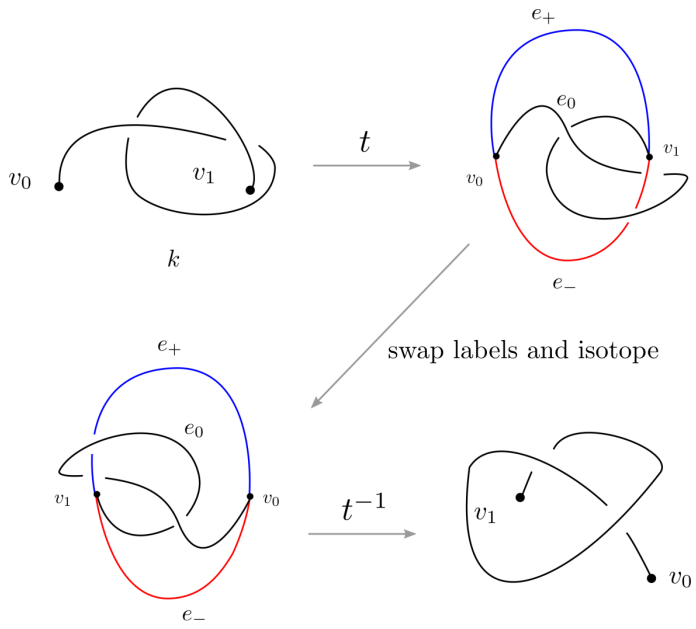

Figure 5.9: A knotoid and its rotation are associated with θ-curves differing from each other by swapping the e_- and e_+ labels.

Call $\Theta^s/_\sim$ the set of simple θ-curves up to relabelling the two vertices. The isomorphism t of Theorem 5.2.4 gives a bijection

$$t_\sim : \mathbb{K}(S^2)/_\sim \longrightarrow \Theta^s/_\sim$$

between unoriented knotoids and elements of $\Theta^s/_\sim$. Furthermore, t also induces a bijection

$$t_\approx : \mathbb{K}(S^2)/_\approx \longrightarrow \Theta^s/_\approx$$

from the set of unoriented knotoids up to rotation and the set of θ-curves up to relabelling the edges e_- and e_+ and the vertices. This latter bijection will be the key element in proving Theorem 4.1.1.

5.3 Double branched coverings

The 3-dimensional interpretation of planar and spherical knotoids suggests a way to associate a knot to every knotoid.

Consider a planar knotoid k, thought of as an embedded arc in the cylinder $D^2 \times I$, with endpoints in $t \times I, h \times I$. The double cover of $D^2 \times I$ branched along $t \times I, h \times I$ is the solid torus $S^1 \times D^2$. This can bee seen in Figure 5.10, that shows how to construct this double branched cover by *cuts*. More precisely, we can cut the cylinder $D^2 \times I$ along two disks (these are the two dashed arcs times I, shown in Figure 5.10), take two copies of the obtained object, and then glue them as shown in the picture. For more details on how to construct branched covers see *e.g.* [[105], Chapter 10.*B*].

Denote the branched covering map by

$$p : S^1 \times D^2 \longrightarrow D^2 \times I$$

The pre-image $p^{-1}(k)$ of the knotoid in the double branched cover is a knot inside the solid torus $S^1 \times D^2$. The knot type of this branched cover is a knotoid invariant; in particular by composing the branched covering construction with any invariant of knots in the solid torus (see *e.g.* [79, 43, 55]) we obtain a new knotoid invariant. Note that by definition, the lifts of line-isotopic embedded arcs are ambient isotopic knots, since isotopies of k preserving the branching set lift to equivariant isotopies.

Remark 5.3.1. From the knotoid diagram obtained by projecting k, it is possible to construct a diagram in the annulus $S^1 \times I$ for $p^{-1}(k)$ by taking the double cover of the disk $D^2 \times \{pt\}$ branched over the endpoints of the diagram, as shown in Figure 5.10.

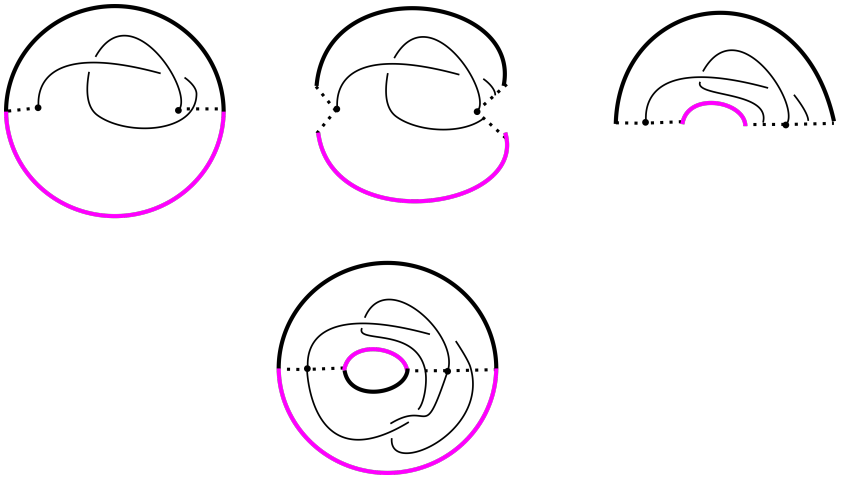

Figure 5.10: The two-fold branched cover of $D^2 \times I$ by $S^1 \times D^2$ can be described by *cuts* (see *e.g.* [[105], Chapter 10.*B*] for a reference). The picture shows the product $D^2 \times I$ seen from above. The black and violet circle in $D^2 \times \{1\}$ (the boundary of $D^2 \times \{1\}$) lifts to two parallel longitudes of the solid torus.

Similarly, given a knotoid $k \in \mathbb{K}(S^2)$ and the associated θ-curve $t(k)$ in S^3, the pre-image of k under the double cover of S^3 branched along the preferred constituent unknot of $t(k)$ is a knot in S^3, see Figure 5.14. Double branched covers of simple θ-curves have been extensively studied in [21], whose main results are discussed and used in Section 5.3.1.

Remark 5.3.2. Consider a diagram representing $k \in \mathbb{K}(S^2)$: we can obtain a diagram for the lift of k by taking the double cover of S^2 branched along the endpoints, as shown in Figure 5.10 and Figure 5.11.

Call $\mathcal{K}(S^1 \times D^2)$ and $\mathcal{K}(S^3)$ the sets of knots in the solid torus and in S^3 respectively, taken up to the appropriate ambient isotopies. Thus, we have the following maps induced by the double branched covers:

$$\gamma_T : \mathbb{K}(D^2) \longrightarrow \mathcal{K}(S^1 \times D^2)$$

$$\gamma_S : \mathbb{K}(S^2) \longrightarrow \mathcal{K}(S^3)$$

Remark 5.3.3. Recall that two knotoids k and $k_{\mathbf{rot}}$ that differ by a rotation lift to θ-curves differing from each other simply by swapping the labels on the e_- and e_+ edges. The double branched covers of such θ-curves produce isotopic knots. Thus,

k and $k_{\mathbf{rot}}$ have the same image under the map γ_S. The same is true for a knotoid k and its reverse $-k$.

Consider a circle in the boundary of $D^2 \times \{pt\}$, as the black and violet one in Figure 5.10. This lifts to two parallel longitudes of the solid torus. We can then define a natural embedding e of the solid torus in S^3 by sending any of these longitudes to the preferred longitude of the solid torus in S^3 arising as the neighbourhood of the standard unknot. By composing γ_T with e we can associate to a knotoid in $\mathbb{K}(D^2)$ a knot in S^3.

Proposition 5.3.4. *Given a knotoid k in $\mathbb{K}(D^2)$, $e(\gamma_T(k)) = \gamma_S(\iota(k))$. Similarly, given $k \in \mathbb{K}(S^2)$ take any planar representative k^{pl} of k. Then, the knot type of $e(\gamma_T(k^{pl}))$ does not depend on the particular choice of k^{pl}.*

In other words, the knot type in S^3 of the lift of a planar knotoid k depends only on its class $\iota(k) \in \mathbb{K}(S^2)$.

Proof. Consider the diagram for k arising from the projection onto $D^2 \times \{pt\}$. The 2-fold cover of the disk branched along the endpoints can be viewed as the restriction of the 2-fold cover of a 2-sphere branched along the endpoints, see Figure 5.11. Thus, isotopies on the sphere below translate into isotopies on the sphere for the lifted diagram.

□

Remark 5.3.5. Note that, as shown in Figure 5.12, non-equivalent knotoids in $\mathbb{K}(D^2)$ that are equivalent in $\mathbb{K}(S^2)$ might lift to different knots in the solid torus.

For knot type knotoids the behaviour under the maps γ_S and γ_T is unsurprisingly trivial.

Proposition 5.3.6. *Consider an oriented knot-type knotoid K. The lift $\gamma_S(K)$ is the connected sum $K'\#rev(K')$, where K' is the knot naturally associated to K (with orientation induced by K) and $rev(K')$ is its inverse.*

Proof. Thanks to Proposition 5.3.4 we can choose a planar diagram for k in which the endpoints lie in the *external region* of the disk, so that there are no intersections (apart from the endpoints themselves) between the diagram and the arc which define the cuts, and the statement is trivially true. □

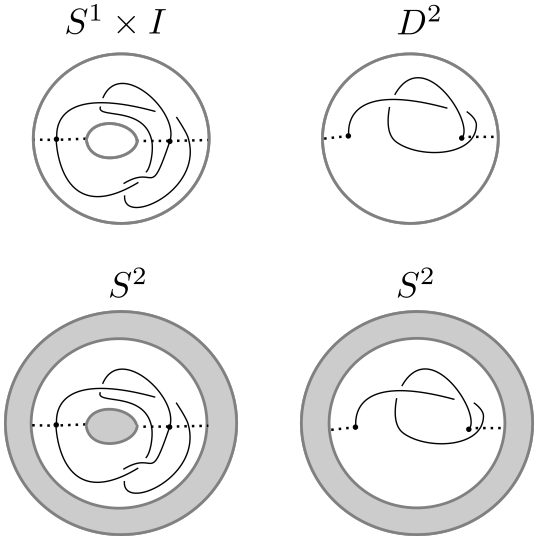

Figure 5.11: On the top, the annulus $S^1 \times I$ as double cover of the disk D^2 branched along two points. On the bottom, the extension of that cover to a double branched cover of the S^2 over the S^2. Isotopies on the sphere on the left-side translate into isotopies on the sphere for the lifted diagrams.

5.3.1 Behaviour under multiplication

In this section we will first discuss the behaviour of γ_S under multiplication of knotoids. Double branched covers of simple θ-curves have been extensively studied in [21].

Definition 5.3.7. *A θ-curve is said to be* prime *if:*

- *it is non-trivial;*
- *it is not the connected sum of a non trivial knot and a θ-curve (as in the top part of Figure 5.13);*
- *it is not the result of a vertex-multiplication of two non-trivial θ-curves (as in the bottom part of Figure 5.13).*

According to Definition 5.3.7, if K is a knot-type knotoid, then $t(K)$ is the vertex multiplication of a non trivial knot and a θ-curve, thus, it is not prime. The following result is attributed to WP Thurston by Moriuchi ([95], Theorem 4.1), and it has been proven in [21].

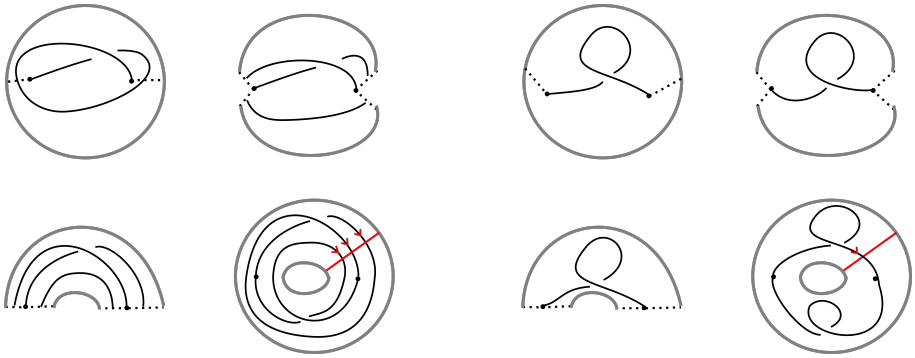

Figure 5.12: Two knotoid diagrams k_1 and k_2 that represent different classes in $\mathbb{K}(D^2)$ such that $\iota(k_1) = \iota(k_2)$ lift to different knots in the solid torus. $\gamma_T(k_2)$ is the core of the solid torus, while $\gamma_T(k_1)$ is the 2_3 knot in Gabrovsek and Mroczkowski's table for knots in the solid torus (see [43]), with winding number equal to 3. However, $e(\gamma_T(k_1)) = e(\gamma_T(k_2)) = \bigcirc$.

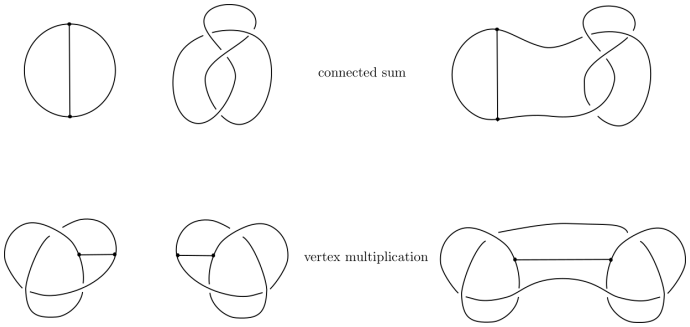

Figure 5.13: On the top, the result of a connected sum between a knot and a θ-curve. On the bottom, the result of a vertex-multiplication of two θ-curves.

Theorem 5.3.8 (Main Theorem in [21])**.** *Consider a simple θ-curve a, with unknotted constituent knot a_1, and let K be the closure of the pre-image of $a \setminus a_1$ under the double cover of S^3 branched along a_1. Then K is prime if and only if a is prime.*

Theorem 5.3.8 together with Theorem 5.2.4 directly imply the following result on knotoids.

Theorem 5.3.9. *The lift $\gamma_S(k)$ of a proper knotoid k is prime if and only if k is prime. In particular $\gamma_S(k_1 \cdot k_2) = \gamma_S(k_1) \# \gamma_S(k_2)$.*

Note that even if the products $k_1 \cdot k_2$ and $k_2 \cdot k_1$ are in general distinct both

as oriented and unoriented knotoids (see the relations described in Section 5.1.2), their lifts are equivalent as knots in S^3. This seems to imply that γ_S cannot tell apart $k_1 \cdot k_2$ and $k_2 \cdot k_1$. Indeed, to distinguish them it is necessary to use the information on the involution defined by the double branched cover construction, as we will see in Section 5.5.2.

5.3.2 Knotoids and strongly invertible knots

Consider a knotoid $k \in \mathbb{K}(S^2)$ and its lift $\gamma_S(k)$ in S^3. The fact that S^3 is the double cover of itself branched along the preferred constituent unknot ◯ of $t(k)$ defines an orientation preserving involution τ of S^3, whose fixed point set $fix(\tau)$ is precisely the unknot ◯. The involution τ reverses the orientation of $\gamma_S(k)$, and the fixed point set intersects $\gamma_S(k)$ in exactly two points (the lifts of the endpoints of k). The involution τ is called a *strong inversion*, and a knot with this property is called a *strongly invertible knot* (a precise definition will be given in Section 5.5).

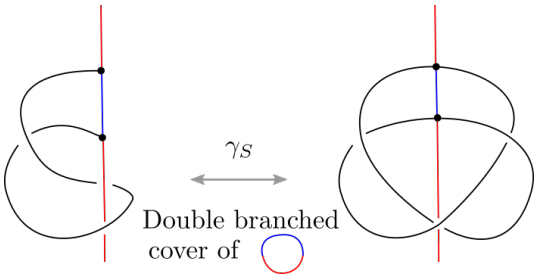

Figure 5.14: The trefoil 3_1 admits a strong inversion. On the left, a simple θ-curve and the associated trefoil knot obtained by taking the double cover of S^3 branched along $e_- \cup e_+$. The fixed point set of τ is the unknot $e_- \cup e_+$, shown as a vertical line on the right side of the picture.

Since not every knot in S^3 admits a strong inversion, this in particular implies that the maps γ_S and γ_T are not surjective.

Remark 5.3.10. We could have inferred the non-surjectivity of the map γ_T from the following observation.

The winding number $[\gamma_T(k)] \in H_1(S^1 \times D^2; \mathbb{Z})$ of the lift $\gamma_T(k)$ of a knotoid k is always odd. This is true since by construction the lifted knot intersects the meridian disk containing the lifted branching points an odd number of times.

In Section 5.5 we will use classical results on symmetry groups of knots to better understand the map γ_S and to prove the 1-1 correspondence of Theorem 4.1.1.

5.4 Trivial knotoid detection

This section is devoted to the proof of two different results on the detection of the trivial knotoid.

Our double branched cover construction provides a way to detect the trivial knotoid $0_1 \in \mathbb{K}(S^2)$, thanks to the following result.

Theorem 5.4.1 (Lemma 2.3 in [21])**.** *A knotoid $k \in \mathbb{K}(S^2)$ lifts to the trivial knot in S^3 if and only if k is the trivial knotoid 0_1 in $\mathbb{K}(S^2)$.*

Theorem 5.4.1 is proven for θ-curves. In the setting of knotoids, a slightly more powerful version of this result holds, allowing for the detection of the trivial planar knotoid $0_1^{\text{pl}} \in \mathbb{K}(D^2)$ as well.

Theorem 5.4.2. *A knotoid $k \in \mathbb{K}(D^2)$ lifts to a knot isotopic to the core of the solid torus if and only if $k = 0_1^{pl}$ in $\mathbb{K}(D^2)$.*

Proof. If k is the trivial knotoid, then its lift is a knot isotopic to the core of the solid torus (see *e.g.* the right side of Figure 5.12). Conversely, suppose that $\gamma_T(k)$ is isotopic to the core C of the solid torus $S^1 \times D^2$. Then, its complement in the solid torus is homeomorphic to the product $T^2 \times I$. Since $T^2 \times I$ arises as a double branched cover, there is an involution τ of $T^2 \times I$ with 4 disjoint arcs as fixed set (see Figure 5.15).

Thanks to the following result we know that the involution defined by the double branched cover respects the product structure on $T^2 \times I$.

Theorem 5.4.3 (Theorem A of [68])**.** *Let h be a PL involution of $F \times I$, where F is a compact surface, such that $h(F \times \partial I) = F \times \partial I$. Then, there exist an involution g of F such that h is equivalent (up to conjugation with homeomorphisms) to the involution of $F \times I$ defined by $(x, t) \mapsto (g(x), \lambda(t))$ for $(x, t) \in F \times I$, and where $\lambda : I \longrightarrow I$ is either the identity or $t \mapsto 1 - t$.*

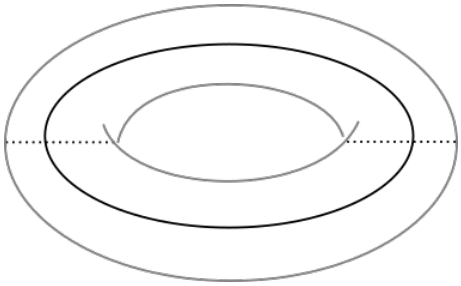

Figure 5.15: $T^2 \times I$ admits an involution with fixed set the union of 4 arcs. These arcs are the intersection between the lines defining the cover and the complement of a tubular neighbourhood of the lifted knot (the core of the solid torus).

The intersection between the fixed set $Fix(\tau)$ and every torus $T^2 \times \{pt\}$ consists of 4 isolated points, as highlighted in Figure 5.15. Involutions of closed surfaces are completely classified; the following result is well known, and it probably should be attributed to [70], but we refer to [34] for a more modern and complete survey.

Theorem 5.4.4 (Theorem 1.11 of [34])**.** *There is only one involution $\bar{\tau}$, up to conjugation with homeomorphisms, for the torus $S^1 \times S^1$ with 4 isolated fixed points. This involution is shown in Figure 5.16; it is orientation preserving and it is induced by a rotation of π about the dotted line indicated in the picture.*

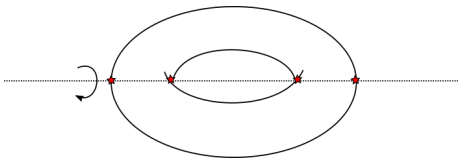

Figure 5.16: The involution of the torus with 4 fixed points, indicated with the red stars.

With an abuse of notation, call $\bar{\tau}$ the involution of $T^2 \times I$ obtained as the product $\bar{\tau} \times Id_I$. Since conjugated involutions produce homeomorphic quotient spaces, thanks to the previous two results we can say that the complement of the trivial knot in the solid torus projects to a homeomorphic copy of the complement of the trivial knotoid in the three-ball. In other words, our quotient space $T^2 \times I/\tau$ is homeomorphic to $T^2 \times I/\bar{\tau}$, the last one being precisely the complement of the trivial knotoid, as in Figure 5.17.

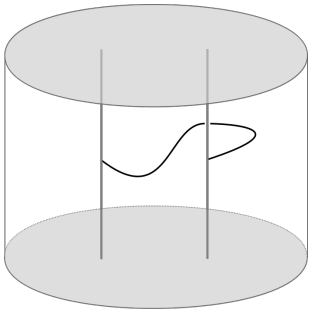

Figure 5.17: The quotient space under the involution is homeomorphic to the complement of the trivial knotoid in the cylinder.

We will be done once we prove that the line isotopy class of the curve in Figure 5.17 is not affected by the action of homeomorphisms; this is a consequence of the following proposition. Let Y be the cylinder $D^2 \times I$, and call $MCG(Y; p, q)$ the group of isotopy classes of automorphisms of Y that leave $p \times I$ and $q \times I$ invariant, where p, q are points in the interior of $D^2 \times \{pt\}$.

Proposition 5.4.5. *$MCG(Y; p, q)$ is isomorphic to $\mathbb{Z}$, and it is generated by a Dehn-twist along the blue rectangle in Figure 5.18.*

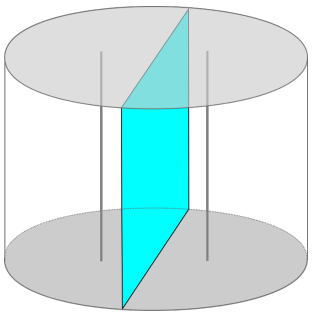

Figure 5.18: $MCG(Y; p, q)$ is generated by a Dehn twist along the boundary of the blue rectangle.

The proof of Proposition 5.4.5 requires a couple of preliminary results. First, note that removing the two lines yields a 3-dimensional genus 2 handlebody H. The homeomorphisms of a handlebody are determined by their behaviour on the boundary. More precisely, the mapping class group of a handlebody can be identified with the subgroup of the mapping class group of its boundary, consisting

of homeomorphisms that can be extended to the handlebody due to the following lemma.

Lemma 5.4.6. *Let H be a genus 2 handlebody. Any homeomorphism $\phi : H \longrightarrow H$ such that $\phi\big|_{\partial H}$ is isotopic to $Id_{\partial H}$ is isotopic to Id_H.*

The previous lemma is well known, and a proof may be found *e.g.* in Chapter 3 of [42].

Remark 5.4.7. Recall that a self homeomorphism of the boundary of a handlebody can be extended to the handlebody if and only if the image of the boundary of every meridian disc is contractible in the handlebody. In particular, Dehn twists along the blue curves in Figure 5.19 do not extend to the handlebody.

Now, cutting the boundary of the handlebody H along the blue curves, as in Figure 5.19, produces a sphere with 4 holes S.

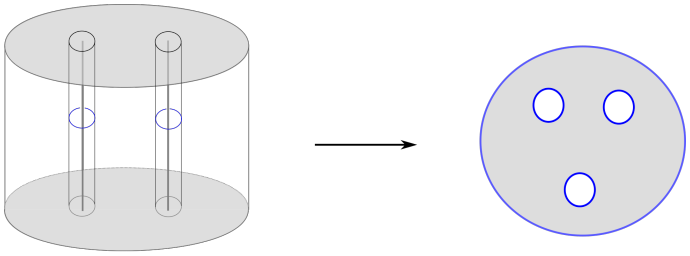

Figure 5.19: Cutting the boundary of the handlebody along the blue curves gives back the sphere with 4 holes S.

A proof for the following lemma can be deduced from *e.g.* the proof of Proposition 2.7, Chapter 2, [39]. Given a surface S with boundary, denote by $MCG(S, \partial S)$ the group of isotopy classes of orientation-preserving homeomorphisms of S that leave each boundary component invariant.

Lemma 5.4.8. *Let S be the sphere with 4 holes. Then, $MCG(S, \partial S)$ is isomorphic to a subgroup of $MCG(T^2)/-Id \cong PSL(2, \mathbb{Z})$.*

Thus, we defined a homomorphism $MCG(Y; p, q) \longrightarrow MCG(S, \partial S)$, and an injective homomorphism $MCG(S, \partial S) \longrightarrow PSL(2, \mathbb{Z})$. An element in the kernel of the composition of these two homomorphisms is then an automorphism of ∂H

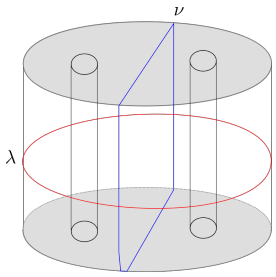

Figure 5.20: $\phi : S \longrightarrow S$ in $MCG(S, \partial S)$ is completely determined by the images of the curves ν and λ.

that leaves the two blue curves in the left side of Figure 5.19 invariant and that is isotopic to the identity on S. Such an element is a product of Dehn twists about the two blue curves of Figure 5.19, but thanks to Remark 5.4.7, the only element in $MCG(Y; p, q)$ of that form is the trivial element. Moreover, Lemma 5.4.8 is proven by exhibiting a bijection between homotopy classes of essential closed curves in T^2 and in S, and this in particular implies that any homeomorphism $\phi : S \longrightarrow S$ leaving each component of ∂S invariant is completely determined by the images of the curves ν and λ in Figure 5.20. Now, $\phi(\nu) = \nu$, since ν is the only essential closed curve in S which is trivial in $H_1(H)$; on the other hand, Remark 5.4.7 implies that $\phi(\lambda)$ is the curve that results from λ by applying a Dehn twist along ν. Putting all together, we obtain a proof for Proposition 5.4.5 and Theorem 5.4.2, as wanted.

□

5.5 Knotoids and strongly invertible knots

5.5.1 Proof of the main correspondence

This section is devoted to the proof of the main result, Theorem 4.1.1 above.

Theorem. *There is a* 1-1 *correspondence between unoriented knotoids, up to rotation, and knots K with a strong inversion τ, up to conjugacy.*

We should point out that the correspondence between knotoids and strongly invertible knots is partially inspired by the construction in [131], Section 2.2. We begin by giving a precise definition of what a strongly invertible knot is. Recall

that $Sym(S^3, K)$ denotes the symmetry group of a knot K, that is, the group of diffeomorphisms of the pair (S^3, K) modulo isotopies, and $Sym^+(S^3, K)$ is the subgroup of $Sym(S^3, K)$ of diffeomorphisms preserving the orientation of S^3.

Definition 5.5.1. *A* strongly invertible knot *is a pair (K, τ), where $\tau \in Sym(S^3, K)$ is called a* strong inversion*, and it is an orientation preserving involution of S^3 that reverses the orientation of K, taken up to conjugacy in $Sym^+(S^3, K)$. Thus, two strongly invertible knots (K_1, τ_1) and (K_2, τ_2) are equivalent if there is an orientation preserving homeomorphism $f : S^3 \longrightarrow S^3$ satisfying $f(K_1) = K_2$ and $f\tau_1 f^{-1} = \tau_2$.*

Call $\mathcal{K}SI(S^3)$ the set of strongly invertible knots (K, τ) in S^3, up to equivalence, and $\mathcal{K}_{SI}(S^3)$ the subset of $\mathcal{K}(S^3)$ consisting of knots that admit a strong inversion. There is then a natural forgetful map $\mathcal{K}SI(S^3) \longrightarrow \mathcal{K}_{SI}(S^3)$. As we saw in Section 5.3.2, the lift of a knotoid through the double branched cover of S^3 is a strongly invertible knot, thus, $\gamma_S(\mathbb{K}(S^2)) \subset \mathcal{K}_{SI}(S^3)$. More precisely, the branching set $e_- \cup e_+$ determines an involution τ. Thus, we can promote γ_S to a map $\gamma_S : \mathbb{K}(S^2) \longrightarrow \mathcal{K}SI(S^3)$. Further, a knotoid k, its reverse $-k$, its rotation $k_{\mathbf{rot}}$ and its reverse rotation $-k_{\mathbf{rot}}$ map to the same element in $\mathcal{K}SI(S^3)$ (see Remark 5.3.3, and note that their associated θ-curves share the same preferred constituent unknot $e_- \cup e_+$). Thus, γ_S descends to a well defined map on the quotient

$$\gamma_{S_\approx} : \mathbb{K}(S^2)/_\approx \longrightarrow \mathcal{K}SI(S^3)$$

On the other hand, given a strongly invertible knot there are four oriented knotoids associated to it, given by the construction explained below. Consider a strongly invertible knot $(K, \tau) \in \mathcal{K}SI(S^3)$; the fixed point set of τ is an unknotted circle (thanks to the positive resolution of the Smith conjecture, [128]). Moreover, τ defines the projection

$$p : S^3 \longrightarrow S^3/\tau \cong S^3$$

that can be interpreted as the double cover of S^3 branched along $Fix(\tau)$.

Remark 5.5.2. The trefoil is a strongly invertible knot. Up to isotopy, we can represent the fixed point set as the z axis in $\mathbb{R}^3$, see the right side of Figure 5.14. On the left of the picture, the θ-curve obtained from the projection.

From (K,τ) we can construct the θ-curve $\theta(K,\tau) = p(Fix(\tau)) \cup p(K)$, where $p(K) = e_0$ and $p(Fix(\tau)) = e_- \cup e_+$, as explained in [107]. Equivalent strongly invertible knots project to equivalent θ-curves (as elements of $\Theta^s/_\approx$), thus, we have a well defined map

$$\beta : \mathcal{K}SI(S^3) \longrightarrow \Theta^s/_\approx$$

The four labelled θ-curves corresponding to the different choices of labelling the edges e_- and e_+ and the vertices v_0 and v_1 are mapped by the isomorphism t of Theorem 5.2.4 to knotoids k,$-k$, $k_{\mathbf{rot}}$ and $-k_{\mathbf{rot}}$ related by reversion and rotation, as discussed in Section 5.3. Thus, we have a well defined map

$$\Pi = t_{\approx}^{-1} \circ \beta$$

from the set of strongly invertible knots to the set $\mathbb{K}(S^2)/_\approx$ of unoriented knotoids in S^2 up to rotation. Since the preferred constituent unknot of $t_\approx(t_\approx^{-1}(\theta(K,\tau))) = \theta(K,\tau)$ is clearly $p(Fix(\tau))$, Π is the inverse of $\gamma_{S_\approx}$. From this and the discussion in Section 5.3.2 we obtain that

$$\gamma_{S_\approx} : \mathbb{K}(S^2)/_\approx \longrightarrow \mathcal{K}SI(S^3)$$

is a bijection, and Theorem 4.1.1 is proven.

5.5.2 Connected sums

Call k_1 the knotoid on the left-side of Figure 5.2, and consider the product $k_1 \cdot k_1$. Its image under γ_S is the composite knot $3_1\#3_1$ (see *e.g.* Figure 5.33, and recall Theorem 5.3.9). We know from Proposition 5.3.6 that the knot-type knotoid k associated to the trefoil knot lifts to $3_1\#3_1$ as well (the trefoil is invertible, thus 3_1 is isotopic to its reverse -3_1). Theorem 4.1.1 implies that $3_1\#3_1$ admits at least two non-equivalent involutions, associated to the equivalence classes in $\mathbb{K}(S^2)/_\approx$ of the knotoids $k_1 \cdot k_1$ and k, respectively. These non-equivalent involutions are shown in Figure 5.21.

Similarly, Figure 5.22 shows two different involutions of the composite knot $3_1\#8_{20}$, defining different composite knotoids.

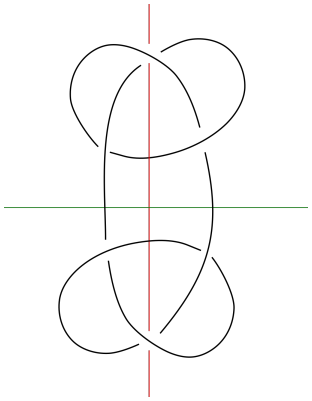

Figure 5.21: The fixed point sets of two non-equivalent involutions are shown here. The one corresponding to the vertical line associates the knot $3_1\#3_1$ to $k_1 \cdot k_1$. The quotient under the involution corresponding to the horizontal line is the one associated to the knot-type knotoid k.

5.5.3 Strong inversions

It is a classical result [73] that every knot admits a finite number of non equivalent strong inversions. For torus and hyperbolic knots[1] a stronger result holds. Recall that we say that a knot K *admits period* 2 if it is fixed by an orientation preserving involution which also preserves the knot orientation. More precisely, K has *cyclic* (respectively *free*) period 2 if there exist a non-trivial $\phi \in Sym^+(S^3, K)$ with $\phi^2 = id$, that preserves the orientation on K, with $fix(\phi)$ an unknot (respectively $fix(\phi) = \varnothing$).

Theorem 5.5.3 (Proposition 3.1, [107])**.** *A torus knot admits exactly one strong inversion. If a hyperbolic knot is strongly invertible, then it admits either* 1 *or* 2 *non equivalent inversions, and it admits exactly* 2 *if and only if it admits (cyclic or free) period* 2*.*

The previous result together with Theorem 4.1.1 proves Corollary 4.1.2.

Corollary. *Given any torus knot K_t there is exactly* 1 *knotoid associated to it, up to rotation and reversion. Given any strongly invertible hyperbolic knot K_h there are either* 1 *or* 2 *knotoids associated to it up to reversion and rotation, depending*

[1]The definition of torus and hyperbolic knots is given in Appendix A.1.

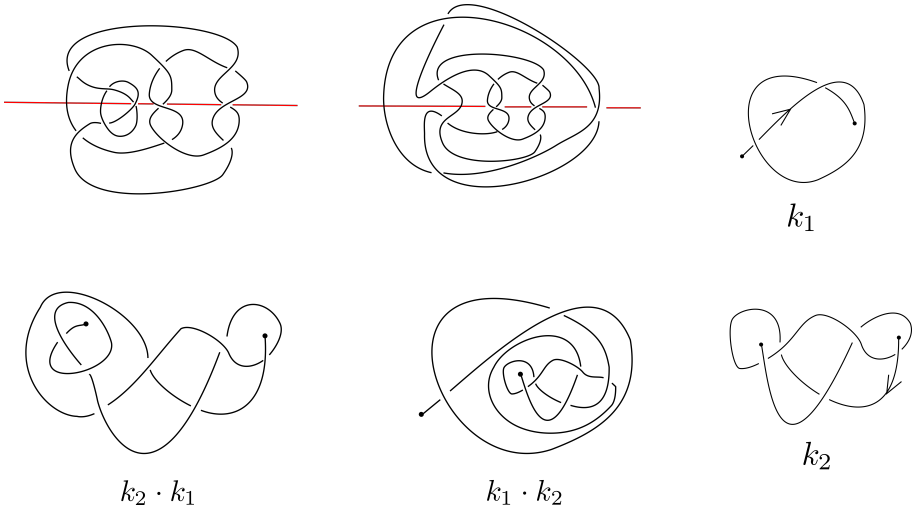

Figure 5.22: Two different involutions of the composite knot $3_1\#8_{20}$, associated to the composite knotoids $k_1 \cdot k_2$ and $k_2 \cdot k_1$.

on whether or not K_h is periodic with period 2. In general, given any strongly invertible knot K there are only finitely many knotoids associated to it.

Thus, to every torus knot there is a single knotoid associated up to reversion and rotation, and to every hyperbolic knot there are at most two. We give the following definition, borrowed from classical knot theory.

Definition 5.5.4. *We will call* torus knotoids *the knotoids whose lifts are torus knots. Similarly, we will call* hyperbolic knotoids *those lifting to hyperbolic knots.*

More generally, only finitely many knotoids are associated with a single knot type. Hence it is natural to ask the following.

Question 5.5.5. *Is there an algorithm to decide whether two knotoids k_1 and k_2 are equivalent?*

Since there are now several known ways to solve the knot recognition problem (for a survey, see *e.g.* [77] and [37]), the next step to answer Question 5.5.5 positively would be to decide whether two given involutions of a knot complement are conjugate homeomorphisms. Using the solution to the equivalence problem for hyperbolic knots [86, 76], since there is an algorithm to decide whether two involutions of a hyperbolic knot complement are conjugate [78], this can be done

in the hyperbolic case. Thus, it is possible to tell if two hyperbolic knotoids k_1 and k_2 represent equivalent classes in $\mathbb{K}(S^2)/_{\approx}$. This is enough to distinguish them as oriented knotoids.

Theorem 5.5.6. *Given two hyperbolic knotoids k_1 and k_2, there is an algorithm to determine whether k_1 and k_2 are equivalent as oriented knotoids.*

Proof. By the previous discussion, we can tell if k_1 and k_2 represent equivalent classes in $\in \mathbb{K}(S^2)/_{\approx}$. Suppose they do, and note that since the mapping class group of a hyperbolic knot is computable [54], we can tell whether their lifts admits or not period 2. If it does, then Corollary 4.1.5 (a proof of which is contained in Section 5.6) tells us that exactly one of the following holds:

- k_1 and k_2 are isotopic as oriented knotoids;
- k_1 is isotopic to $k_{\mathbf{2rot}}$.

We can then consider the diagrams of k_1 and k_2 given as an input, and any diagram of $k_{\mathbf{2rot}}$. Now, if two diagrams represent equivalent knotoids, then there exists a finite sequence of Reidemeister moves and isotopies taking one to the other. Since we know that k_1 is equivalent to one between k_2 and $k_{\mathbf{2rot}}$, after a finite number of Reidemeister moves and isotopies performed on k_1, this will transform into either k_2 or $k_{\mathbf{2rot}}$. Similarly, if the lift of k_1 and k_2 does not admit period 2, Corollary 4.1.5 ensures that exactly one of the following holds:

- k_1 and k_2 are isotopic;
- k_1 is isotopic to $-k_2$;
- k_1 is isotopic to $k_{\mathbf{2rot}}$;
- k_1 is isotopic to $-k_{\mathbf{2rot}}$.

And we can distinguish between these possibilities exactly as before. □

Remark 5.5.7. Note that Question 5.5.5 can be answered positively using the correspondence between knotoids and θ-curves (Theorem 5.2.4). Indeed, given two θ-curves, we can consider their complements in S^3, together with the data of the

meridians of the three edges. We could then let Haken's algorithm [50, 117]) run to decide whether or not the obtained 3-manifolds are equivalent. However, the algorithm of Theorem 5.5.6 appears to be practical, whereas Haken's algorithm is not.

5.5.4 An example: the $T_{2,2k+1}$-torus knotoids

Every $T_{2,2k+1}$-torus knot admits a diagram of the form shown in the upper part of Figure 5.23, where its unique involution τ is represented as a straight line.

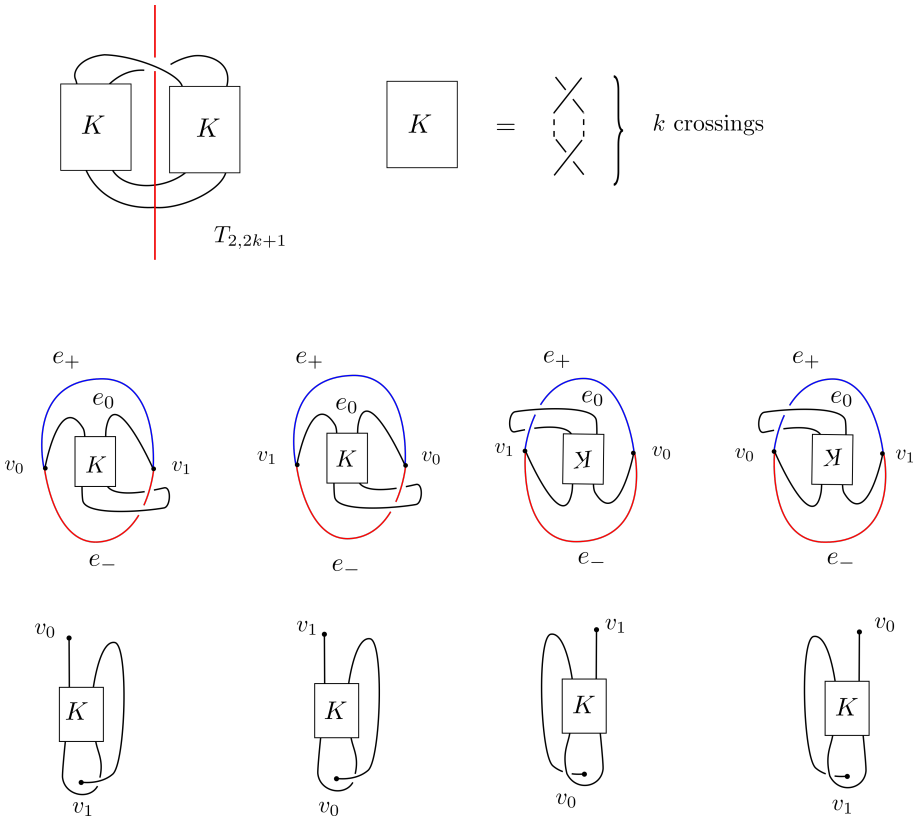

Figure 5.23: On the top, a diagram representing the torus knot $T_{2,2k+1}$. The K box contains k consecutive crossings of the same sign, as shown on the top-right side of the picture. Note that rotating K by π does not change it. The unique involution τ of $T_{2,2k+1}$ gives 4 labelled θ-curves and their associated oriented knotoids. These are related to one another by reversion and rotation.

Recall that, as defined in Section 5.5.1, the inverse of $\gamma_{S_\approx}$ is given by $\Pi = t_\approx^{-1} \circ \beta$, where β is the map from the set of strongly invertible knots $\mathcal{K}SI(S^3)$ to the set

$\Theta^s/_\approx$ of equivalence classes of simple and labelled θ-curves, and $t_\approx$ is the bijection $t_\approx : \mathbb{K}(S^2)/_\approx \longrightarrow \Theta^s/_\approx$. In the equivalence class of $\beta(T_{2,2k+1})$ there are *a priori* 4 distinct labelled θ-curves. These are shown in the middle of Figure 5.23, over their associated knotoids. Using these canonical representatives of $\Pi(T_{2,2k+1}, \tau)$ we can prove the following.

Proposition 5.5.8. *Every $T_{2,2k+1}$-torus knotoid is reversible.*

Proof. First, observe that it is enough to prove that one of the knotoids in Figure 5.23 is reversible, since rotation and reversion commute. The proof is contained in Figure 5.24.

□

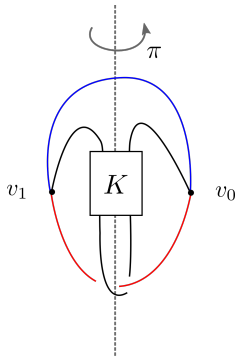

Figure 5.24: A proof that the $T_{2,2k+1}$-torus knotoids are reversible. The rotation by π sends the θ-curve associated to a $T_{2,2k+1}$-torus knotoid into the one corresponding to its reverse.

The previous proposition, together with Corollary 4.1.2 implies that there are at most 2 oriented knotoids associated to every $T_{2,2k+1}$-torus knot. These knotoids are reversible and related by a rotation.

5.6 Amphichirality, reversibility and rotatability in hyperbolic knotoids

In this section we show how Corollary 4.1.2 can be improved in two different ways, by considering properties of the symmetry groups of hyperbolic knots. Much of this section uses the machinery of *orbifolds*, which is revised in Appendix A.2.

5.6.1 Reversible knotoids

Even if the maps γ_S and γ_T cannot distinguish between two knotoids differing only in the orientation, using γ_S it is possible to tell whether a hyperbolic knotoid is reversible or not, and whether it is rotatable or not. The following lemma follows from Theorem 5.2.4.

Lemma 5.6.1. *An oriented knotoid $k \in \mathbb{K}(S^2)$ is reversible (respectively rotatable) if and only if there is an isotopy taking the θ-curve $t(k)$ back to itself, that preserves each edge but swaps the two vertices (respectively, that preserves e_0, and swaps e_+ and e_- and the vertices).*

Furthermore, we can prove that the isotopies of the previous lemma have order 2.

Proposition 5.6.2. *A hyperbolic, oriented knotoid $k \in \mathbb{K}(S^2)$ is reversible (respectively, equivalent to the reverse of its rotation) if and only if there is an order two orientation preserving homeomorphism of S^3 taking the θ-curve $t(k)$ back to itself, that preserves each edge but swaps the two vertices (respectively, that preserves e_0 and swaps the two vertices and e_- and e_+).*

Proof. One direction is clear. So suppose that k is a hyperbolic knotoid that is either reversible or equivalent to the reverse of its rotation. Let $t(k)$ be the corresponding θ-curve, with edges labelled e_-, e_+ and e_0, and where $e_- \cup e_+$ is the preferred constituent unknot. By hypothesis, $\gamma_S(k)$ is a hyperbolic knot. The involution on the hyperbolic manifold $S^3 \setminus \text{int}(N(\gamma_S(k)))$ is realised by a hyperbolic isometry τ by Theorem A.2.1. The quotient $(S^3 \setminus \text{int}(N(\gamma_S(k)))/\tau$ is therefore a hyperbolic orbifold $\mathcal{O}$. Its underlying space is the 3-ball $S^3 \setminus \text{int}(N(e_0))$, and its singular locus is the intersection with $e_- \cup e_+$. Now, we are assuming that k is either reversible or equivalent to the reverse of its rotation. Hence, by Lemma 5.6.1, there is a homeomorphism ρ of S^3 taking $t(k)$ back to itself, that preserves each edge but swaps the two vertices, or that swaps both the vertices and the edges e_- and e_+. In both cases, this therefore induces a homeomorphism of $\mathcal{O}$ that preserves its singular locus. By Mostow rigidity, this is homotopic to an isometry $\overline{\rho}$ of $\mathcal{O}$. In both cases, the action of $\overline{\rho}^2$ on $\partial\mathcal{O}$ is isotopic to the identity,

via an isotopy that preserves the singular points throughout. Hence, because it is an isometry of a Euclidean pillowcase orbifold, $\overline{\rho}^2$ is the identity. Therefore, $\overline{\rho}^2$ is actually equal to the identity on $\mathcal{O}$. So, in both cases, $\overline{\rho}$ extends to the required order two homeomorphism of S^3, taking $t(k)$ back to itself, that preserves each edge but swaps the two vertices or that preserves e_0 and swaps the vertices and the two other edges. □

Sakuma and Kodama [71] proved that, given an invertible hyperbolic knot K with a strong involution τ, the existence of such symmetries for the θ-curve $\theta(K,\tau)$ is completely determined by $Sym(S^3,K)$.

Theorem 5.6.3 (Proposition 1.2, [71])**.** *Given an invertible hyperbolic knot K with a strong inversion τ, then $Sym(S^3,K)$ admits cyclic (respectively free) period 2 if and only if there exist an orientation preserving involution of S^3 fixing setwise $\theta(K,\tau)$ that preserves each edge but swaps the two vertices (respectively, that preserves e_0, and swaps e_+ and e_- and the vertices)*[2]*.*

As an immediate corollary of Theorem 5.6.3 and Lemma 5.6.2 we have the following characterisation for hyperbolic knotoids, which is a restatement of Theorem 4.1.3.

Theorem 5.6.4. *A hyperbolic, oriented knotoid $k \in \mathbb{K}(S^2)$ is reversible if and only if $\gamma_S(k)$ has cyclic period 2. Analogously, it is equivalent to the reverse of its rotation if and only if $\gamma_S(k)$ has free period 2.*

5.6.2 Hyperbolic knotoids are not rotatable

Recall that a knotoid $k \in \mathbb{K}(S^2)$ is called rotatable if it is isotopic to its rotation $k_{\mathbf{rot}}$. For hyperbolic knotoids, we show that this is never the case.

Theorem 5.6.5. *A hyperbolic knotoid is never rotatable.*

Proof. Associated to the hyperbolic knotoid k, there is the θ-curve $t(k)$, which has three edges e_0, e_- and e_+, and where $e_- \cup e_+$ is the preferred constituent unknot.

[2]In [71] Sakuma and Kodama call $\theta(K,\tau)$ *strongly reversible* in the first case, and say that $\theta(K,\tau)$ has *period* 2 *centred in* $e_0 = p(K)$ in the second case.

By hypothesis, $\gamma_S(k)$ is a hyperbolic knot. As in the proof of Proposition 5.6.2, the involution on the hyperbolic manifold $S^3 \setminus \text{int}(N(\gamma_S(k)))$ is realised by a hyperbolic isometry τ. The quotient $(S^3 \setminus \text{int}(N(\gamma_S(k)))/\tau$ is a hyperbolic orbifold $\mathcal{O}$. Its underlying space is the 3-ball $S^3 \setminus \text{int}(N(e_0))$, and its singular locus is the intersection with $e_- \cup e_+$. Let $k_{\mathbf{rot}}$ be the knotoid obtained by rotating k. If we suppose that $k_{\mathbf{rot}}$ and k are equivalent, then by Lemma 5.6.2 there is a homeomorphism of S^3 taking $t(k)$ back to itself that swaps the edges labelled e_- and e_+ and leaves all other labels unchanged. This therefore induces a homeomorphism $h\colon \mathcal{O} \to \mathcal{O}$ that preserves the singular locus. It is homotopic to an isometry $\overline{h}\colon \mathcal{O} \to \mathcal{O}$.

We claim that $\overline{h}$ is not equal to the identity, but that $(\overline{h})^2$ is the identity. First observe that h swaps the two components of the singular locus. These are distinct geodesics in $\mathcal{O}$. Thus, the isometry $\overline{h}$ also swaps these two geodesics and therefore is not the identity. On the other hand, h^2 acts as the identity on $\partial N(t(k))$. Hence, the restriction of $(\overline{h})^2$ to $\partial\mathcal{O}$ is isotopic to the identity, via an isotopy that preserves the singular points of $\partial\mathcal{O}$. But any isometry of a Euclidean pillowcase orbifold that is isotopic to the identity via an isotopy preserving the singular points must be equal to the identity. So the restriction of the isometry $(\overline{h})^2$ to $\partial\mathcal{O}$ is the identity and hence $(\overline{h})^2$ is the identity on $\mathcal{O}$. By the double branched cover construction, we obtain $p\colon S^3 - \text{int}(N(\gamma_S(k))) \to \mathcal{O}$ that is an orbifold covering map. This induces a homomorphism $p_*\colon \pi_1(S^3 - \text{int}(N(\gamma_S(k))) \to \pi_1(\mathcal{O})$. The image of this homomorphism is an index 2 subgroup of $\pi_1(O)$. This subgroup consists of those loops in $S^3 - \text{int}(N(t(k)))$ that have even linking number with the unknot $e_- \cup e_+$.

Now $\overline{h}$ lifts to an isometry $\phi\colon S^3 \setminus \text{int}(N(\gamma_S(k))) \to S^3 \setminus \text{int}(N(\gamma_S(k)))$. This is because $\overline{h}_*\colon \pi_1(\mathcal{O}) \to \pi_1(\mathcal{O})$ preserves the subgroup $p_*\pi_1(S^3 - \text{int}(N(\gamma_S(k)))$. This lift ϕ swaps the arcs $p^{-1}(e_- \cap \mathcal{O})$ and $p^{-1}(e_+ \cap \mathcal{O})$. It preserves each of the meridians of $\gamma_S(k)$ at the endpoints of these arcs. To see this, pick a small arc α in $\partial\mathcal{O}$ near one of the endpoints of k, joining a point of $e_- \cap \partial\mathcal{O}$ to a point of $e_+ \cap \partial\mathcal{O}$. This is preserved by h and hence the Euclidean geodesic representative for α is preserved by $\overline{h}$. The inverse image of this geodesic in $S^3 \setminus \text{int}(N(\gamma_S(k)))$ is therefore a meridian of $\gamma_S(k)$ that is preserved by ϕ. Hence, ϕ extends to an involution of S^3 that fixes $\gamma_S(k)$. But no such symmetry exists, by the solution to the Smith Conjecture, since $\gamma_S(k)$ is a non-trivial knot. □

Remark 5.6.6. Consider a hyperbolic knotoid k, and suppose that its lift $\gamma_S(k)$ admits simultaneously free and cyclic period 2. Then, by Theorem 5.6.4, k is equivalent both to $-k$ and to $-k_{\mathbf{rot}}$. This imply that k is equivalent to its rotation $k_{\mathbf{rot}}$, contradicting Theorem 5.6.5. Thus, Theorem 5.6.5 and Theorem 5.6.4 imply that a strongly invertible hyperbolic knot K can not admit simultaneously free and cyclic period 2. We believe that this statement holds for hyperbolic knots in general, but we weren't able to find a reference.

Thus, we obtain Corollary 4.1.5 below as an improvement of Corollary 4.1.2, dealing with hyperbolic knotoids.

Corollary. *Given any strongly invertible hyperbolic knot K there are exactly 4 distinct oriented knotoids associated to it. Moreover, one of the following holds.*

- *If K has cyclic period 2, these are two inequivalent reversible knotoids k^1, k^2 and their rotations $k^1_{\boldsymbol{rot}}$, $k^2_{\boldsymbol{rot}}$;*
- *if K has free period 2, these are two inequivalent knotoids k^1, k^2 (each equivalent to the reverse of its rotation) and their reverses $-k^1$, $-k^2$;*
- *if K does not have period 2, these are a knotoid k, its reverse $-k$, its rotation $k_{\boldsymbol{rot}}$ and its reverse rotation $-k_{\boldsymbol{rot}}$.*

Proof. By Theorem 5.5.3, K has either 1 or 2 strong inversions up to equivalence. It has exactly 2 if and only if K has period 2.

Suppose first that K does not have period 2. Then, up to reversion and rotation, it is associated with just one knotoid k. Moreover, by Theorems 5.6.4 and 5.6.5, k, $-k$, k_{rot} and $-k_{rot}$ are all distinct.

Suppose that K has cyclic period 2. Then, it is associated with two knotoids k^1 and k^2 that are distinct, even up to rotation and reversion. By Theorem 5.6.4, k^1 is equivalent to $-k^1$. Hence, k^1_{rot} is equivalent to $-k^1_{rot}$. By Theorem 5.6.5, k^1 and $-k^1$ are distinct from k^1_{rot} and $-k^1_{rot}$. Similar statements are true for k^2.

Finally, suppose that K has free period 2. Then again it is associated with two knotoids k^1 and k^2 that are distinct up to reversion and rotation. By Theorem 5.6.4, k^1 is equivalent to $-k^1_{rot}$. Hence, $-k^1$ is equivalent to k^1_{rot}. By Theorem 5.6.5, k^1 and $-k^1_{rot}$ are distinct from $-k^1$ and k^1_{rot}. Again, similar statements are true for k^2. □

In particular, the knotoids in Figure 5.25 are all not reversible. In fact, their images under the double branched cover construction are the knot 8_{20}, which is hyperbolic with symmetry group isomorphic to the dihedral group D_1 (thus, it does not admit period 2).

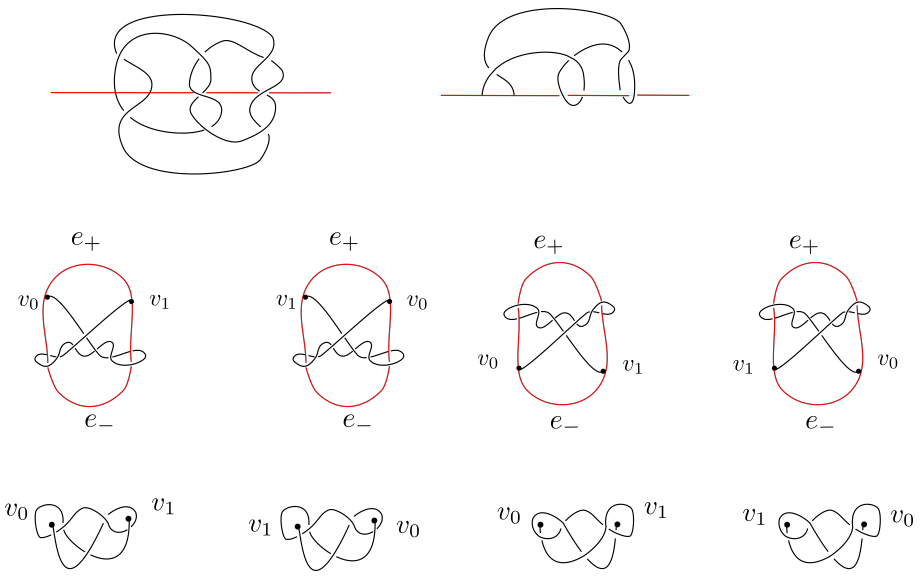

Figure 5.25: There are 4 oriented and not reversible knotoids associated to the knot 8_{20}. These are related to each other by reversion and/or rotation.

5.6.3 Amphichiral strongly invertible knots

It is possible to give a further refinement of Corollary 4.1.2 in the case of amphichiral hyperbolic knots.

Definition 5.6.7. *Recall that a knot K is called* amphichiral *if there exists an orientation-reversing homeomorphism of S^3 fixing the knot (setwise). Note that this implies that K is equivalent to its mirror K_m.*

Consider an invertible, hyperbolic, amphichiral knot K, and suppose that it admits period 2. From Theorem 5.5.3 it follows that K admits two non-equivalent involutions τ_1 and τ_2. Let ϕ be the (isotopy class of) the orientation reversing homeomorphism of Definition 5.6.7; from [[107], Proposition 3.4], we know that τ_1

and τ_2 are conjugated through ϕ

$$\tau_2 = \phi \circ \tau_1 \circ \phi^{-1}$$

Thus, (K, τ_1) is equivalent to $m(K, \tau_2)$, where $m(K, \tau_2)$ is the strongly invertible knot obtained from (K, τ_2) by reversing the orientation of S^3, and the following holds.

Proposition 5.6.8. *Given an invertible, hyperbolic, amphichiral knot K admitting period 2, and let τ_1 and τ_2 be the two non-equivalent strong involutions of K. Then $\Pi(K, \tau_1)$ is the equivalence class in $\mathbb{K}(S^2)/_{\approx}$ containing the mirror images of the knotoids in $\Pi(K, \tau_2)$.*

Note that Theorem 5.6.4 tells us that the oriented knotoids in the equivalence classes of $\Pi(K, \tau_1)$ and $\Pi(K, \tau_2)$ are all either reversible or equivalent to the reverse of their rotations, and Theorem 5.6.8 tells us that each class contains the mirror reflections of the other.

Example: the Figure Eight knot

We work out the case of the figure eight knot (4_1 in the Rolfsen table) as an example of Proposition 5.6.8. The 4_1 knot is known to be hyperbolic, invertible, amphichiral and it admits period 2; thus, it admits two distinct inversions τ_1 and τ_2, shown in the upper part of Figure 5.26.

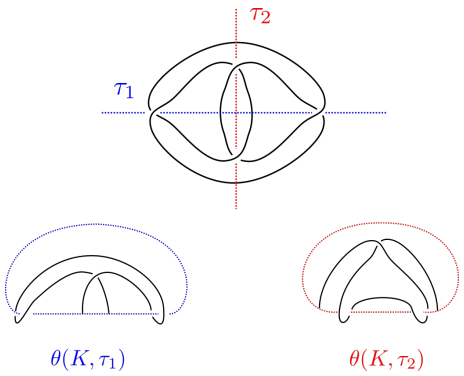

Figure 5.26: On the top, a diagram for 4_1 with the fixed point sets of τ_1 and τ_2 represented as straight lines. On the bottom, the θ-curves $\theta(4_1, \tau_1)$ and $\theta(4_1, \tau_2)$.

By considering the quotients under τ_1 and τ_2 we obtain two elements $\theta(4_1, \tau_1)$ and $\theta(4_1, \tau_2)$ of $\Theta^s/_{\approx}$, shown in the bottom of Figure 5.26. Their constituent knots are two unknots and the torus knot 5_1, and two unknots and the mirror image of 5_1 respectively. Since it is well known that $5_1 \nsim m5_1$, it follows that $\theta(4_1, \tau_1)$ and $\theta(4_1, \tau_2)$ represent different elements of $\Theta^s/_{\approx}$.

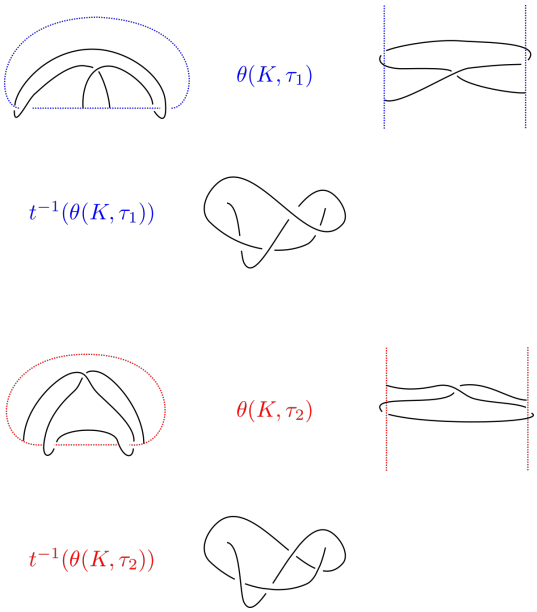

Figure 5.27: On the top: from $\theta(4_1, \tau_1)$ to $\Pi(4_1, \tau_1)$. On the bottom: from $\theta(4_1, \tau_2)$ to $\Pi(4_1, \tau_2)$. The two knotoids are the mirror image of one another.

In figure 5.27 we show how to obtain two specific representatives of the equivalence classes $\Pi(4_1, \tau_1)$ and $\Pi(4_1, \tau_2)$. It is clear from the picture that these knotoids are one the mirror image of the other.

5.6.4 Strongly invertible composite knots

As a corollary of Theorem 4.1.1 and Corollary 4.1.5, we have the following result dealing with strong involutions of composite knots.

Proposition 5.6.9. *Consider a knot K isotopic to the connected sum of $\#_{i=1}^{n} K_h^i$, where $n \geq 2$ and every K_h^i is a strongly invertible, hyperbolic knot. Suppose that these hyperbolic knots are pairwise distinct. Then, the number of non-equivalent strong involutions of K is equal to $4^{n-1}(n!)$.*

Proof. By Theorem 4.1.1, the number of different involutions of $K = \#_{i=1}^{n} K_h^i$ is equal to the number of elements of $\mathbb{K}(S^2)/_{\approx}$ whose image under γ_S is a knot isotopic to K. Theorem 5.3.8 implies that every knotoid k with $\gamma_S(k) = K$ is decomposable as $k = \cdot_{j=1}^{n} k_j$ where each k_j belong to the equivalence class $\Pi(K_h^i, \tau) \in \mathbb{K}(S^2)/_{\approx}$ for a unique (K_h^i, τ). By hypothesis, the summands of $\#_{i=1}^{n} K_h^i$ are pairwise distinct, thus, none of the k_j is a knot-type knotoid. Thus, Theorem 5.1.4 implies that this decomposition is unique in $\mathbb{K}(S^2)$. There are $n!$ ways to order the factors of $k = \cdot_{j=1}^{n} k_j$, and each arrangement corresponds to a different element in $\mathbb{K}(S^2)$. Moreover, by Corollary 4.1.5, each K_h^i is associated to exactly 4 inequivalent oriented knotoids. Depending on whether or not K_h^i has period 2, these can be either

- two inequivalent reversible knotoids k_i^1, k_i^2 and their rotations $k_{i\mathbf{rot}}^1$, $k_{i\mathbf{rot}}^2$, contained in the two classes $\Pi(K_h^i, \tau_1)$ and $\Pi(K_h^i, \tau_2)$;
- two inequivalent knotoids k_i^1, k_i^2 (each equivalent to the reverse of its rotation) and their reverses $-k^1$, $-k^2$, contained in the two classes $\Pi(K_h^i, \tau_1)$ and $\Pi(K_h^i, \tau_2)$;
- a knotoid k_i, its reverse $-k_i$, its rotation $k_{i\mathbf{rot}}$ and its reverse rotation $-k_{i\mathbf{rot}}$, contained in $\Pi(K_h^i, \tau)$.

Choosing a different oriented knotoid associated to the same hyperbolic knot in the decomposition $k = \cdot_{j=1}^{n} k_j$ corresponds to creating a different element in $\mathbb{K}(S^2)$. Thus, there are a total of $4^n(n!)$ different composite knotoids in $\mathbb{K}(S^2)$ whose double branched cover is a knot isotopic to K. Since for every knotoid $k' = k'_1 \cdot k'_2 \dots k'_{m-1} \cdot k'_m$ it holds $k'_{\mathbf{rot}} = k'_{1\mathbf{rot}} \cdot k'_{2\mathbf{rot}} \dots k'_{m-1\mathbf{rot}} \cdot k'_{m\mathbf{rot}}$ and $-k' = -k'_m \cdot -k'_{m-1} \cdots - k'_2 \cdot -k'_1$, by considering reversion and reflection on the composite knotoids, the claim follows. □

5.7 On the map γ_T: an example

It is often hard to distinguish non-equivalent planar knotoids which represent the same class in $\mathbb{K}(S^2)$. In what follows, we show how we can efficiently use the map γ_T to this end. Consider the pair of knotoids k_1 and k_2 in $\mathbb{K}(D^2)$ of Figure 5.28.

They both represent the trivial knotoid in $\mathbb{K}(S^2)$, and they share the same loop arrow polynomial [47].

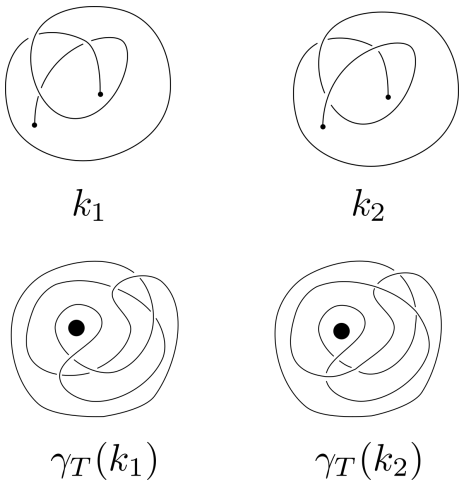

Figure 5.28: On the top, the knotoids k_1 and k_2 in $\mathbb{K}(D^2)$. On the bottom, their images under γ_T.

The images of knotoids k_1 and k_2 under γ_T are two knots in the solid torus. To distinguish them, we can consider the following construction. We can embed the solid torus in S^3 as done in Section 5.3, but this time after giving a full twist along the meridian of $S^1 \times D^2$. We then obtain two knots in S^3, shown in Figure 5.29, that can be easily shown to be the knots 9_{46} and 5_2 by computing the Alexander and Jones polynomials. These invariants are in fact enough to distinguish them since, according to knotinfo [22], the knots 5_2 and 9_{46} are uniquely determined by their Alexander and Jones polynomials among all knots up to 12 crossings. Note that this procedure may be applied to several similar cases, highlighting the power of the map γ_T. We emphasise that the authors are not aware of any other method other than using γ_T that is capable of distinguishing k_1 and k_2. This example was kindly suggested by Dimos Goundaroulis.

Remark 5.7.1. As mentioned in Section 5.3, after applying the map γ_T one could directly compare the resulting knots in the solid torus by using invariants for knots in the solid torus, see *e.g.* [79, 43, 55]. Alternatively, one could also consider the two-component link L in S^3 obtained as the union of $\gamma_T(k)$ with the meridian of the solid torus $S^1 \times D^2$.

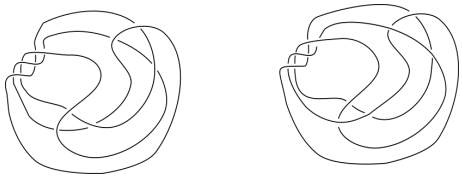

Figure 5.29: By embedding the solid torus in S^3 as in Section 5.3 after giving a full twist along the meridian, we obtain a pair of knots in S^3.

5.8 Gauss Code and Computations

The oriented Gauss code $GC(D)$ for a knot diagram D and a point a in D is a pair (C, S), where C is a $2n$-tuple and S an n-tuple, n being the number of crossings of the diagram. Given a diagram D, $GC(D)$ is constructed as follows: assign a number between 1 and n to each crossing, and pick a point a in the diagram, which is not a double point. Start *walking* along the diagram from a, following the orientation, and record every crossing encountered (in order) by adding an entry to C consisting of the corresponding number, together with a sign + for overpassing and − for underpassing, until you reach the starting point a again. Note that each crossing is encountered twice. S is the n-tuple whose i^{th} entry is equal to 1 if the i^{th} crossing is positive and -1 otherwise. As an example, the Gauss code associated to the diagram in Figure 5.30 is equal to:

$$GC(D) = ((1, -2, 3, -1, 2, -3), (1, 1, 1))$$

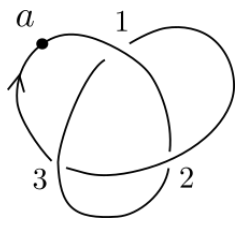

Figure 5.30: Computing the Gauss code for a knot diagram.

Gauss codes can be easily extended to knotoid diagrams, see [49]. The procedure is basically the same, but in this case the starting point a coincides with the tail of the diagram. As an example, the Gauss code for the knotoid in Figure 5.31

is equal to:

$$GC(D) = ((-1, 1, 2, -3, -2, 3), (1, 1, 1))$$

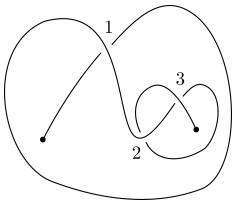

Figure 5.31: Computing the Gauss code for a knotoid.

The information encoded in $GC(D)$ is enough to reconstruct D, both in the case of knot and knotoid diagrams.

5.8.1 Generalised Gauss code for knotoids

Gauss code for knotoid diagrams may be generalised to contain also the information about the intersection with the branching set. We will call the *generalised Gauss code*(indicated as $gGC(D)$) the pair (C, S) where S is the same as in $GC(D)$, while C contains also entries equal to b every time every time the diagram intersects with the arcs that connect the branched points (*i.e.* the endpoints) with the boundary of the disk containing the diagram. For instance, the Gauss code for the knotoid in Figure 5.32 is:

$$-1, b, b, 1, 2, -3, b, -2, 3/1, 1, 1$$

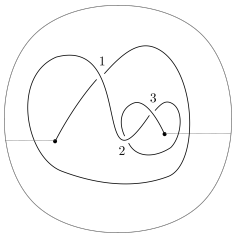

Figure 5.32: Computing the generalised Gauss code for a knotoid.

5.8.2 Gauss code for the lifts

Given a diagram D representing a knotoid k with $gGC(D) = (C, S)$ it is possible to compute $GC(\gamma_S(D))$, where $\gamma_S(D)$ is the diagram representing $\gamma_S(k)$ obtained with the *cuts* technique, as in Figure 5.10.

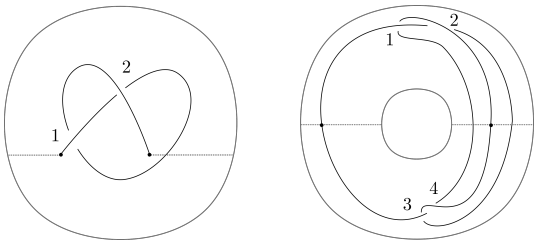

Figure 5.33: Computing the Gauss code for the lift: an example.

Consider the knotoid diagram D on the left-side of Figure 5.33 with $gGC(D) = ((1, -2, b, -1, 2), (1, 1)$. Label the crossings in $\gamma_S(D)$ as shown on the right-side of Figure 5.33: every half of the annulus is a copy of the disk in which D lies, keep the same enumeration on the top-half and increase by 2 the labels in the bottom one. Now, start computing $GC(\gamma_S(D))$: notice that until we reach an intersection between the diagram and one of the arcs splitting the annulus, the entries added in $GC(\gamma_S(D))$ are equal to the first entries in $gGC(D)$. After an intersection point, the path continues on the bottom half of the annulus, and the next entries added in $GC(\gamma_S(D))$ are equal to the corresponding ones in $gGC(D)$, but with every label increased by 2. Once we reach the lift of the head, the path along the knot continues, and it is the same path we have just done, but in the opposite direction and on opposite halves of the annulus. Thus, the last entries added are a copy of the entries written so far, added in the opposite order and with labels corresponding to opposite halves of the annulus and thus:

$$GC(\gamma_S(D)) = ((1, -2, -3, 4, 2, -1, -4, 3), S)$$

To compute S, note that the sign of a crossing in the top-half is the same as its corresponding crossing in the bottom-half. Moreover, since the labels corresponding to each crossings in $gGC(D)$ appear once before the entry b and once

after, the signs of the first two crossings in the knot diagram are changed, and the complete Gauss code is

$$GC(\gamma_S(D)) = ((1, -2, -3, 4, 2, -1, -4, 3), (-1, -1, -1))$$

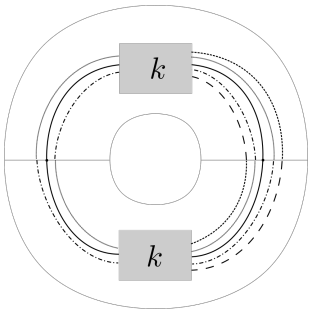

Figure 5.34: Computing the Gauss code of the lift $\gamma_S(D)$.

The previous procedure can be generalised to produce an algorithm. Thus, consider the diagram in Figure 5.34, and start walking along the knot from the lift of the tail. Every time we pass from one half of the annulus to the other, the path on the diagram follows as in the knotoid diagram, but on a different half. Moreover, as before, once we reach the lift of the head of the knotoid, the path proceeds as the one just traced, in the opposite direction and on different halves as before. Now, suppose that on $gGC(D)$ the two appearances of the same label happen without the occurrence of a b entry between them. This means that in $\gamma_S(D)$ we are going to reach the top-lift of the crossing twice without passing to the other half (thus, without swapping the orientation), and the same holds for the bottom-lift of the crossings. In this case the signs of both the lifted crossings in $\gamma_S(D)$ are equal to the sign of the corresponding one in D. Putting everything together, we obtain the following algorithm, that can be easily implemented.

Input: generalised Gauss code of the knotoid, $\mathbf{n}$ = number of crossings in the knotoid diagram;

- go through the knotoid code: copy the entries until you find a b;
- until you reach the point corresponding to the head of the knotoid: after reaching a b

- if the number of b-entries encountered is odd, add entries equals to the knotoid ones, but changing the labels by adding n to them. Do that until you reach another b;
- if the number of b-entries encountered is even, add entries equals to the knotoid ones. Do that until you reach another b.

- After reaching the head: copy the entries added so far, starting from the last one, and changing the labels by subtracting n if they are greater than n, and adding n otherwise;

- Consider the k crossing in the knotoid diagram:
  - if the corresponding labels in the knotoid code appear twice with an even (or zero) number of b-entries between them, then the sign of the k and $k+n$ crossings in the knot diagram are equal to the sign of the starting crossing;
  - if the corresponding labels in the knotoid code appear twice with an odd number of b-entries between them, then the sign of the k and $k+n$ crossings in the knot diagram are opposite to the sign of the starting crossing.

Output: Gauss code for the lifted knot diagram.

Chapter 6

f-distance of knotoids and protein structure

The work described here is joint with Dimos Goundaroulis [9]. Note that from now on we will denote knotoids following the enumeration due to Goundaroulis [47]. In particular, 3_1 will denote the knot-type knotoid associated to the trefoil knot.

6.1 f-distance of knotoids

Recall that forbidden moves define an unknotting operation for knotoids, meaning that any knotoid diagram can be transformed into the trivial one by a finite sequence of these moves. In analogy to the case of knots and crossing changes, we are able to define a distance on knotoids using forbidden moves.

Definition 6.1.1. *Given two knotoids k_1 and k_2, their* forbidden move distance *or f-distance $d_f(k_1, k_2)$ is the minimal number of forbidden moves, across all representatives of k_1 and k_2, needed to transform k_1 into k_2.*

In what follows we will use the bijections

$$t_{\approx} : \mathbb{K}(S^2)/_{\approx} \longrightarrow \Theta^s/_{\approx}$$

and

$$\gamma_{S_{\approx}} : \mathbb{K}(S^2)_{\approx} \longrightarrow \mathcal{K}SI(S^3)$$

to give a characterisation of forbidden moves in terms of operations on θ-curves and on strongly invertible knots.

6.1.1 Crossing changes on θ-curves

A forbidden move on k corresponds to performing a strand passage (*i.e.* a crossing change) on the θ-curve $t_{\approx}(k)$, see Figure 6.1. More precisely, a forbidden move induces a strand passage between the arc e_0 and either e_+ or e_-.

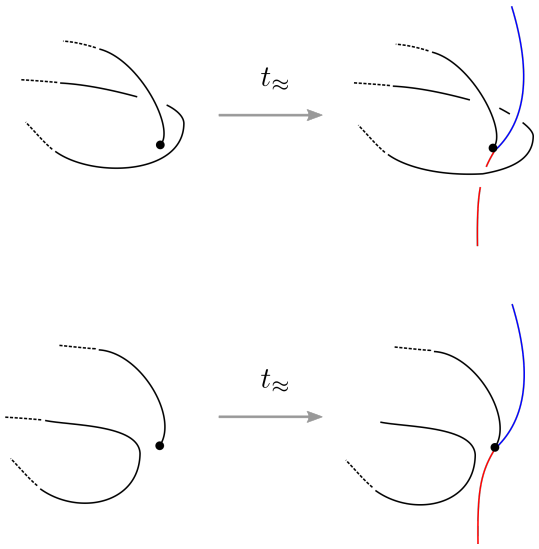

Figure 6.1: A forbidden move between two knotoids k_1 and k_2 induces a strand passage between the arcs e_0 and $e_\pm$ between the corresponding θ-curves.

Remark 6.1.2. Call $K_k^\pm$ the constituent knot of $t_{\approx}(k)$ given by $e_0 \cup e_\pm$. From the previous construction, it follows that a forbidden move induces a crossing change on exactly one between K_k^+ and K_k^-. In particular, this specific strand passage cannot change simultaneously both these constituent knots of $t_{\approx}(k)$.

Remark 6.1.3. Note that given a knotoid k, the pair (K_k^+, K_k^-) can be obtained by computing overpassing closure $\omega_-(k)$ and the mirror image of the underpassing closure $\omega_-(k)$ of k.

6.1.2 Band surgeries on strongly invertible knots

A *band surgery* (also known as *band attachment*) is an operation which changes a link into another link.

Definition 6.1.4. *Let L_1 be a link and $b : I \times I \longrightarrow S^3$ an embedding such that $L_1 \cap b(I \times I) = b(I \times \partial I)$. The link $L_2 = (L_1 \setminus b(I \times \partial I)) \cup b(\partial I \times I)$ is said to be obtained from L_1 by a* band surgery *along the band $B = b(I \times I)$, see Figure 6.2.*

The band surgery is called *coherent* if it respects the orientation of L_1 and L_2, otherwise it is called *non-coherent*, see Figure 6.2. A non-coherent band surgery it is often called a H_2-move (see *e.g.* [1], [56]). Contrary to the case of coherent band surgeries, H_2-moves preserve the number of the components of links. This means that the result of an H_2-move performed on a knot will always be a knot.

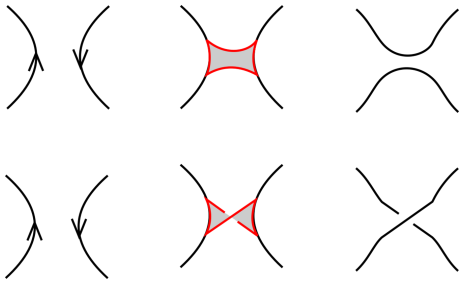

Figure 6.2: Local pictures for a coherent (top) and a non-coherent (bottom) band surgery.

Consider two knotoids that differ by a forbidden move, as on the left of Figure 6.3: it is easy to see that their lifts are related by a single $H(2)$-move (see the right part of Figure 6.3).

Moreover, the band surgery is *equivariant* with respect to the involutions of the two knots (see Figure 6.1).

Definition 6.1.5. *Consider a strongly invertible knot (K_1, τ_1). We say that the strongly invertible knot (K_2, τ_2) is obtained from (K_1, τ_1) by an* equivariant band surgery *if the knots K_1 and K_2 are related by an H_2-move, such that:*

- *$fix(\tau_1)$ intersects the band $b(I \times I)$ transversally exactly once in its interior and the band is invariant under τ_1;*

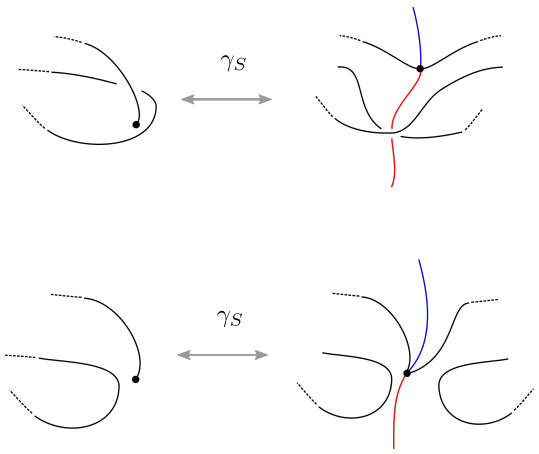

Figure 6.3: Two knotoids that differ by a forbidden move have lifts related by a single band surgery.

- (K_2, τ_2) *and* (K_1', τ_1) *are equivalent as strongly invertible knots*[1]*, where* K_1' *is the knot obtained from* K_1 *by doing the band surgery.*

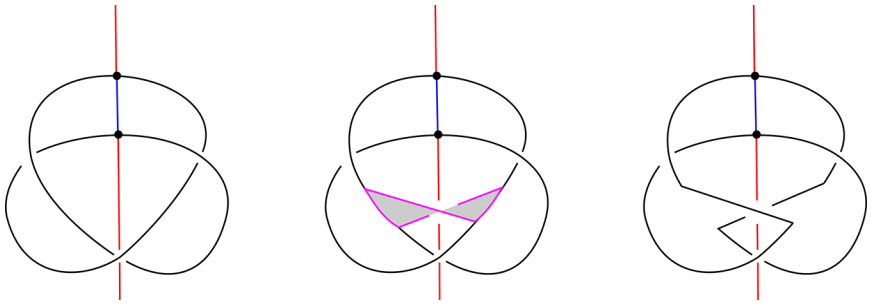

Figure 6.4: The strongly invertible knots $(3_1, \tau)$ and $(0_1, \tau')$ are related by an equivariant band surgery.

An example of an equivariant band surgery is shown in Figure 6.4.

6.1.3 Main result

We are now able to prove our main result.

Theorem 6.1.6. *Consider two equivalence classes of knotoids* k_1 *and* k_2 *up to rotation and reversion. The following are equivalent:*

[1]Recall from Definition 5.5.1 that two strongly invertible knots (K, τ) and (K', τ') are *equivalent* if K and K' are equivalent as knots in S^3, and τ and τ' are conjugated in $Sym^+(S^3, K)$.

- *k_1 and k_2 differ by a single forbidden move;*
- *their corresponding θ-curves $t_{\approx}(k_1)$ and $t_{\approx}(k_2)$ differ by a strand passage of the edge e_0 over either e_+ or e_-;*
- *their corresponding strongly invertible knots $\gamma_{S_{\approx}}(k_1)$ and $\gamma_{S_{\approx}}(k_2)$ differ by an equivariant band surgery.*

Proof. Thanks to the discussion of the previous subsections, it is enough to show the following.

- Given two strongly invertible knots related by an equivariant band surgery, their corresponding θ-curves are related by a strand passage of e_0 through either e_+ or e_-;
- given two θ-curves related by a strand passage of e_0 through either e_+ or e_-, their corresponding knotoids differ by a forbidden move.

Consider then an equivariant band surgery between two strongly invertible knots (K_1, τ_1) and (K_2, τ_2). Up to ambient isotopies fixing the circle $fix(\tau_1)$ the band surgery locally looks like the one in the top part Figure 6.5, with possibly the opposite twists on the band. On the quotient $S^3/\tau_1 \approx S^3$ this results in a strand passage between the arcs e_0 and one between e_+ or e_- in the θ-curve $p(fix(\tau)) \cup p(K)$, as shown in the bottom of Figure 6.5.

Analogously, consider a simple θ-curve. Up to label preserving ambient isotopies fixing the circle $e_- \cup e_+$, any strand passage between the arc e_0 and the arc $e_\pm$ locally looks like the one shown in the top part of Figure 6.6 (up to changing the crossing between e_0 and $e_\pm$). The bottom right part of Figure 6.6 shows how this translates into a forbidden move on the corresponding knotoid. The case where the crossing between e_0 and $e_\pm$ is the opposite one is similar.

□

6.1.4 Lower bounds on the f-distance

We use Theorem 6.1.6 to produce lower bounds for the forbidden move-distance between equivalence classes of knotoids up to the four involutions of Figure 5.2.

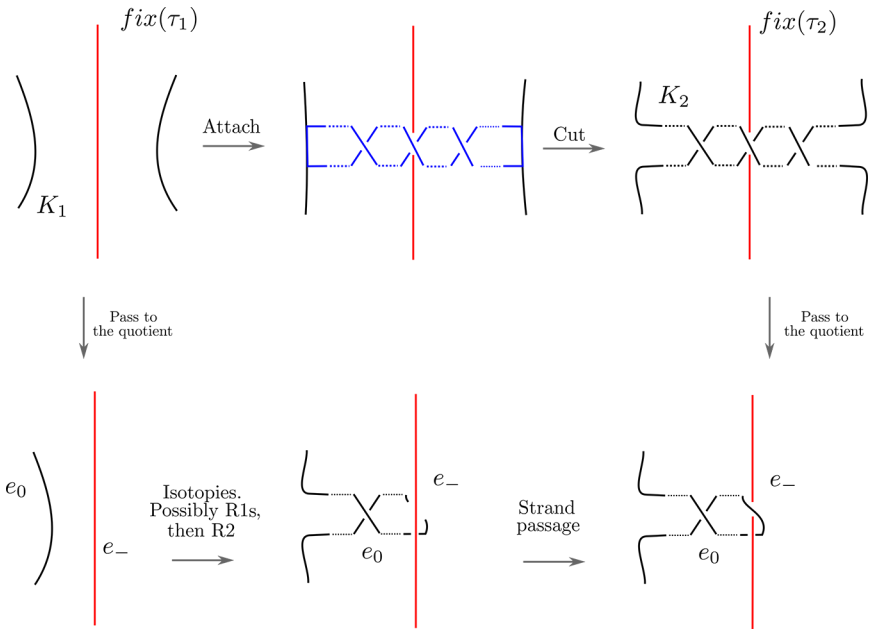

Figure 6.5: On the top, two strongly invertible knots (K_1, τ_1) and (K_2, τ_2) related by an equivariant band surgery. Up to ambient isotopies fixing the circle $fix(\tau_1)$ (and up to inverting the crossings), the band looks like the one in the middle of the top row. The band has an odd number of twists. On the bottom, the corresponding effect on the associated θ-curves. If the band has $2n + 1$ twists, the θ-curves are related by a sequence of n Reidemeister moves of type I (R1s) followed by a a Reidemeister move of type II (R2) and by a single strand passage.

With a little abuse of notation, we will still call these equivalence classes *knotoids*.

The *H_2-Gordian distance* $d_{H_2}(K, K')$ between two knots K and K' is defined as the minimal number of equivariant band surgeries connecting K and K' [1]. As an immediate consequence of Theorem 6.1.6, given two knotoids k_1 and k_2, with corresponding strongly invertible knots $\gamma_{S_\approx}(k_1) = (K_1, \tau_1)$ and $\gamma_{S_\approx}(k_2) = (K_2, \tau_2)$, we have that

$$d_f(k_1, k_2) \geq d_{H_2}(K_1, K_2). \tag{6.1}$$

Analogously, given two knotoids k_1 and k_2, consider the pairs $(K^+_{k_1}, K^-_{k_1})$ and $(K^+_{k_2}, K^-_{k_2})$. We can define their *Gordian distance* $d_{\text{pair}}((K^+_{k_1}, K^-_{k_1}), (K^+_{k_2}, K^-_{k_2}))$ as the minimum between $d(K^+_{k_1}, K^+_{k_2}) + d(K^-_{k_1}, K^-_{k_2})$ and $d(K^+_{k_1}, K^-_{k_2}) + d(K^-_{k_1}, K^+_{k_2})$, where d is the usual Gordian distance between knots. From Remark 6.1.2 it follows

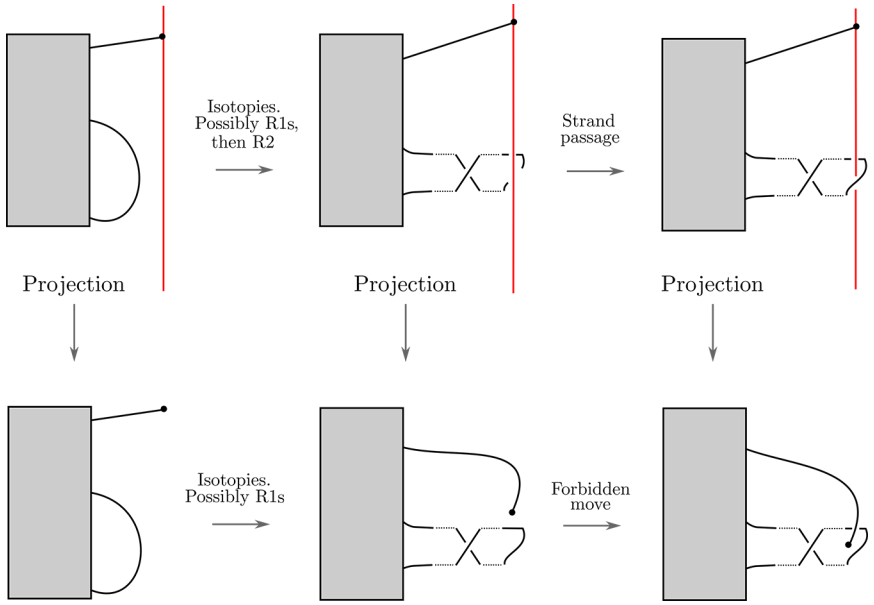

Figure 6.6: On the top row, two θ-curves related by a strand passage between the arc e_0 and the arc $e_\pm$. Up to label preserving ambient isotopies fixing the circle $e_- \cup e_+$ we can make the strand passage look like in the picture. The effect on the corresponding projections giving the knotoids is to perform a sequence of Reidemeister moves of type I followed by a single forbidden move.

that

$$d_f(k_1, k_2) \geq d_{\text{pair}}((K^+_{k_1}, K^-_{k_1}), (K^+_{k_2}, K^-_{k_2})). \tag{6.2}$$

Thus, as a corollary of Theorem 6.1.6 we have the following.

Corollary 6.1.7. *Let 0_1 denote the trivial knotoid. If K is a non trivial knot-type knotoid then $d_f(K, 0_1) \geq 2u(K)$, where $u(K)$ is the unknotting number of K considered as a knot in S^3.*

Proof. If K is a knot type knotoid, its corresponding constituent knots $K^\pm_K$ are both isotopic to K. Thus, $d_f(K, 0_1) \geq 2u(K^\pm_K)$ where $u(K^\pm_K)$ is the unknotting number of the constituent knot.

□

Note that we do not expect the equality to hold in general, since in $K^\pm_K$ the unknotting crossing change might involve only the arc $e_\pm$, and thus it would not

correspond to a forbidden move.

6.2 Computing f-distances of S^2-knotoids

As mentioned above, the main theorem provides lower bounds for f-distances between isotopy classes of knotoids. Since our aim is to build a table of f-distances, this is information alone is not sufficient. For this reason, we computed the f-distance between all non-composite knotoid diagrams, including non-minimal crossing representations, with up to six crossings with the help of a computer program written in `python 3.7`, available at [45].

Roughly, our strategy works as follows. First, all $2,363,766$ knotoid diagrams with up to six crossings (both of minimal and non-minimal crossing number representation) [47] are encoded using the oriented Gauss codes for knotoids (see Section 5.8). We note here that from now on, we shall be using the terms knotoid diagram and oriented Gauss code interchangeably. Moreover, we will not take into consideration composite knotoids. Each knotoid diagram is then identified using the arrow polynomial for knotoids ([49] and Section 5.1.1) and the classification of S^2-knotoids provided by [47]. Let now $\mathcal{K}$ be the set of all knotoid diagrams with up to six crossings and let $G(V, E)$ be an undirected graph such that:

$$\begin{aligned} V(G) &= \mathcal{K} \\ E(G) &= \{(v, u) \mid (v, u) \in \mathcal{K}^2,\ v \overset{f}{\sim} u,\ v \neq u\}, \end{aligned}$$

where $v \overset{f}{\sim} u$ denotes a pair of knotoid diagrams (v, u) that are related by a single forbidden move. In other words, G is the undirected graph whose vertices are knotoid diagrams and two diagrams are related with a single forbidden move if and only if the corresponding vertices of G are connected with an edge. Our program builds G and then searches for all paths between all possible pairs of vertices. Finally, the set of all diagrams is partitioned into isotopy classes and the path of minimal distance between two isotopy classes determines their numerical f-distance, d_f^{num}. From this we can obtain upper bounds for the f-distances between isotopy classes of knotoids by computing their experimental f-distances which are defined as:

$$d_f^{\exp}(v,u) = \min\left\{d_f^{\mathrm{num}}(v,x) \mid x \in (u, u_{\mathbf{mir}}, u_{\mathbf{sym}}, u_{\mathbf{rot}}, -u)\right\}.$$

By comparing the upper bounds with the lower bounds discussed in Section 6.1.4 we are able to produce Table B.1 (shown in Appendix B) containing the f-distances between equivalence classes of knotoids with minimal crossing number ≤ 4. Most of the lower bounds in Table B.1 are obtained using the inequality (6.2). Gordian distances between knot types are taken from [94], while H_2-distances from [61] and [62].

Note that this could be improved by considering in the experimental approach a higher threshold for the maximum crossing number. This means that non-minimal representations of higher crossing number for the ambiguous entries in Table B.1 will be considered, which may help decreasing their upper bounds. Unfortunately, our available computational power prohibited us from exploring this possibility.

Example 6.2.1. Computing lower bounds using inequality (6.2) it is quite straightforward. Indeed, given a knotoid k we obtain the constituent knots $K_k^{\pm}$ as explained in Remark 6.1.3. Then, using values for the Gordian distance taken from [94] we compute d_{pair} for each pair of knotoids.

To illustrate how our method works in the case of inequality (6.1), we will prove as an example that $d_f(3_1, 4_7) = 2$. Given a knot K, it is well known (see *e.g.* [105]) that the double cover of S^3 branched along K is a closed 3-manifold $\Sigma(K)$ whose homeomorphism class depends solely on the knot K. Let's denote by $\delta(K)$ the dimension of the first homology of $\Sigma(K)$ with coefficients in $\mathbb{Z}_3$, $\delta(K) = \dim(H_1(\Sigma(K), \mathbb{Z}_3))$. The value of the Jones polynomial of K at $t^{1/2} = e^{i\pi/6}$ can be computed as $V(K,\omega) = \pm(i\sqrt{3})^{\delta(K)}$ [61, Proposition 5.1]. If two knots K and K' have H_2-distance 1 then the ratio $V(K,\omega)/V(K',\omega) \in \{\pm 1, \pm i\sqrt{3}^{\pm 1}\}$, which is the content of [61, Lemma 5.2].

We shall apply these to the pair $(3_1, 4_7)$. Recall from Proposition 5.3.6 that knotoid 3_1 lifts to a connected sum of trefoil knots $3_1\#3_1$. Additionally, it is known (see *e.g.* [61]) that $\delta(3_1\#3_1) = 2$ and, thus, $V(3_1\#3_1, \omega) = \pm 3$. On the other hand, 4_7 lifts to the torus knot 8_{19}, and in this case we have (see *e.g.* [15]) that $H_1(\Sigma(8_{19}), \mathbb{Z}) \cong \mathbb{Z}_3$. Thus, $\delta(8_{19}) = 1$. The ratio $V(3_1\#3_1, \omega)/V(8_{19}, \omega) \notin \{\pm 1, \pm i\sqrt{3}^{\pm 1}\}$ and so 3_1 and 4_7 cannot have H_2-distance equal to 1. Finally, from

Table B.3 we see that $d_f^{\exp}(3_1, 4_7) = 2$ and therefore we have that $d_f(3_1, 4_7) = 2$. In a similar way we can compute lower bounds for the f-distance of corresponding to the entries in red of tables B.1 and B.2, since in these cases the knotoids lift to knots K with $\delta(K) = 1$.

6.3 Application to the study of proteins' topology

As mentioned in Section 4.2, the topology of a protein is often currently studied by approximating its corresponding knotoid distribution. This is obtained by computing the knotoid type of those projections defined by sampling a finite number of points in the surrounding 2-sphere.

The data of the approximated distribution of a given protein is often summarised in a plot called *the projection map* [46]. The projection map is in fact the Voronoi diagram $\mathcal{VD}(s)$ of S^2 with respect to the set s of sampled points. In the projection map, each cell is colour-coded according to the knotoid type it produces. Thus, we obtain a picture for the projection map, as the surrounding 2-sphere divided into coloured regions.

We will call the *knotoid spectrum*, denoted by $spec(s)$, the set of distinct labels in $\mathcal{VD}(s)$. By construction, there is a bijection between the number of different colours in a projection map $\mathcal{VD}(s)$ and the number of different knotoids in the knotoid spectrum $spec(s)$ of the analysed curve (see Fig. 6.7).

6.3.1 On the optimal number of projections.

The projection map obviously depends heavily on the sample size of projections; if too few points are sampled, then the overall topology of the analysed curve will not be well approximated. Therefore, it is important to understand the optimal number of different projections needed to obtain a faithful representation of the global topology of a protein.

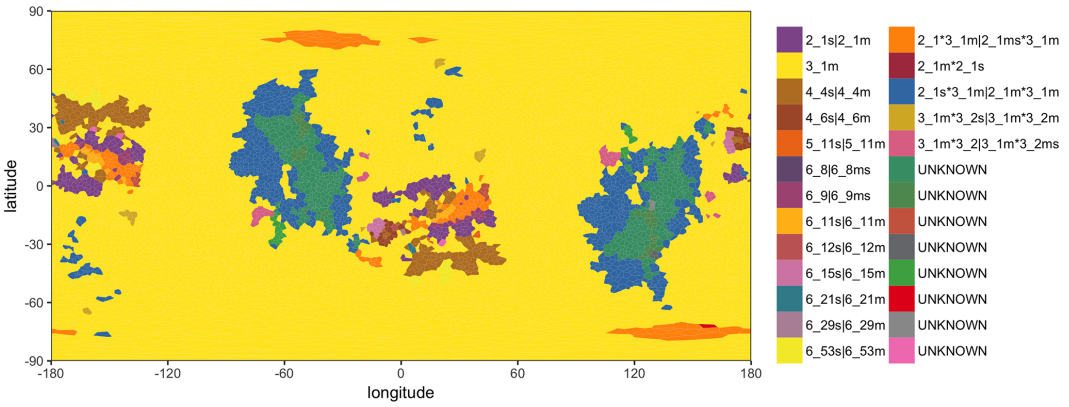

Figure 6.7: The projection map for the protein N-acetyl-L-ornithine transcarbamylase complexed with N-acetyl-L-ornirthine (pdb code: 3kzn). To create this map we used $10,000$ projections. We can see that the predominate knotoid type is $3_{1_{\mathbf{mir}}}$, since it corresponds to the region with the largest area. The colour scale on the right shows the colour - knotoid type correspondence. Note that the | symbol in the knotoid name stands for "or", meaning that knotoid names separated with | share the same arrow polynomial. The label "UNKNOWN" corresponds to knotoids with crossing number > 6. Finally, the multiplication of knotoids is indicated by an asterisk $*$.

Recall that small perturbations in the choice of the direction of projections can either leave the corresponding knotoid type unchanged (*i.e.* by changing the knotoid diagram by isotopies of S^2) or have the effect of performing a forbidden move (recall Figure 5.1) on the knotoid diagram. Thus, when the spectrum is well approximated two knotoids corresponding to adjacent regions are related by a single forbidden move.

Therefore, when the number of sample points is small, there is a higher chance for cells corresponding to knotoids with $d_f > 1$ to appear next to each other. Given a protein with dominant knotoid k_0, we define the *interface error*, $er(s)$, associated to the sample of size s, as the ratio between the number of regions adjacent to the dominant region whose corresponding knotoids k_i are such that $d_f(k_i, k_0) > 1$ and the number of all adjacent regions to k_0.

We expect to see $er(s)$ decreasing as the number s of projections increases.

In our analysis, we concentrated on proteins with predominate knotoid type 3_1. There are 457 such proteins [59] in total deposited in the Protein Data Bank [12].

We remark here that in this project we only focused on proteins catalogued as knotted in the KnotProt databes [59]. In future, it might be interesting to extend our discussion to unknotted proteins, since these might present non-trivial topology as well when studied using the knotoid approach. All proteins of interest are analysed using 50, 100, 500, 1,000, 5,000 and, finally, 10,000 projections. Each time we compute $er(s)$ for the respective Voronoi diagram. In more detail, for each Voronoi diagram we build a graph where the vertices correspond to the regions of the map and the edges correspond to common boundaries between regions. We compute $er(s)$ by counting the number of graph edges between 3_1 and knotoids that give $d_f > 1$ and taking the ratio over the total number of edges that have 3_1 as one of its endpoints, loops excluded.

The values of the f-distances are taken from Table B.2, and these are computed as detailed in Section 6.2.

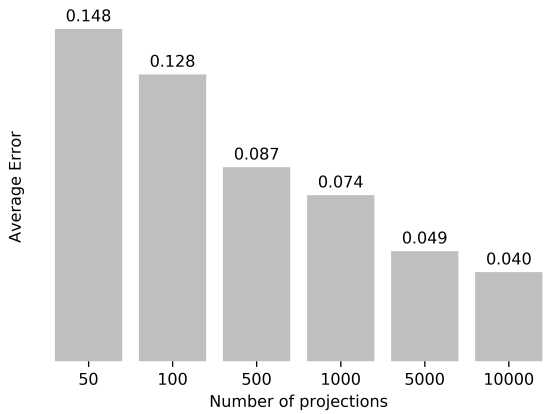

Figure 6.8: The diminishing effect of increasing the number of projections on the average interface error $er(s)$ of a protein chain.

Our analysis shows that for 5,000 and 10,000 projections the interface error is smaller than 0.05. Moreover, computing the projection map of a protein using 5,000 projections is feasible for any good laptop. We thus suggest 5,000 as a threshold for the sample size.

6.3.2 On deeply and shallow knotted proteins.

A protein is called deeply knotted when several amino acids can be removed from both termini of the protein structure before converting it to the trivial knot. More precisely, the *knotted core* of a protein is defined as the shortest subchain for which a non trivial knotoid is detected in the approximation map, while a *tail* is a segment between one terminal of a knotted chain and its knotted core.

The knotted core of a protein is believed to have an important biological role in the protein's function [84, 24], and recent studies show that the formation of deep knots with characteristic structural motifs provides a favourable environment for active sites in enzymes [31]. In particular, it seems that the knotted cores and especially their borders present more intra-chain contacts than other sites [31]. These regions appear to be more thermally stable. Even more interestingly, some knotted proteins have homologues without a knot, and these unknotted counterparts form local entanglements that retain the structural characteristics of the knotted cores [31, 101].

The length of the knotted core of a protein is currently determined by computationally expensive subchain analysis [33, 30].

In our work, we use the results on the f-distance to answer numerically the following question:

Q: Can we define a numerical measure capable of indicating whether a protein is deeply knotted or not?

Naively, one might guess that for shallow knotted proteins the probability of finding *simpler* knotoids adjacent to the dominant one should be higher than in the case of deep knots. This is because the two tails of the knot are less probable to interact with the rest of the chain in a way that will produce "simplifying" forbidden move. With this in mind, we define the following.

Definition 6.3.1. *Let k_0 be the knotoid in S^2 corresponding to the predominate type of a given protein. An interface knotoid, denoted by k_{int}, is a knotoid such that:*

$$d_f(k_0, k_{\text{int}}) = 1 \quad \textit{and} \quad d_f(k_{\text{int}}, 0_1) \leq d_f(k_0, 0_1)$$

We then define the *relative area* A_{rel} as the ratio of the sum of *areas* of interface knotoids in $\mathcal{VD}$ over the area of the predominate, namely:

$$\mathcal{A}_{\text{rel}} = \frac{1}{\mathcal{A}_p} \sum_{k \in \mathcal{K}_{\text{int}}} \mathcal{A}_k, \tag{6.3}$$

where $\mathcal{K}_{\text{int}}$ is the set of all interface knotoids of the predominate knotoid, $\mathcal{A}_p$ is the area in $\mathcal{VD}$ of the predominate knotoid and $\mathcal{A}_k$ is the area in $\mathcal{VD}$ of the knotoid k. Note that each area is computed as the number of distinct Voronoi cells in the same region.

As mentioned earlier, to determine the depth of a protein knot one has to analyse all of its subchains. Computationally this is achieved by progressively trimming the chain from each side and evaluating its knotoid type until the knotted core is obtained[2]. We subsequently define an abstract measure of depth, denoted by $D(k)$, as follows:

$$D(k) = \frac{\ell_N(k)\,\ell_C(k)}{\ell_T(k)^2}$$

where k is a knotoid, $\ell_T(k)$ is the total length of the chain of k, $\ell_N(k)$ and $\ell_C(k)$ are the lengths[3] of the two tails of k (*i.e.* the two sides of the chain not involved in the knotted core).

As in the previous section, we perform statistical analysis on proteins having the 3_1 as dominant knotoids. From Theorem 6.1.6 we have that 2_1 is the only knotoid (between knotoids with 6 or fewer crossings) having distance 1 from both 3_1 and 0_1. In fact, it is straightforward to check that all the knotoids k with less than 6 crossings and $d_f(k, 3_1) = 1$ have distance > 1 from 0_1 using inequality 6.2, as shown in Table B.2. In this case Eq. 6.3 becomes:

$$\mathcal{A}_{\text{rel}} = \frac{\mathcal{A}_{2_1}}{\mathcal{A}_{3_1}}$$

[2]The method discussed here to localise the shortest knotted portion of a protein with non-trivial topology is known as the *top-down* one. As discussed in [119] there is also a *bottom-up* method. These methods are not necessarily equivalent [119].

[3]For each analysed protein, the values of the tails' lengths were taken from the KnotProt database [30].

We compute $\mathcal{A}_{\text{rel}}$ and $D(k)$ for all of the 457 studied proteins. In more detail, we first compute the projection map for each protein using the optimal value of $5,000$ projections that was determined in the previous section. From each projection map we then compute the corresponding $\mathcal{A}_{\text{rel}}$ and $D(k)$.

Our analysis shows a strong inverse Spearman correlation[4] (~ -0.8138), which is clearly visible in Figure 6.9 and Figure 6.10. We also observe a partition of the set of all proteins with a 3_1 into two separate clusters, one in upper left corner of the scatterplot and one in the lower-lower right. In the upper cluster includes the deep 3_1-proteins while the lower one is the cluster of shallow 3_1-proteins.

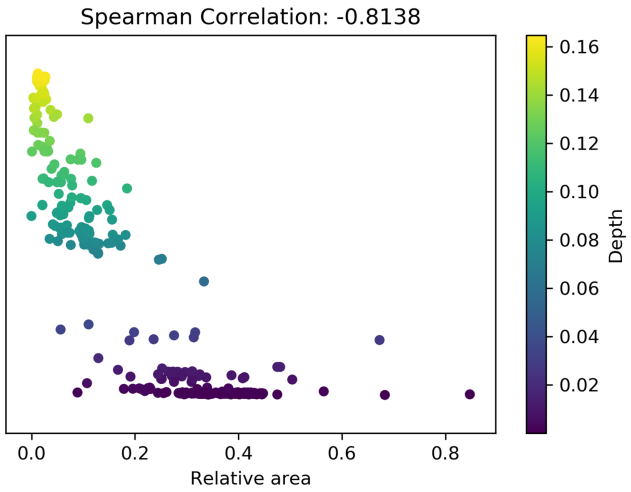

Figure 6.9: Scatterplot of values of $\mathcal{A}_{\text{rel}}$ against $D(k)$. The colour map on the right indicates the different values of $D(k)$. The higher the value, the deeper a knot is. Two distinct clusters of points, in terms of $D(k)$, are visible in the graph indicating a well defined separation between deeply and shallowly knotted proteins.

Our analysis is performed using a modified version of the software KnotoID [33], and our code is available online at [45].

[4]The Spearman correlation is a measure of the monotonicity of the relationship between two datasets. We computed it using Python's `scipy.stats.spearmanr` function.

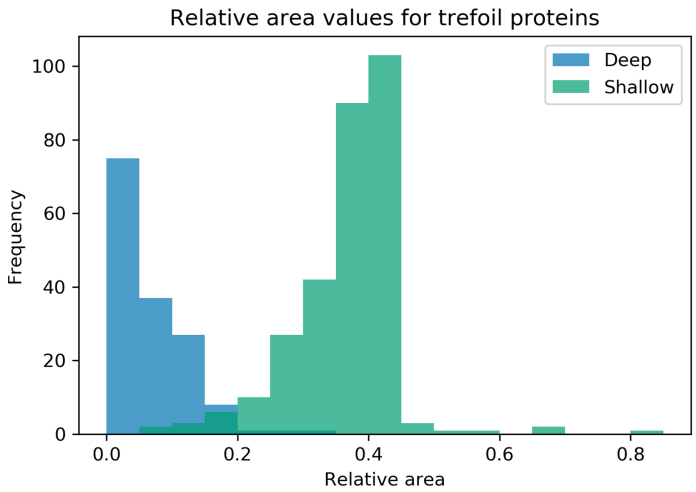

Figure 6.10: The two histograms for the deeply knotted protein group and the shallowly knotted group.

6.4 Conclusions

Concluding, our computations show how, remarkably, we can infer subtle information about the geometry of the protein and about its knot depth, directly from a refined topological analysis based on the properties of knotoids and of their f-distance.

Our result provides a "proof of concept", demonstrating that the knotoid distribution can be used to easily extract and characterise geometric and topological features of proteins. To fully exploit this tool it might be useful to find a more compact and discretised way of representing it. To this end, there is a natural way to associate a planar graph to knotoid distribution of a knotted protein.

More precisely, given the projection map associated to a given protein, we can construct a graph by adding a vertex for each coloured region in the map, and by adding an edge between two vertices if and only if the corresponding regions are adjacent.

Each vertex is then labelled according to the corresponding colour (*i.e.* the label is the knotoid type of the associated projection). These graphs provide "easy to handle" combinatorial objects that might be applied to tackle complex problems such as the protein folding problem, both in the knotted and unknotted case.

Appendices

Appendix A

Miscellanea on knots and manifolds

A.1 Torus, satellite and hyperbolic knots

What follows is a list of basic definitions for knots in S^3. More details can be found in *e.g.* [2].

We will denote by $\nu(K)$ the interior of a regular neighbourhood of the knot K.

Definition A.1.1. *A knot K is called* hyperbolic *if its complement $S^3 \setminus \nu(K)$ is a homogenous hyperbolic 3-manifold, that is, it admits a finite-volume complete Riemannian metric of constant negative curvature.*

A torus link is a knot which can be embedded on the torus as a simple closed curve.

Definition A.1.2. *The torus link $T_{p,q}$ of order (p, q) is the link that wraps around the torus $S^1 \times S^1$, p times along the longitudinal direction and q times along the meridional one.*

When p and q are coprime $T_{p,q}$ is a knot. Torus knots are all chiral, they are invertible and have symmetry group $\mathbb{Z}_2$.

Definition A.1.3. *A knot K is called a* satellite knot *if $S^3 \setminus \nu(K)$ contains an incompressible, non boundary-parallel torus.*

Take a non trivial knot K_1 inside a solid torus $S^1 \times D^2$. Here, by non trivial, we mean that K_1 can not be contained in a ball $D^3 \subset S^1 \times D^2$, and K_1 can not be isotopic to the core of the solid torus. If we tie up the solid torus into a non trivial knot[1], then $K = \phi(K_1)$ is a satellite knot. All satellite knots can be constructed through this procedure.

As a consequence of Thurston's Geometrisation of knot complements [25], it is known that every knot is precisely one of the following: hyperbolic, a torus knot, or a satellite knot.

Theorem A.1.4. *Every non trivial knot in S^3 is either a torus knot, a satellite knot or a hyperbolic knot.*

Note that composite knots are a particular case of a satellite knots. In particular, torus and hyperbolic knots are prime.

A.2 Hyperbolic Geometry

Informally, an orbifold is a space where each point x has an open neighbourhood of the form $\mathbb{R}^n/\Gamma$ for some finite subgroup Γ of $O(n)$, and where x is taken to be the image of the origin. However, it is more than just a topological space, since the orbifold also keeps track of the group Γ attached to x. This is called the *local group* of x. The *singular locus* of the orbifold is the set of points with non-trivial local group.

The most basic example of an orbifold is the quotient of a smooth manifold M by a finite group of diffeomorphisms. In this paper, we will only consider the case of the group $\mathbb{Z}_2$ acting on a smooth manifold by an orientation-preserving involution τ. In this case, the quotient M/τ is again a manifold and its singular locus is a properly embedded 1-manifold.

The most significant structural result about 3-orbifolds is the Orbifold Theorem [25, 13], which gives a version of the Geometrisation Conjecture for orbifolds. Rather than state the precise theorem, we observe the following well-known consequence.

[1] *i.e.* through a non trivial embedding $\phi : S^1 \times D^2 \longrightarrow S^3$. Here, by non trivial we mean that $\phi(V)$ is the regular neighbourhood of a non trivial knot.

Theorem A.2.1. *Let Γ be a finite group of diffeomorphisms of a finite-volume hyperbolic 3-manifold M. Then Γ is conjugate to a group of isometries.*

Proof. Mostow Rigidity implies that Γ is homotopic to a group of isometries, but this is weaker than our desired conclusion. Instead, we use the Orbifold Theorem. This implies that the orbifold M/Γ is hyperbolic. Hence, M has a hyperbolic structure upon which Γ acts by isometries. By Mostow Rigidity, this hyperbolic structure is isometric to our given one, via an isometry h. Thus, h is our required conjugating diffeomorphism. □

There is a notion of the fundamental group $\pi_1(\mathcal{O})$ of an orbifold $\mathcal{O}$ and of a covering map between orbifolds. For a definition of these terms, see *e.g.* [109] or [25].

Appendix B

The f-distance tables

	0_1	2_1	3_1	3_2	4_1	4_2	4_3	4_4	4_5	4_6	4_7	4_8
0_1	0	1	2	1	2	1	2	2	2	3	1	1
2_1	1	0	1	2	3	1	1	1	1	2	1	1
3_1	2	1	0	3	4	2	2	1	2	1	2	2
3_2	1	2	3	0	1	2	2-3	3	1	3-4	2	2
4_1	2	3	4	1	0	3	3-4	4	2	4-5	3	3
4_2	1	1	2	2	3	0	1-2	1	2	2	1-2	1
4_3	2	1	2	2-3	3-4	1-2	0	2	2	1	1-2	1
4_4	2	1	1	3	4	1	2	0	2	1	1-2	1
4_5	2	1	2	1	2	2	2	2	0	2-3	1-2	2
4_6	3	2	1	3-4	4-5	2	1	1	2-3	0	2-3	2
4_7	1	1	2	2	3	1-2	1-2	1-2	1-2	2-3	0	1-2
4_8	1	1	2	2	3	1	1	1	2	2	1-2	0

Table B.1: The f-distance table for equivalence classes of knotoids with minimal crossing number ≤ 4. In a few cases (*e.g* for the pair $(4_1, 4_6)$) lower and upper bounds do not coincide. In these cases we write upper and lower bounds separated by a dash, indicating the interval of possible values of the f-distances. Entries in the table are colour coded accordingly to how lower bounds were computed. Lower bounds for the entries in blue are computed using the inequality 6.2, while the ones in red using the inequality 6.1. We are not able to produce lower bounds for entries in orange.

	3_1		3_1		3_1		3_1		3_1
5_1	2	6_6	3	6_{35}	2	6_{64}	3	6_{93}	3
5_2	2	6_7	3	6_{36}	2	6_{65}	2-3	6_{94}	2
5_3	2	6_8	1-2	6_{37}	2-4	6_{66}	2	6_{95}	2
5_4	2	6_9	1-2	6_{38}	2-3	6_{67}	2	6_{96}	2
5_5	3	6_{10}	2	6_{39}	1-2	6_{68}	2	6_{97}	2-3
5_6	2	6_{11}	1-2	6_{40}	2	6_{69}	2	6_{98}	2
5_7	3	6_{12}	2	6_{41}	2	6_{70}	3	6_{99}	2-4
5_8	2	6_{13}	2	6_{42}	3	6_{71}	4	6_{100}	2-3
5_9	2	6_{14}	3	6_{43}	3	6_{72}	2	6_{101}	3
5_{10}	3	6_{15}	1	6_{44}	2	6_{73}	2	6_{102}	3
5_{11}	1	6_{16}	1	6_{45}	1-2	6_{74}	3-4	6_{103}	3
5_{12}	2	6_{17}	2	6_{46}	3-4	6_{75}	3	6_{104}	3
5_{13}	4	6_{18}	2	6_{47}	2	6_{76}	3	6_{105}	2
5_{14}	3	6_{19}	2-3	6_{48}	2-3	6_{77}	2	6_{106}	1
5_{15}	4	6_{20}	3-4	6_{49}	3	6_{78}	3	6_{107}	2
5_{16}	2	6_{21}	2	6_{50}	2-3	6_{79}	3-4	6_{108}	2-3
5_{17}	2	6_{22}	2-3	6_{51}	2	6_{80}	2-4	6_{109}	2-3
5_{18}	2	6_{23}	2-3	6_{52}	3	6_{81}	2	6_{110}	3
5_{19}	2	6_{24}	2-3	6_{53}	1	6_{82}	2-3	6_{111}	2
5_{20}	1	6_{25}	3	6_{54}	4	6_{83}	1-3	6_{112}	1-2
5_{21}	3	6_{26}	2	6_{55}	2	6_{84}	2	6_{113}	3
5_{22}	2	6_{27}	2-3	6_{56}	2	6_{85}	2-3	6_{114}	2
5_{23}	3	6_{28}	2	6_{57}	4	6_{86}	2-4	6_{115}	1-2
5_{24}	1-2	6_{29}	2	6_{58}	2	6_{87}	2	6_{116}	2
6_1	4	6_{30}	1-2	6_{59}	1	6_{88}	1	6_{117}	3
6_2	2	6_{31}	3	6_{60}	3	6_{89}	2	6_{118}	1-3
6_3	2	6_{32}	3	6_{61}	3	6_{90}	2	6_{119}	2-3
6_4	3	6_{33}	3	6_{62}	1-2	6_{91}	2-3	6_{120}	2-3
6_5	2	6_{34}	2-3	6_{63}	2-3	6_{92}	2-3	6_{121}	2-4

Table B.2: The f-distances between equivalence classes of knotoids with minimal crossing number ≤ 6 and the 3_1 knotoid. In a few cases (*e.g* for the 6_{99} knotoid) lower and upper bounds do not coincide. In these cases we write upper and lower bounds separated by a dash, indicating the interval of possible values of the f-distances. Entries in the table are colour coded accordingly to how lower bounds were computed. Lower bounds for the entries in blue are computed using the inequality 6.2, while the ones in red using the inequality 6.1. We are not able to produce lower bounds for entries in orange.

	0_1	2_1	2_1^m	2_1^{ms}	2_1^s	3_1	3_1^m	3_2	3_2^m	3_2^{ms}	3_2^s	4_1	4_2	4_2^m
0_1	0	1	1	1	1	2	2	1	1	1	1	2	1	1
2_1	1	0	2	2	2	1	3	2	2	2	2	3	1	2
2_1^m	1	2	0	2	2	3	1	2	2	2	2	3	2	1
2_1^{ms}	1	2	2	0	2	1	3	2	2	2	2	3	2	2
2_1^s	1	2	2	2	0	3	1	2	2	2	2	3	2	2
3_1	2	1	3	1	3	0	4	3	3	3	3	4	2	3
3_1^m	2	3	1	3	1	4	0	3	3	3	3	4	3	2
3_2	1	2	2	2	2	3	3	0	2	2	1	1	2	2
3_2^m	1	2	2	2	2	3	3	2	0	1	2	1	2	2
3_2^{ms}	1	2	2	2	2	3	3	2	1	0	2	1	2	2
3_2^s	1	2	2	2	2	3	3	1	2	2	0	1	2	2
4_1	2	3	3	3	3	4	4	1	1	1	1	0	3	3
4_2	1	1	2	2	2	2	3	2	2	2	2	3	0	2
4_2^m	1	2	1	2	2	3	2	2	2	2	2	3	2	0
4_2^{ms}	1	2	2	1	2	2	3	2	2	2	2	3	2	2
4_2^s	1	2	2	2	1	3	2	2	2	2	2	3	2	2
4_3	2	1	3	3	3	2	4	3	3	3	3	4	2	3
4_3^m	2	3	1	3	3	4	2	3	3	3	3	4	3	2
4_3^{ms}	2	3	3	1	3	2	4	3	3	3	3	4	3	3
4_3^s	2	3	3	3	1	4	2	3	3	3	3	4	3	3
4_4	2	2	3	1	3	1	4	3	3	3	3	4	3	3
4_4^m	2	3	2	3	1	4	1	3	3	3	3	4	3	3
4_4^{ms}	2	1	3	2	3	1	4	3	3	3	3	4	2	3
4_4^s	2	3	1	3	2	4	1	3	3	3	3	4	3	2
4_5	2	3	1	3	3	4	2	1	3	3	2	2	3	2
4_5^m	2	1	3	3	3	2	4	3	1	2	3	2	2	3
4_5^{ms}	2	3	3	3	1	4	2	3	2	1	3	2	3	3
4_5^s	2	3	3	1	3	2	4	2	3	3	1	2	3	3
4_6	3	2	4	2	4	1	5	4	4	4	4	5	3	4
4_6^m	3	4	2	4	2	5	1	4	4	4	4	5	4	3
4_6^{ms}	3	2	4	2	4	1	5	4	4	4	4	5	3	4
4_6^s	3	4	2	4	2	5	1	4	4	4	4	5	4	3
4_7	1	2	1	2	2	3	2	2	2	2	2	3	2	2
4_7^m	1	1	2	2	2	2	3	2	2	2	2	3	2	2
4_7^{ms}	1	2	2	2	1	3	2	2	2	2	2	3	2	2
4_7^s	1	2	2	1	2	2	3	2	2	2	2	3	2	2
4_8	1	1	2	2	2	2	3	2	2	2	2	3	2	2
4_8^m	1	2	1	2	2	3	2	2	2	2	2	3	2	2
4_8^{ms}	1	2	2	1	2	2	3	2	2	2	2	3	2	2
4_8^s	1	2	2	2	1	3	2	2	2	2	2	3	2	2

Table B.3: Table of experimental f-distances of all knotoids with up to 4 crossings (part 1).

	4_2^{ms}	4_2^{s}	4_3	4_3^{m}	4_3^{ms}	4_3^{s}	4_4	4_4^{m}	4_4^{ms}	4_4^{s}	4_5	4_5^{m}	4_5^{ms}	4_5^{s}
0_1	1	1	2	2	2	2	2	2	2	2	2	2	2	2
2_1	2	2	1	3	3	3	2	3	1	3	3	1	3	3
2_1^{m}	2	2	3	1	3	3	3	2	3	1	1	3	3	3
2_1^{ms}	1	2	3	3	1	3	1	3	2	3	3	3	3	1
2_1^{s}	2	1	3	3	3	1	3	1	3	2	3	3	1	3
3_1	2	3	2	4	2	4	1	4	1	4	4	2	4	2
3_1^{m}	3	2	4	2	4	2	4	1	4	1	2	4	2	4
3_2	2	2	3	3	3	3	3	3	3	3	1	3	3	2
3_2^{m}	2	2	3	3	3	3	3	3	3	3	3	1	2	3
3_2^{ms}	2	2	3	3	3	3	3	3	3	3	3	2	1	3
3_2^{s}	2	2	3	3	3	3	3	3	3	3	2	3	3	1
4_1	3	3	4	4	4	4	4	4	4	4	2	2	2	2
4_2	2	2	2	3	3	3	3	3	2	3	3	2	3	3
4_2^{m}	2	2	3	2	3	3	3	3	3	2	2	3	3	3
4_2^{ms}	0	2	3	3	2	3	2	3	3	3	3	3	3	2
4_2^{s}	2	0	3	3	3	2	3	2	3	3	3	3	2	3
4_3	3	3	0	4	4	4	3	4	2	4	4	2	4	4
4_3^{m}	3	3	4	0	4	4	4	3	4	2	2	4	4	4
4_3^{ms}	2	3	4	4	0	4	2	4	3	4	4	4	4	2
4_3^{s}	3	2	4	4	4	0	4	2	4	3	4	4	2	4
4_4	2	3	3	4	2	4	0	4	2	4	4	3	4	2
4_4^{m}	3	2	4	3	4	2	4	0	4	2	3	4	2	4
4_4^{ms}	3	3	2	4	3	4	2	4	0	4	4	2	4	3
4_4^{s}	3	3	4	2	4	3	4	2	4	0	2	4	3	4
4_5	3	3	4	2	4	4	4	3	4	2	0	4	4	3
4_5^{m}	3	3	2	4	4	4	3	4	2	4	4	0	3	4
4_5^{ms}	3	2	4	4	4	2	4	2	4	3	4	3	0	4
4_5^{s}	2	3	4	4	2	4	2	4	3	4	3	4	4	0
4_6	3	4	3	5	3	5	2	5	2	5	5	3	5	3
4_6^{m}	4	3	5	3	5	3	5	2	5	2	3	5	3	5
4_6^{ms}	3	4	3	5	3	5	2	5	2	5	5	3	5	3
4_6^{s}	4	3	5	3	5	3	5	2	5	2	3	5	3	5
4_7	2	2	3	2	3	3	3	3	3	2	2	3	3	3
4_7^{m}	2	2	2	3	3	3	3	3	2	3	3	2	3	3
4_7^{ms}	2	2	3	3	3	2	3	2	3	3	3	3	2	3
4_7^{s}	2	2	3	3	2	3	2	3	3	3	3	3	3	2
4_8	2	2	2	3	3	3	3	3	2	3	3	2	3	3
4_8^{m}	2	2	3	2	3	3	3	3	3	2	2	3	3	3
4_8^{ms}	2	2	3	3	2	3	2	3	3	3	3	3	3	2
4_8^{s}	2	2	3	3	3	2	3	2	3	3	3	3	2	3

Table B.4: Table of experimental f-distances of all knotoids with up to 4 crossings (part 2).

	4_6	4_6^m	4_6^{ms}	4_6^s	4_7	4_7^m	4_7^{ms}	4_7^s	4_8	4_8^m	4_8^{ms}	4_8^s
0_1	3	3	3	3	1	1	1	1	1	1	1	1
2_1	2	4	2	4	2	1	2	2	1	2	2	2
2_1^m	4	2	4	2	1	2	2	2	2	1	2	2
2_1^{ms}	2	4	2	4	2	2	2	1	2	2	1	2
2_1^s	4	2	4	2	2	2	1	2	2	2	2	1
3_1	1	5	1	5	3	2	3	2	2	3	2	3
3_1^m	5	1	5	1	2	3	2	3	3	2	3	2
3_2	4	4	4	4	2	2	2	2	2	2	2	2
3_2^m	4	4	4	4	2	2	2	2	2	2	2	2
3_2^{ms}	4	4	4	4	2	2	2	2	2	2	2	2
3_2^s	4	4	4	4	2	2	2	2	2	2	2	2
4_1	5	5	5	5	3	3	3	3	3	3	3	3
4_2	3	4	3	4	2	2	2	2	2	2	2	2
4_2^m	4	3	4	3	2	2	2	2	2	2	2	2
4_2^{ms}	3	4	3	4	2	2	2	2	2	2	2	2
4_2^s	4	3	4	3	2	2	2	2	2	2	2	2
4_3	3	5	3	5	3	2	3	3	2	3	3	3
4_3^m	5	3	5	3	2	3	3	3	3	2	3	3
4_3^{ms}	3	5	3	5	3	3	3	2	3	3	2	3
4_3^s	5	3	5	3	3	3	2	3	3	3	3	2
4_4	2	5	2	5	3	3	3	2	3	3	2	3
4_4^m	5	2	5	2	3	3	2	3	3	3	3	2
4_4^{ms}	2	5	2	5	3	2	3	3	2	3	3	3
4_4^s	5	2	5	2	2	3	3	3	3	2	3	3
4_5	5	3	5	3	2	3	3	3	3	2	3	3
4_5^m	3	5	3	5	3	2	3	3	2	3	3	3
4_5^{ms}	5	3	5	3	3	3	2	3	3	3	3	2
4_5^s	3	5	3	5	3	3	3	2	3	3	2	3
4_6	0	6	2	6	4	3	4	3	3	4	3	4
4_6^m	6	0	6	2	3	4	3	4	4	3	4	3
4_6^{ms}	2	6	0	6	4	3	4	3	3	4	3	4
4_6^s	6	2	6	0	3	4	3	4	4	3	4	3
4_7	4	3	4	3	0	2	2	2	2	2	2	2
4_7^m	3	4	3	4	2	0	2	2	2	2	2	2
4_7^{ms}	4	3	4	3	2	2	0	2	2	2	2	2
4_7^s	3	4	3	4	2	2	2	0	2	2	2	2
4_8	3	4	3	4	2	2	2	2	0	2	2	2
4_8^m	4	3	4	3	2	2	2	2	2	0	2	2
4_8^{ms}	3	4	3	4	2	2	2	2	2	2	0	2
4_8^s	4	3	4	3	2	2	2	2	2	2	2	0

Table B.5: Table of experimental f-distances of all knotoids with up to 4 crossings (part 3).

Bibliography

[1] Tetsuya Abe and Taizo Kanenobu. Unoriented band surgery on knots and links. *arXiv preprint arXiv:1112.2449*, 2011.

[2] Colin Conrad Adams. *The knot book: an elementary introduction to the mathematical theory of knots*. American Mathematical Soc., 2004.

[3] VI Arnold. Plane curves, their invariants, perestroikas and classifications. *Singularities and Bifurcations, Adv. in Sov. Math*, 21:1–16, 1993.

[4] Sebastian Baader. Note on crossing changes. *Quarterly Journal of Mathematics*, 57(2):139–142, 2006.

[5] Agnese Barbensi, Dorothy Buck, Heather A Harrington, and Marc Lackenby. Double branched covers of knotoids. *arXiv preprint arXiv:1811.09121, to appear in Communications in Analysis and Geometry*, 2018.

[6] Agnese Barbensi and Daniele Celoria. DNAandGrids. `https://github.com/agnesedaniele/DNAandGrids`, 2019.

[7] Agnese Barbensi and Daniele Celoria. The Reidemeister graph is a complete knot invariant. *Algebraic & Geometric Topology*, 20(2):643–698, 2020.

[8] Agnese Barbensi, Daniele Celoria, Heather A. Harrington, Andrzej Stasiak, and Dorothy Buck. Grid diagrams as tools to investigate knot spaces and topoisomerase-mediated simplification of DNA topology. *Science Advances*, 6(9), 2020.

[9] Agnese Barbensi and Dimos Goundaroulis. f-distance of knotoids and protein structure. *arXiv preprint arXiv:1909.08556*, 2019.

[10] Andrew D Bates, Anthony Maxwell, et al. *DNA topology*. Oxford University Press, USA, 2005.

[11] David Bates, B Montgomery Pettitt, Gregory R Buck, and Lynn Zechiedrich. Importance of disentanglement and entanglement during dna replication and segregation: Comment on:disentangling dna molecules by alexander vologodskii. *Physics of life reviews*, 18:160, 2016.

[12] Helen M Berman, Philip E Bourne, John Westbrook, and Christine Zardecki. The protein data bank. pages 394–410, 2003.

[13] Michel Boileau, Bernhard Leeb, and Joan Porti. Geometrization of 3-dimensional orbifolds. *Annals of mathematics*, pages 195–290, 2005.

[14] Daniel Bölinger, Joanna I Sułkowska, Hsiao-Ping Hsu, Leonid A Mirny, Mehran Kardar, José N Onuchic, and Peter Virnau. A Stevedore's protein knot. *PLoS computational biology*, 6(4), 2010.

[15] M Borodzik and S Friedl. Knotorious world wide web page, 2011.

[16] Maciej Borodzik and Stefan Friedl. On the algebraic unknotting number. *Transactions of the London Mathematical Society*, 1(1):57–84, 2014.

[17] Dorothy Buck. DNA topology. *Applications of knot theory (Proc. Sympos. Appl. Math., 66, Amer. Math. Soc., 2009)*, pages 47–79, 2009.

[18] Gregory R Buck and E Lynn Zechiedrich. DNA disentangling by type-2 topoisomerases. *Journal of molecular biology*, 340(5):933–939, 2004.

[19] D Andrew Burden and Neil Osheroff. Mechanism of action of eukaryotic topoisomerase II and drugs targeted to the enzyme. *Biochimica et Biophysica Acta (BBA)-Gene Structure and Expression*, 1400(1-3):139–154, 1998.

[20] Yannis Burnier, Cedric Weber, Alessandro Flammini, and Andrzej Stasiak. Local selection rules that can determine specific pathways of DNA unknotting by type II DNA topoisomerases. *Nucleic acids research*, 35(15):5223–5231, 2007.

[21] Jack S Calcut and Jules R Metcalf-Burton. Double branched covers of theta-curves. *Journal of Knot Theory and Its Ramifications*, 25(08):1650046, 2016.

[22] Jae Choon Cha and Charles Livingston. Knotinfo: an online table of knot invariants.

[23] James J Champoux. DNA topoisomerases: structure, function, and mechanism. *Annual review of biochemistry*, 70(1):369–413, 2001.

[24] Thomas Christian, Reiko Sakaguchi, Agata P Perlinska, Georges Lahoud, Takuhiro Ito, Erika A Taylor, Shigeyuki Yokoyama, Joanna I Sulkowska, and Ya-Ming Hou. Methyl transfer by substrate signaling from a knotted protein fold. *Nature structural & molecular biology*, 23(10):941, 2016.

[25] Daryl Cooper, Craig David Hodgson, and Steve Kerckhoff. *Three-dimensional orbifolds and cone-manifolds*, volume 5. Mathematical society of Japan, 2000.

[26] Lucia Coronel, Enzo Orlandini, and Cristian Micheletti. Non-monotonic knotting probability and knot length of semiflexible rings: the competing roles of entropy and bending energy. *Soft matter*, 13(23):4260–4267, 2017.

[27] Lucia Coronel, Antonio Suma, and Cristian Micheletti. Dynamics of supercoiled dna with complex knots: large-scale rearrangements and persistent multi-strand interlocking. *Nucleic acids research*, 46(15):7533–7541, 2018.

[28] Alexander Coward and Marc Lackenby. An upper bound on Reidemeister moves. *American Journal of Mathematics*, 136(4):1023–1066, 2014.

[29] Peter Cromwell. Arc presentations of knots and links. *Banach Center Publications*, 42:57–64, 1998.

[30] Pawel Dabrowski-Tumanski, Pawel Rubach, Dimos Goundaroulis, Julien Dorier, Piotr Sułkowski, Kenneth C Millett, Eric J Rawdon, Andrzej Stasiak, and Joanna I Sulkowska. Knotprot 2.0: a database of proteins with knots and other entangled structures. *Nucleic acids research*, 47(D1):D367–D375, 2018.

[31] Pawel Dabrowski-Tumanski, Andrzej Stasiak, and Joanna I Sulkowska. In search of functional advantages of knots in proteins. *PloS one*, 11(11):e0165986, 2016.

[32] Richard W Deibler, Jennifer K Mann, L Sumners De Witt, and Lynn Zechiedrich. Hin-mediated DNA knotting and recombining promote replicon dysfunction and mutation. *BMC molecular biology*, 8(1):44, 2007.

[33] Julien Dorier, Dimos Goundaroulis, Fabrizio Benedetti, and Andrzej Stasiak. Knoto-ID: a tool to study the entanglement of open protein chains using the concept of knotoids. *Bioinformatics*, 34(19):3402–3404, 2018.

[34] Daniel Dugger. Involutions on surfaces. *Journal of Homotopy and Related Structures*, 14(4):919–992, 2019.

[35] HA Dye and Louis H Kauffman. Virtual crossing number and the arrow polynomial. *Journal of Knot Theory and Its Ramifications*, 18(10):1335–1357, 2009.

[36] Ivan Dynnikov. Arc-presentations of links: monotonic simplification. *Fundamenta Mathematicae*, 1(190):29–76, 2006.

[37] Ivan Alekseyevich Dynnikov. Recognition algorithms in knot theory. *Russian Mathematical Surveys*, 58(6):1093, 2003.

[38] Tobias Ekholm, Lenhard Ng, and Vivek Shende. A complete knot invariant from contact homology. *Inventiones mathematicae*, 211(3):1149–1200, 2018.

[39] Benson Farb and Dan Margalit. *A primer on mapping class groups (pms-49)*. Princeton University Press, 2011.

[40] Alessandro Flammini, Amos Maritan, and Andrzej Stasiak. Simulations of action of DNA topoisomerases to investigate boundaries and shapes of spaces of knots. *Biophysical journal*, 87(5):2968–2975, 2004.

[41] Erica Flapan. Infinitely periodic knots. *Canadian Journal of Mathematics*, 37(1):17–28, 1985.

[42] Anatolij T Fomenko and Sergei Vladimirovich Matveev. *Algorithmic and computer methods for three-manifolds*. Springer Science and Business Media, 2013.

[43] Boštjan Gabrovšek and Maciej Mroczkowski. Knots in the solid torus up to 6 crossings. *Journal of Knot Theory and Its Ramifications*, 21(11):1250106, 2012.

[44] Cameron McA Gordon and J Luecke. Knots are determined by their complements. *Journal of the American Mathematical Society*, 2(2):371–415, 1989.

[45] Dimos Goundaroulis. f-distance. `https://github.com/dgound/f-distance`, 2019.

[46] Dimos Goundaroulis, Julien Dorier, Fabrizio Benedetti, and Andrzej Stasiak. Studies of global and local entanglements of individual protein chains using the concept of knotoids. *Scientific reports*, 7(1):6309, 2017.

[47] Dimos Goundaroulis, Julien Dorier, and Andrzej Stasiak. A systematic classification of knotoids on the plane and on the sphere. *arXiv preprint arXiv:1902.07277*, 2019.

[48] Dimos Goundaroulis, Neslihan Gügümcü, Sofia Lambropoulou, Julien Dorier, Andrzej Stasiak, and Louis Kauffman. Topological models for open-knotted protein chains using the concepts of knotoids and bonded knotoids. *Polymers*, 9(9):444, 2017.

[49] Neslihan Gügümcü and Louis H Kauffman. New invariants of knotoids. *European Journal of Combinatorics*, 65:186–229, 2017.

[50] Wolfgang Haken et al. Theory of normal surfaces: an isotopic criterion for the circular node. *Acta Mathematica*, 105(3-4):245–375, 1961.

[51] Rudolph Halin. About the maximum number of foreign infinite paths in graphs. *mathematical news*, 30(1-2):63–85, 1965.

[52] Joel Hass and Tahl Nowik. Invariants of knot diagrams. *Mathematische Annalen*, 342(1):125–137, 2008.

[53] Allison Henrich and Louis H Kauffman. Unknotting unknots. *The American Mathematical Monthly*, 121(5):379–390, 2014.

[54] Shawn R Henry and Jeffrey R Weeks. Symmetry groups of hyperbolic knots and links. *Journal of Knot Theory and Its Ramifications*, 1(02):185–201, 1992.

[55] Jim Hoste and Mark E Kidwell. Dichromatic link invariants. *Transactions of the American Mathematical Society*, 321(1):197–229, 1990.

[56] Jim Hoste, Yasutaka Nakanishi, and Kouki Taniyama. Unknotting operations involving trivial tangles. *Osaka Journal of Mathematics*, 27(3):555–566, 1990.

[57] Xia Hua, Diana Nguyen, Barath Raghavan, Javier Arsuaga, and Mariel Vazquez. Random state transitions of knots: a first step towards modeling unknotting by type II topoisomerases. *Topology and its Applications*, 154(7):1381–1397, 2007.

[58] Sophie E Jackson, Antonio Suma, and Cristian Micheletti. How to fold intricately: using theory and experiments to unravel the properties of knotted proteins. *Current opinion in structural biology*, 42:6–14, 2017.

[59] Michal Jamroz, Wanda Niemyska, Eric J Rawdon, Andrzej Stasiak, Kenneth C Millett, Piotr Sułkowski, and Joanna I Sulkowska. Knotprot: a database of proteins with knots and slipknots. *Nucleic acids research*, 43(D1):D306–D314, 2014.

[60] David Joyce. A classifying invariant of knots, the knot quandle. *Journal of Pure and Applied Algebra*, 23(1):37–65, 1982.

[61] Taizo Kanenobu. Band surgery on knots and links. *Journal of Knot Theory and Its Ramifications*, 19(12):1535–1547, 2010.

[62] Taizo Kanenobu. Band surgery on knots and links, III. *Journal of Knot Theory and Its Ramifications*, 25(10):1650056, 2016.

[63] Vsevolod Katritch, Jan Bednar, Didier Michoud, Robert G Scharein, Jacques Dubochet, and Andrzej Stasiak. Geometry and physics of knots. *Nature*, 384(6605):142–145, 1996.

[64] Vsevolod Katritch, Wilma K Olson, Alexander Vologodskii, Jacques Dubochet, and Andrzej Stasiak. Tightness of random knotting. *Physical Review E*, 61(5):5545, 2000.

[65] Louis H Kauffman and Sofia Lambropoulou. Hard unknots and collapsing tangles. *Introductory lectures on knot theory, Ser. Knots Everything*, 46:187–247, 2012.

[66] Arkady B Khodursky, E Lynn Zechiedrich, and Nicholas R Cozzarelli. Topoisomerase IV is a target of quinolones in escherichia coli. *Proceedings of the National Academy of Sciences*, 92(25):11801–11805, 1995.

[67] Hyoungjun Kim, Sungjong No, and Seungsang Oh. Equilateral stick number of knots. *Journal of Knot Theory and Its Ramifications*, 23(07):1460008, 2014.

[68] Paik Kee Kim and Jeffrey L Tollefson. Pl involutions of fibered 3-manifolds. *Transactions of the American Mathematical Society*, 232:221–237, 1977.

[69] Rob Kirby. Manifold theory. *Algebraic and Geometric Topology, Part 2*, 2:273, 1978.

[70] Felix Klein. Über realitätsverhältnisse bei der einem beliebigen geschlechte zugehörigen normalkurve der φ. *mathematical annals*, 42(1):1–29, 1893.

[71] Kouzi Kodama and Makoto Sakuma. Symmetry groups of prime knots up to 10 crossings. In *Knots*, volume 90, pages 323–340. de Gruyter, 1992.

[72] Dimitrios Kodokostas and Sofia Lambropoulou. Rail knotoids. *arXiv preprint arXiv:1812.09493*, 2018.

[73] Sadayoshi Kojima. Finiteness of symmetries on 3-manifolds. 1983.

[74] Ph G Korablev and Ya K May. Knotoids and knots in the thickened torus. *Siberian Mathematical Journal*, 58(5):837–844, 2017.

[75] Martin I Krzywinski, Jacqueline E Schein, Inanc Birol, Joseph Connors, Randy Gascoyne, Doug Horsman, Steven J Jones, and Marco A Marra. Circos: An information aesthetic for comparative genomics. *Genome Research*, 2009.

[76] Greg Kuperberg. Algorithmic homeomorphism of 3-manifolds as a corollary of geometrization. *arXiv preprint arXiv:1508.06720*, 2015.

[77] Marc Lackenby. Elementary knot theory. *arXiv preprint arXiv:1604.03778*, 2016.

[78] Marc Lackenby. Links with splitting number one. *arXiv preprint arXiv:1808.05495*, 2018.

[79] Sofia Lambropoulou. Knot theory related to generalized and cyclotomic hecke algebras of type b. *arXiv preprint math/0405504*, 2004.

[80] Nicole CH Lim and Sophie E Jackson. Molecular knots in biology and chemistry. *Journal of Physics: Condensed Matter*, 27(35):354101, 2015.

[81] Zhirong Liu, Jennifer K. Mann, E. Lynn Zechiedrich, and Hue Sun Chan. Topological information embodied in local juxtaposition geometry provides a statistical mechanical basis for unknotting by type-2 DNA topoisomerases. *J. Mol. Biol.*, 361(2):268–285, Aug 2006.

[82] Zhirong Liu, E. Lynn Zechiedrich, and Hue Sun Chan. Inferring global topology from local juxtaposition geometry: interlinking polymer rings and ramifications for topoisomerase action. *Biophys. J.*, 90(7):2344–2355, Apr 2006.

[83] Rhonald C Lua and Alexander Y Grosberg. Statistics of knots, geometry of conformations, and evolution of proteins. *PLoS computational biology*, 2(5), 2006.

[84] Anna L Mallam and Sophie E Jackson. The dimerization of an α/β-knotted protein is essential for structure and function. *Structure*, 15(1):111–122, 2007.

[85] Anna L Mallam and Sophie E Jackson. Knot formation in newly translated proteins is spontaneous and accelerated by chaperonins. *Nature chemical biology*, 8(2):147, 2012.

[86] Jason Fox Manning. Algorithmic detection and description of hyperbolic structures on closed 3–manifolds with solvable word problem. *Geometry & Topology*, 6(1):1–26, 2002.

[87] Marc L Mansfield. Are there knots in proteins? *Nature structural biology*, 1(4):213–214, 1994.

[88] Julien Marché. About the Gordian graph at infinity. *Comptes Rendus Mathematique*, 340(5):363–368, 2005.

[89] Kenneth Millett, Akos Dobay, and Andrzej Stasiak. Linear random knots and their scaling behavior. *Macromolecules*, 38(2):601–606, 2005.

[90] Kenneth C Millett, Eric J Rawdon, Andrzej Stasiak, and Joanna I Sułkowska. Identifying knots in proteins, 2013.

[91] Yasuyuki Miyazawa. A distance for diagrams of a knot. *Topology and its Applications*, 159(4):1122–1131, 2012.

[92] José María Montesinos Amilibia. Three-manifolds as 3-fold branched covers of s^3. *Quarterly Journal of Mathematics*, 27(1):85–94, 1976.

[93] Hyeyoung Moon. Calculating knot distances and solving tangle equations involving montesinos links. 2010.

[94] Hyeyoung Moon. Calculating knot distances and solving tangle equations involving montesinos links. 2010.

[95] Hiromasa Moriuchi. An enumeration of theta-curves with up to seven crossings. *Proceedings of the East Asian School of Knots, Links, and Related topics*, pages 171–185, 2004.

[96] Brendan Owens. Unknotting information from Heegaard Floer homology. *arXiv preprint math/0506485*, 2005.

[97] Brendan Owens and Saso Strle. Immersed disks, slicing numbers and concordance unknotting numbers. *arXiv preprint arXiv:1311.6702*, 2013.

[98] Peter Ozsváth and Zoltán Szabó. Knots with unknotting number one and Heegaard Floer homology. *Topology*, 44(4):705–745, 2005.

[99] Peter S Ozsváth, András I Stipsicz, and Zoltán Szabó. *Grid homology for knots and links*, volume 208 of *Mathematical Series and Monographs*. American Mathematical Soc., 2015.

[100] Michael Polyak. Minimal generating sets of Reidemeister moves. *arXiv preprint arXiv:0908.3127*, 2009.

[101] Raffaello Potestio, Cristian Micheletti, and Henri Orland. Knotted vs. unknotted proteins: evidence of knot-promoting loops. *PLoS computational biology*, 6(7), 2010.

[102] Dusan Racko, Fabrizio Benedetti, Dimos Goundaroulis, and Andrzej Stasiak. Chromatin loop extrusion and chromatin unknotting. *Polymers*, 10(10):1126, 2018.

[103] Kurt Reidemeister. Elementare begründung der knotentheorie. In *Abhandlungen aus dem Mathematischen Seminar der Universität Hamburg*, volume 5, pages 24–32. Springer, 1927.

[104] Joaquim Roca. In silico, in vitro and in vivo imageries of type ii topoisomerases. comment on" disentangling dna molecules" by alexander vologodskii. *PhLRv*, 18:147–149, 2016.

[105] Dale Rolfsen. *Knots and links*, volume 346. American Mathematical Soc., 2003.

[106] Valentin V Rybenkov, Christian Ullsperger, Alexander V Vologodskii, and Nicholas R Cozzarelli. Simplification of DNA topology below equilibrium values by type II topoisomerases. *Science*, 277(5326):690–693, 1997.

[107] Makoto Sakuma. On strongly invertible knots. In *Algebraic and Topological Theories. Papers from the Symposium Dedicated to the Memory of Dr. Takehiko Miyata (Kinosaki, 1984), Kinokuniya Company Ltd., Tokyo*, pages 176–196, 1986.

[108] Álvaro San Martín, Piere Rodriguez-Aliaga, José Alejandro Molina, Andreas Martin, Carlos Bustamante, and Mauricio Baez. Knots can impair protein degradation by ATP-dependent proteases. *Proceedings of the National Academy of Sciences*, 114(37):9864–9869, 2017.

[109] Peter Scott. The geometries of 3-manifolds. *Bulletin of the London Mathematical Society*, 15(5):401–487, 1983.

[110] Andrzej Stasiak, Jacques Dubochet, Vsevolod Katritch, and Piotr Pieranski. Ideal knots and their relation to the physics of real knots. *Ideal knots*, 19:1–19, 1998.

[111] Tanya Stuchinskaya, Lesley A Mitchenall, Allyn J Schoeffler, Kevin D Corbett, James M Berger, Andrew D Bates, and Anthony Maxwell. How do type II topoisomerases use ATP hydrolysis to simplify DNA topology beyond equilibrium? investigating the relaxation reaction of nonsupercoiling type II topoisomerases. *Journal of molecular biology*, 385(5):1397–1408, 2009.

[112] Joanna I Sułkowska, Jeffrey K Noel, and Jose N Onuchic. Energy landscape of knotted protein folding. *Proceedings of the National Academy of Sciences*, 109(44):17783–17788, 2012.

[113] Joanna I Sułkowska, Eric J Rawdon, Kenneth C Millett, Jose N Onuchic, and Andrzej Stasiak. Conservation of complex knotting and slipknotting patterns in proteins. *Proceedings of the National Academy of Sciences*, 109(26):E1715–E1723, 2012.

[114] DeWitt Sumners and SG Whittington. Knots in self-avoiding walks. *Journal of Physics A: Mathematical and General*, 21(7):1689, 1988.

[115] William R. Taylor. A deeply knotted protein and how it might fold. *Nature*, 406:916–919, 2000.

[116] The Sage Developers. *SageMath, the Sage Mathematics Software System (Version 8.6)*, 2019. `https://www.sagemath.org`.

[117] Abigail Thompson. Algorithmic recognition of 3-manifolds. *Bulletin of the American Mathematical Society*, 35(1):57–66, 1998.

[118] Sonia Trigueros, Javier Salceda, Ignacio Bermúdez, Xavier Fernández, and Joaquim Roca. Asymmetric removal of supercoils suggests how topoisomerase II simplifies DNA topology. *Journal of molecular biology*, 335(3):723–731, 2004.

[119] Luca Tubiana, Enzo Orlandini, and Cristian Micheletti. Probing the entanglement and locating knots in ring polymers: A comparative study of different arc closure schemes. *Progress of Theoretical Physics Supplement*, 191:192–204, 2011.

[120] Vladimir Turaev. Knotoids. *Osaka Journal of Mathematics*, 49(1):195–223, 2012.

[121] Jussi Väisälä. Gromov hyperbolic spaces. *Expositiones Mathematicae*, 23(3):187–231, 2005.

[122] Peter Virnau, Anna Mallam, and Sophie Jackson. Structures and folding pathways of topologically knotted proteins. *Journal of Physics: Condensed Matter*, 23(3):033101, 2010.

[123] Peter Virnau, Leonid A Mirny, and Mehran Kardar. Intricate knots in proteins: Function and evolution. *PLoS computational biology*, 2(9):e122, 2006.

[124] Alexander Vologodskii. Theoretical models of DNA topology simplification by type IIA DNA topoisomerases. *Nucleic acids research*, 37(10):3125–3133, 2009.

[125] Alexander Vologodskii. Disentangling dna molecules. *Physics of life reviews*, 18:118–134, 2016.

[126] Alexander V Vologodskii, Wentao Zhang, Valentin V Rybenkov, Alexei A Podtelezhnikov, Deepa Subramanian, Jack D Griffith, and Nicholas R Cozzarelli. Mechanism of topology simplification by type II DNA topoisomerases. *Proceedings of the National Academy of Sciences*, 98(6):3045–3049, 2001.

[127] AV Vologodskii, AV Lukashin, MD Kamenetskii, and VV Anshelevich. The knot problem in statistical mechanics of polymer chains. *Soviet Journal of Experimental and Theoretical Physics*, 39:1059, 1974.

[128] Friedhelm Waldhausen. Über involutionen der 3-sphäre. *Topology*, 8(1):81–91, 1969.

[129] James C Wang. DNA topoisomerases. *Annual review of biochemistry*, 65(1):635–692, 1996.

[130] James D Watson, Francis HC Crick, et al. Molecular structure of nucleic acids. *Nature*, 171(4356):737–738, 1953.

[131] Liam Watson. Khovanov homology and the symmetry group of a knot. *Advances in Mathematics*, 313:915–946, 2017.

[132] Jie Yan, Marcelo O Magnasco, and John F Marko. Kinetic proofreading can explain the supression of supercoiling of circular DNA molecules by type-II topoisomerases. *Physical Review E*, 63(3):031909, 2001.

[133] Riccardo Ziraldo, Andreas Hanke, and Stephen D Levene. Kinetic pathways of topology simplification by type-ii topoisomerases in knotted supercoiled dna. *Nucleic acids research*, 47(1):69–84, 2019.